FRACTALCOMS

Exploring the limits of Fractal Electrodynamics for the future telecommunication technologies
IST-2001-33055

Task 3.1 Final Report

Advanced meshing of fractal structures

Deliverable reference:	**D5**
Contractual Date of Delivery to the EC:	**January 31., 2003**
Author(s):	**Juan M. Rius**
Participant(s):	**UPC**
Workpackage:	**WP3**
Security:	**Public**
Nature:	**Deliverable**
Version:	**2.0**
Date:	**January 25, 2003**

Total number of pages: 8 pages + 5 reports attached

Abstract:

Special purpose meshing tools have been developed for the numerical simulation of pre-fractal structures, so that the aims of this project can be reached: A high-order point-based discretization scheme based on Nystrom method with singular kernel correction has been explored, the best way to model and mesh wire pre-fractal antennas has been studied, advanced adaptive meshing facilities have been developed for fractal domains, new basis functions for vertex-connected structures have been introduced and a specific treatment of T-junctions and similar complex connections has been provided.

Keyword list: Numerical simulations, meshing, pre-fractal antennas.

ADVANCED MESHING OF FRACTAL STRUCTURES

1. INTRODUCTION

This task is essentially aimed at developing special purpose meshing tools for the numerical simulation of pre-fractal structures, so that the aims of this project can be reached. The work to do in this task is, from Annex-1 to the contract between the consortium and the EC:

a) A high-order point-based discretization scheme based on Nystrom method with singular kernel correction will be explored.

b) Advanced adaptive meshing facilities will be developed for fractal domains. In a first phase, conventional meshing algorithms will be adapted to the requirements of the present project. In a second phase, the production of fractal meshes for the discretization of fractal domains will be evaluated and, if possible, the corresponding algorithms will be developed and coded.

c) New basis functions for vertex-connected structures will be introduced.

d) Specific treatment of T-junctions and similar complex connections will be provided.

2. NYSTROM METHOD HIGH-ORDER DISCRETIZATION SCHEME

(Report - WP3 T3.1 UPC T0+12 Nystrom)

Formulation and software code has been developed for the analysis of electrostatic problems with potential equation and Nystrom method. The kernel singularity has been corrected by Strain's method, using polynomial testing functions. The charge is therefore represented by a underlying polynomial basis. The results for objects with open surfaces are very bad, since the charge is singular at edges and cannot be expanded by the underlying polynomial quadrature basis. On the contrary, when the unknown charge is a polynomial, Nystrom method gives very small errors, up to machine precision.

Close form formulas for evaluating the integrals that arise in the computation of Strain correction have been derived for problems with singular kernel and polynomial unknown. However, it has not been possible to derive Strain correction formulas for problems having both singular kernel and unknown. Problems of this kind are the Electric Field Integral Equation (EFIE) and the electrostatic potential equation on open surfaces. For that reason, Nystrom method can be currently applied to electromagnetic problems only on closed surfaced, which is not the case of the antennas under consideration.

For those reasons, Nystrom method is not adequate for the analysis of pre-fractal antennas, since:

- Nystrom method is based on quadrature integration rules that relay in underlying polynomial basis. Since the rapidly varying -almost discontinuous- current and charge in pre-fractals cannot be expanded by a polynomial basis, Nystrom method looses its power of accurate integrations with few samples and results will be very poor.
- Nystrom method forces the EFIE equation in a point-matching fashion. Since the near field is also rapidly-varying, it is best to use a weighted residual procedure such as method of moments.

On the other hand, since the integrals of the current or charge along pre-fractal antennas converge very fast with the number of iterations (result of WP2 and Task 3.2), then it is possible to discretize the EFIE in highly-iterated pre-fractals using the conventional Galërkin - Method of Moments, which is in essence a weighted residual procedure.

In conclusion, we think that the **Method of Moments with Galërkin testing** (weak formulation) **is the most robust approach to discretize the EFIE in pre-fractals**. This assumption has been corroborated by the excellent results of numerical simulations in tasks 3.2, 3.3 and 3.4.

3. MODELING PRE-FRACTAL ANTENNAS

(Report - WP3 T3.1 UPC T0+12 Meshing wire antennas)

Modeling highly-iterated pre-fractal wire antennas is a challenging problem. It has been shown in [Deliverable D6, Task 3.2 Final Report] and [Report - WP3 T3.2 UPC T0+12 Prefractal wire modeling] that several difficulties arise with Pocklington integral equation and thin-wire models, even with the extended kernel.

The possibility of modeling the wire cylindrical surface with a triangle mesh is not practical do to cylinder intersections at corners, the huge computational cost required and, in difficult problems, there is no convergence with mesh refinement.

For that reason, we propose here to model pre-fractal wires using a narrow strip. Two strip models are considered: the planar and the extrusion strip. Both lead to similar results for low-iteration pre-fractals, but the extrusion strip, unlike the planar one, can model highly-iterated pre-fractals in which the strip width is comparable to the pre-fractal segment length.

For both kinds of strips, the discretization in triangles of size much smaller than the wavelength makes the linear system very badly-conditioned. For that reason, iterative solvers fail, even with huge pre-conditioners. A direct solver can be used with more than 10,000 unknowns thanks to the block-solution algorithm developed at UPC.

A numerical integration and mesh refinement convergence study has been done. The extrusion strip model shows good convergence with both refinement of mesh size and refinement of EFIE source and testing integration, for both the cases of electrically very small and self-resonant antennas.

4. MESHING PRE-FRACTAL ANTENNAS

(Report - WP3 T3.1 CIMNE T0+12 GiD)

Software facilities have been developed in order to mesh a wide range of fractal geometries in the most automatic and adaptive way with while keeping the user interaction to a minimum.

The starting point of this task is the commercial pre and post-processing software package named GiD that has been developed at CIMNE. This software has been developed for giving support to all the necessary operations for the preparation of data for numerical analysis involving any type of geometrical discretization of the analysis domain, like in the case of the numerical algorithms used in the FRACTALCOMS project. Since standard CAD systems are not prepared for the generation of fractal geometries, the main activity in Task 3.1 has consisted in providing GiD with new software facilities for the automatic generation and meshing of fractal geometries. In addition, special adaptive mesh facilities have been added to the software in order to allow an enhancing of the quality of the numerical results in certain areas of the analysis domain.

The main technical aspect of the new tools added to GiD for the generation and meshing of fractal geometries is the recursive definition of the fractal geometry. Following the indications from UPC, this definition is based in the use of a geometrical Initiator and a geometrical Generator. The generation of the fractal geometry is based on a recursive process in which each segment of the Initiator is substituted by the Generator. Both the Initiator and the Generator can be selected from an existing list or manually defined by the user.

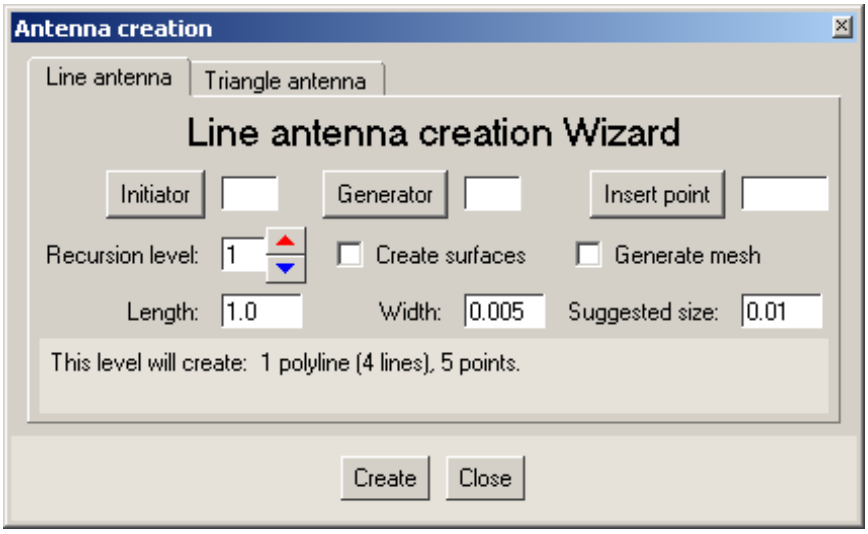

If the thin-wire approximation is not used, the recursive definition of the fractal geometry produces a wire antenna that needs to be widened in order to get a strip. This process is produced by widening each linear segment of the obtained geometry. Special care has to be taken in order to avoid overlapping between strips from consecutive segments at the corner points. This process is executed automatically after defining the with of the strip antenna.

The next step is the generation of the mesh for the numerical analysis of the fractal antenna. This process is performed in a completely automatic way after defining the size and the type (triangular or quadrilateral) of the elements. In addition, it is also possible to generate adapted meshes with a non uniform distribution of sizes after some manual definition of the desired size at each part of the domain.

During the first year of the project an increasing interest in antennas created from planar fractal geometries has been detected. This has suggested to enlarge the software capabilities developed during the first year in order to deal with this alternative type of geometries. Even taking into account that Task 3.1 has finished at T0+12, CIMNE agrees in being active for the second year in order to allow for the mentioned software improvements. This will allow to introduce the generation of planar geometries in GiD and, also, to introduce some minor improvements in the treatment of the wire geometries. The expansion of CIMNE activity will be carried out using some remaining man months that have not been completely consumed during the first year project. This will allow to develop this additional activity without any additional budget.

5. NEW BASIS FUNCTIONS

(Report - WP3 T3.1 EPFL T0+6 Quadrangular basis)

EPFL has developed a new set of basis functions defined on quadrangular regions. Particular cases of these functions are the well-known rooftop and Rao, Wilton and Glisson (RWG) basis.

These new functions will be very useful for the project because they simplify enormously the electric connection between different patches of the pre-fractal that share only one vertex. As a result, it will be easier to build adaptive meshes having less unknowns and modeling better the variation of the current in the pre-fractal geometry.

Three cases of quadrangular basis functions have been considered:

- With constant normal component of the current at one edge. The divergence of the current (charge) is not constant.
- With constant divergence of the current, but non-constant normal component of the current at the edge.
- Having both properties of constant divergence of the current and constant normal component of the current at one edge.

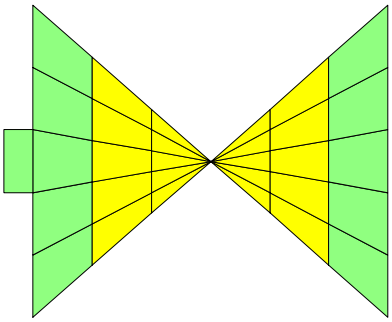

The best results are obtained with the 3rd option. The agreement with the conventional rooftop and RWG functions is very good.

The potential of quadrangular basis functions for solving connectivity problems has been shown in the simulation of a bow-tie antenna with different feeding zone sizes. The results are very promising.

6. TREATMENT OF T-JUNCTIONS

(Report - WP3 T3.1 EPFL T0+12 Tjunctions)

When building prefractal antennas of intricate shape (Koch, fractal tree) with microstrip or printed technology, discontinuities such as right-angle bends, T-junctions and crossings are encountered. In a boundary element discretisation, brute force approach would require an important computer effort and time for such complicated structures and would prevent us to analyse but the very first fractal iterations. Knowing the electromagnetic behaviour of these connections (mainly the distribution of currents and charges), a model could be created in order to substitute a brute force discretisation in the junctions. In the present work, a study of currents and charges in a T-junction is done in order to know which kind of global basis function would serve best as model for this type of junctions. This global basis should allow us to analyse pre-fractal antennas up to the iteration limit imposed by current technology.

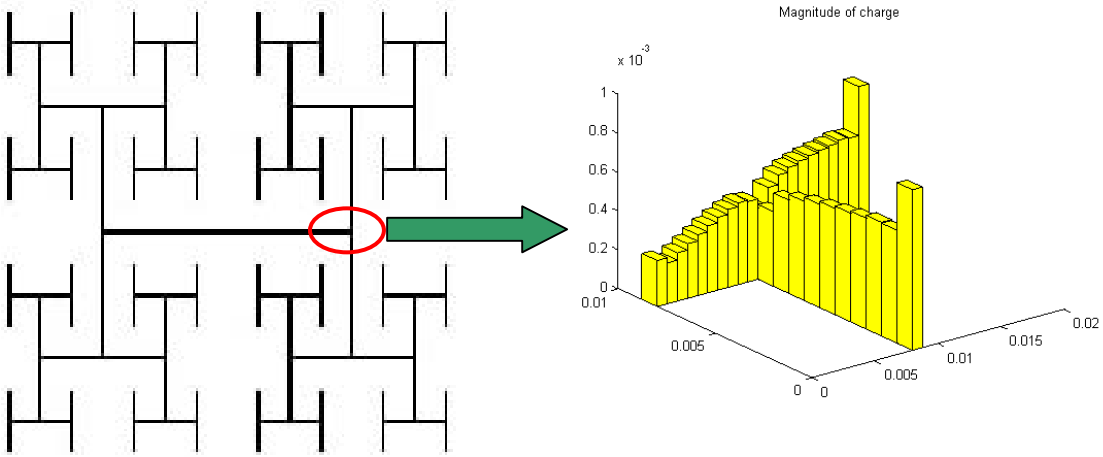

Different models for analysing printed junctions have been discussed. First, the quasistatic model has led us to two results, namely: The current distribution tends to be solenoidal at low frequencies and Kirchoff's law should be satisfied in small junctions. Then a transmission line (TL) model has been studied to have some useful global indications about the charge and current behaviour. In this case Kirchoff's law must still be satisfied but opposite to quasistatic approaches, the TL model allows prediction of charge behaviour in the arms connected at the junction. Indeed the TL predictions are frequently a good approximation at the global level.

These global results have been corroborated with a full-wave model. For low frequencies the general behaviour of charge and current along the line for the transmission line model and in the full-wave model is the same, except, of course, in the junction. For high frequencies radiation phenomena take place, and so transmission line model is no longer valid. But even at low frequencies, radiation is generated at the junction. This results in a net decrease of charge level at the junction which has been

systematically observed in our numerical experiments. This feature of the charge must be included in the pre-fractal antenna model if accurate predictions are required.

With the full-wave model the structure has been studied once with a rough mesh and once with a very high number of unknowns, to know in detail which is the evolution of currents and charges on the T-junction, for different kind of excitation. With a high degree of detail results show with precision the zones where current and charge maxima or minima can be found. For low frequencies, in the junction and without taking into account singularities, the charge can be said to be constant, but it is no longer the case for high frequencies. All this information must be used in order to define a global basis function that reproduces these characteristics, and thus it can be used to substitute the detailed fine mesh in the junction without loss in precision and accuracy of results.

Summarizing, this study has set up the basic strategy for the modelling of connections and junctions in pre-fractal antennas. Some observed effects deserve further study in order to reach a correct interpretation. For instance the electromagnetic behaviour of junctions seems to depend critically on the kind and type of excitation.

At a first glance, this seems to render hopeless a global, unique approach for junctions in fractals. But save for the case of a junction containing eventually the excitation, most junctions in fractal structures are essentially excited by the fractal itself and hence there is room for a systematic time-saving treatment.

FRACTALCOMS

Exploring the limits of Fractal Electrodynamics for the future telecommunication technologies
IST-2001-33055

Nystrom's method over planar structures

Author(s):	**Sergio López, Juan M. Rius**
Participant(s):	**UPC**
Workpackage and task:	**WP3, T3.1**
Security:	**Public**
Nature:	**Report**
Version and date:	**1.0, 30-12-2002**

Total number of pages: 11

Abstract:

One of task 3.1 objective is solving the Maxwell's equations over planar structures using the Nyström's method. This problem began to be studied the last century's last decade and stand off for its difficulty to handle the singular behaviour of the equations' kernels. Moreover, over planar structures we have the problem of the singular behaviour of the sources in edges and corners. To study the method utility in this context we have not chosen the habitual equations EFIE and MFIE otherwise we have chosen the potential integral equation which is easier to handle, and then in function of the results we would increase the difficulty level. In this report we show the obtained advances and conclusions on existing techniques to treat this problem.

Keyword list: Numerical integration, analytical integration, Gaussian rules, BEM, singular functions.

RELATED WP AND TASKS (FROM THE PROJECT DESCRIPTION)

WP3: Software simulation tool

Task 3.1: Advanced meshing of fractal structures

(a) A high-order point-based discretization scheme based on Nystrom method with singular kernel correction will be explored

1 INTRODUCTION

The Nyström's method is presented as an efficient mechanism to solve integral equations. The idea consists on discretize this equations using a quadrature or cubature rule, since a proper description of the integration domain has been done in order to do it. Doing this we succeed in transform the integral equation in a matricial equation whose solution will be computed by matrix inversion. Now we show these steps in an explicit way:

Suppose you have the next integral equation:

$$\Phi(r) = \int_S K(r - r')\Psi(r')dr'$$

Where Φ is the known function, Ψ is the unknown function, *K* is the kernel and *s* is the integration domain.

Suppose you have a quadrature or cubature rule of N points with its weights w_n and their respective abcisae r_n. This rule will be some kind of Gaussian rule, since this quadrature rules have good properties like rapid convergence, stability, positivity of the weights and mathematical elegance. After the process of discretization of the equation shown above we have the next equation:

$$\Phi(r_m) \cong \sum_{n=1}^{N} w_n \cdot K(r_m - r_n) \cdot \Psi(r_n)$$

This is a matricial equation which can be expressed in a more explicit way:

$$\begin{bmatrix} w_1 \cdot K(r_1 - r_1) & \ldots & w_N \cdot K(r_1 - r_N) \\ \ldots & & .... \\ w_1 \cdot K(r_N - r_1) & \ldots & w_N \cdot K(r_N - r_N) \end{bmatrix} \cdot \begin{bmatrix} \Psi(r_1) \\ \ldots \\ \Psi(r_N) \end{bmatrix} = \begin{bmatrix} \Phi(r_1) \\ \ldots \\ \Phi(r_N) \end{bmatrix}$$

This is a square system of equations which can be written in compact form:

$$[K_{mn}] \cdot [\Psi_n] = [\Phi_m]$$

Where *K* is the Nyström's matrix. We can solve this system inverting *K* , then:

$$[\Psi_n] = [K_{mn}]^{-1} \cdot [\Phi_m]$$

Now we have discrete values of the unknowed function from which $\Psi(r)$ will be interpolated.

Up to now all seems perfect but we are doing implicit assumptions as the Nyström's matrix has inverse and the product between the kernel and the unknown function is smooth varying so then it can be efficiently integrated by the Gaussian quadrature rule. Under these conditions the Nyström's method has the next advantages:

- The solution found with this method has the same error as the quadrature rule used. If a high-order quadrature rule is used the solution represents a high-order approximation to the exact solution.
- Use of the Nyström's method reduces dramatically the precomputation time, since to fill the matrix only kernel evaluations are required instead of N^2 numerical double integrations like in the Galerkin method where the number of unknowns is N.

Unfortunately in electromagnetic problems the kernels can not be regulars otherwise they can be near singulars, singulars even hypersingulars, specially when x_m is close to x_n or x_m is equal to x_n. Moreover if the integration domain is not regular, it has geometric singularities as edges and corners, a singular behaviour of the unknown function is expected in this areas. That means that some elements of the Nyström's matrix can be infinity and the matrix has not got inverse, even if the matrix had got inverse is possible than the product between the kernel and the unknown function were not regular, then we lost the convergence properties that we had got thanks to the Gaussian rule. In the last years some methods that attempt to solve these problems have appeared in the literature about this subject. We discuss about these methods and we show some results in the next sections.

2 LOCAL CORRECTIONS

2.1 The Strain´s method.

One way to avoid the existence of infinities in the Nyström's matrix is the incorporation of the Strain's method. This method consists in modifying the value of the kernel in the vicinity of the singularity. Doing this we can avoid the infinities and the kernel's fast varying zones in order to maintain the properties of the Gaussian rule. The new values of the kernel are called *local corrections*. To compute these corrections we have to compute the kernel's moments in small domain called D_m which contains a set of source points x_n and is centered in the field point x_m. This moments are the integral over D_m of the product between the kernel and a set of K functions called *testing functions*, which typically are the functions for which the quadrature or cubature rule are exact, like monomials of the form $x^m y^n$ in our case. Finally we extract the value of the local corrections, denoted by L_{mn}, by solving the next system of equations:

$$\sum_{n=1}^{Np} w_n L_{mn} f^{(k)}(x_m - x_n) = \int_{D_m} G(x_m - x') \cdot f^{(k)}(x_m - x') \cdot ds'$$

Where G is the free space Green's function which is our kernel. This system represents K constrains (one for each testing function $f^{(k)}$) on Np local correction coefficients (one for each of Np source points in the vicinity of the mth field point). Doing this for each field point we can built a sparse matrix of local corrections so that the kernel's sampled values in the Nyström's matrix will be L_{mn}, if x_n is inside of D_m, or $G(x_m-x_n)$ otherwise. If the integrals at right hand side of the above equation are numerically computed can suppose an increase of the global computation time.

Doing this the Nyström-Strain's method has the next advantages:

- *Faster precomputation:* Unlike the method which requires N^2 numerical double integrations to fill the impedance matrix, the Nyström method requires less tan N^2 kernel evaluations and $O(N)$ calculations of local correction coefficients.
- *Elimination of multipatch parametric basis functions:* Conventional method of moments scattering codes require basis functions with a certain level of continuity across patch boundaries to facilitate differentiation. Now the requirement to use elemental sources with guaranteed continuity between patches disappears because continuity of the source distribution is achieved as a natural consequence of accurately solving the integral equation.

- *More amenable to fast solution algorithms:* Implementation of a fast method that requires segregation of the discretized scatterer into groups is simpler and more natural with a point-based discretization.
- *Iterative solver memory reduction:* With the Nyström method, the memory requirement for an iterative solver using the full impedance matrix can be reduced from $O(N^2)$ (storing the full impedance matrix) to $O(N)$ (storing only the local correction matrix).
- *Symmetry exploitation:* Whit Nyström's method is simpler reflecting the geometrical representations in the matrix representation.

2.2 Formulation for local corrections' integrals.

One of the most important advances that the UPC's Electromagnetic and Photonics Engineering Group has obtained is the analytical formulation to compute the integrals of the local corrections system over a triangular mesh of the surface, when these integrals are singular. This integrals can be singular, when all points lie in the same plane, or near-singular if we have unconnected surfaces like for example a capacitor or we have curved surfaces. In the near-singular case we have only obtained analytical integration for the internal integral but in the singular case, which is the case of planar structures, all the integration process is completely analytical. This has the benefit to reduce dramatically the computation time of local corrections that is a critical phase. We have obtained this formulation in two ways which will be explained below.

2.2.1 *BEM's z-formulae technique.*

This technique consists of solving the next integral equation:

$$I(z)=\int_T \frac{x^{l_1}y^{l_2}}{\sqrt{x^2+y^2+z^2}}dxdy=\int_T f(x,y,z)dxdy=\int_T f(\underline{x},z)dxdy$$

To solve this integral we must explode the homogeneity of the integrand though the Euler identity, integrating and subsequently applying Green's theorem, then we obtain the linear *continuation differential equation*:

$$\frac{\partial I(z)}{\partial z}-\frac{\alpha}{z}I(z)=\frac{1}{z}\cdot\int_{\partial\Omega} f\cdot(ydx-xdy)$$

At this point we have to differentiate between the near singular and the singular cases.

- *Near-singular integration technique.*

To obtain a close formulation we need to solve the differential equation showed before, arriving to the next expression:

$$I(z)=z^{\alpha}\int_{\partial\Omega}\left[F(\pm\infty)-F(\underline{x},z)\right]\cdot\underline{x}\cdot ds \qquad (A)$$

Where $\underline{x}\cdot ds=x\cdot dy-y\cdot dx$ and *F* is called *primitive boundary function* (PBF) which has analytical resolution and it has the next form:

$$F(\underline{x},z)=\int\frac{1}{z^{\alpha+1}}f(\underline{x},z)dz$$

The resolution of expression (A) is showed in the next page:

$$
\underset{(p=\alpha+1)}{I(z)} = \begin{cases}
\bullet \text{for } \alpha=1: \\
\displaystyle\int_{\partial\Omega} \frac{x^m y^n \sqrt{x^2+y^2+z^2}}{(x^2+y^2)}\,\underline{x}ds - z\cdot\int_{\partial\Omega}\frac{x^m y^n}{(x^2+y^2)}\,\underline{x}ds \\
\bullet \text{for } \alpha \text{ odd with } \alpha\geq 3: \\
\displaystyle\frac{(p-2)!!}{(p-1)!!}\cdot\left\{(-1)^{p/2}\cdot z^{\alpha}\left[\int_{\partial\Omega}\frac{x^m y^n}{(x^2+y^2)^{p/2}}\,\underline{x}ds - \frac{1}{z}\cdot\int_{\partial\Omega}\frac{x^m y^n\sqrt{x^2+y^2+z^2}}{(x^2+y^2)^{p/2}}\,\underline{x}ds\right] - \sum_{k=1}^{(p-2)/2}(-1)^k\frac{(p-1-2k)!!}{(p-2k)!!}\cdot z^{2k-2}\cdot\int_{\partial\Omega}\frac{x^m y^n\sqrt{x^2+y^2+z^2}}{(x^2+y^2)^k}\,\underline{x}ds\right\} \\
\bullet \text{ for } \alpha \text{ even with } \alpha\geq 2: \\
\displaystyle\frac{(p-2)!!}{(p-1)!!}\cdot\left[(-1)^{(p+3)/2}\cdot z^{\alpha}\cdot\int_{\partial\Omega}\frac{x^m y^n\cdot \operatorname{asinh}\left(\frac{x^2+y^2}{z\sqrt{x^2+y^2}}\right)}{(x^2+y^2)^{(p-1)/2}\cdot\sqrt{(x^2+y^2)}}\,\underline{x}ds - \sum_{k=1}^{(p-1)/2}(-1)^k\frac{(p-1-2k)!!}{(p-2k)!!}\cdot z^{2k-2}\cdot\int_{\partial\Omega}\frac{x^m y^n\sqrt{x^2+y^2+z^2}}{(x^2+y^2)^k}\,\underline{x}ds\right]
\end{cases}
$$

The contour integrals of the expression showed before are the addition of three integrals which result from the parameterization of the contour's triangles. These integrals have the form:

$$\pm\int_{t_a}^{t_b}\left[\frac{1}{\sqrt{C\cdot t^2+B\cdot t+A}}\cdot \mathrm{a\,sinh}\left(\frac{\sqrt{C\cdot t^2+B\cdot t+A}}{z}\right)\right]^i\cdot\left[\sqrt{C\cdot t^2+B\cdot t+A+z^2}\right]^j\cdot\frac{t^u\cdot(M\cdot t+N)^v}{(C\cdot t^2+B\cdot t+A)^k}\cdot N dt$$

Where the pair (i,j) can be *(0,0)*, *(0,1)* or *(1,0)*. These integrals have not analytical resolution but all the integrands are smooth varying, then we have used a Gauss-Legendre rule to compute it.

- *Singular integration technique*

To compute de singular integrals we have used the next theorem:

Theorem: *For* $\alpha>0$ *and homogeneous functions* $f(\underline{x},z)$ *bounded for* $(\underline{x},0)\in\partial\Omega$ *the continuation singular integral is bounded and can be computed by:*

$$I(0)=\frac{1}{\alpha}\int_{\partial\Omega} f(\underline{x},0)\cdot\underline{x}ds$$

These integrals have analytical resolution and are the addition of a set of integrals. In this case each one of these integrals has the form:

$$\int\frac{t^k}{\sqrt{A+B\cdot t+C\cdot t^2}}dt$$

This expression can be computed across this recursion:

$$\begin{cases}
\bullet\text{For k>2:}\\
\int\frac{t^k}{\sqrt{A+Bt+Ct^2}}dt=\frac{t^{k-1}\sqrt{A+Bt+Ct^2}}{k\cdot C}-\frac{(2k-1)\cdot B}{2\cdot k\cdot C}\int\frac{t^{k-1}}{\sqrt{A+Bt+Ct^2}}dt-\frac{(k-1)\cdot A}{k\cdot C}\int\frac{t^{k-2}}{\sqrt{A+Bt+Ct^2}}dt\\
\bullet\text{For k=2:}\\
\int\frac{t^k}{\sqrt{A+Bt+Ct^2}}dt=\left(\frac{t}{2\cdot C}-\frac{3\cdot B}{4\cdot C^2}\right)\cdot\sqrt{A+Bt+Ct^2}+\left(\frac{3\cdot B^2}{8\cdot C^2}-\frac{A}{2\cdot C}\right)\cdot\int\frac{1}{\sqrt{A+Bt+Ct^2}}dt\\
\bullet\text{For k=1:}\\
\int\frac{t}{\sqrt{A+Bt+Ct^2}}dt=\frac{\sqrt{A+Bt+Ct^2}}{C}-\frac{B}{2\cdot C}\int\frac{1}{\sqrt{A+Bt+Ct^2}}dt\\
\bullet\text{For k=0 :}\\
\int\frac{1}{\sqrt{A+Bt+Ct^2}}dt=\frac{1}{\sqrt{C}}\cdot\mathrm{a\,sinh}\left(\frac{2\cdot C\cdot t+B}{\sqrt{\Delta}}\right)
\end{cases}$$

2.2.2 Singularity cancellation technique.

This technique consists of subdividing the region of integration in three subtriangles with the field point at one vertex, and then performs the integration using polar coordinates. The elements that operate on the integration of each subtriangle are showed in the next figure:

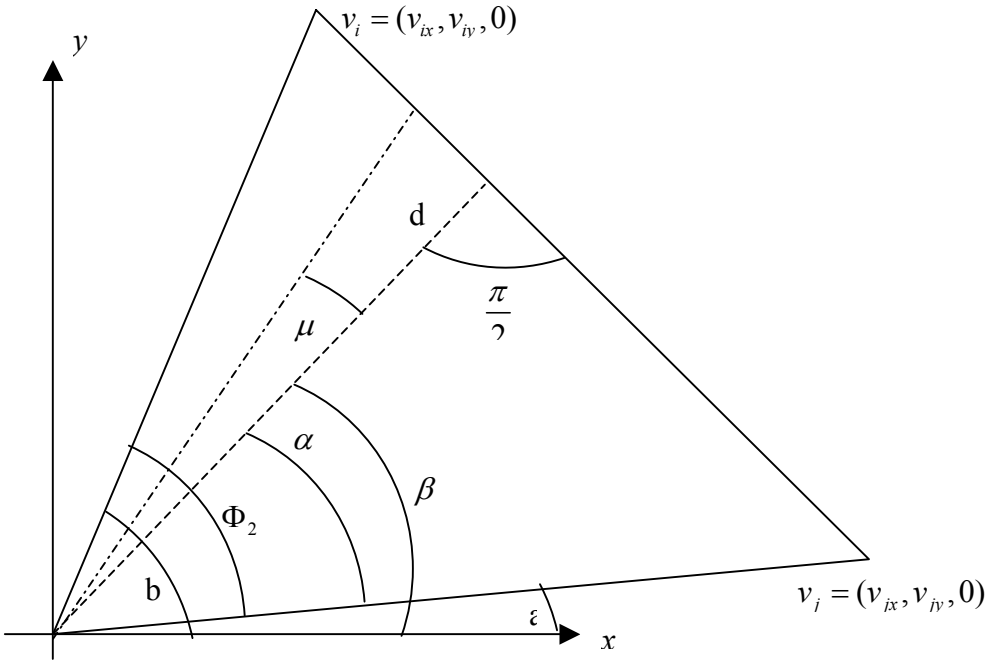

- *Near-singular integration technique:*

After the polar transformation we can obtain an integral of this form:

$$I(z) = \int_{-\alpha}^{\Phi_2 - \alpha} \int_{0}^{d/\cos(\mu)} \frac{r^{n+m+1} \cdot \cos^m(\mu+\beta) \cdot \sin^n(\mu+\beta)}{\sqrt{r^2+z^2}} \cdot dr \cdot d\mu$$

This integral can be expressed on this way:

$$I(z) = \int_{-\alpha}^{\Phi_2 - \alpha} \cos^m(\mu+\beta) \cdot \sin^n(\mu+\beta) \cdot F_p(\mu) \cdot d\mu \qquad \text{(B)}$$

Where $p = m+n+1$ and $F_p(\mu)$ has the next expression:

$$F_p(\mu) = \int_{0}^{d/\cos(\mu)} \frac{r^p}{\sqrt{r^2+z^2}} \cdot dr$$

This integral has analytical resolution across the following recursion:

$$F_p(\mu) = \begin{cases} \bullet \text{If p=0:} \\ \ln\left(\frac{d}{\cos(\mu)} + \sqrt{\left(\frac{d}{\cos(\mu)}\right)^2 + z^2}\right) - \ln(|z|) \\ \bullet \text{If p=1:} \\ \sqrt{\left(\frac{d}{\cos(\mu)}\right)^2 + z^2} - |z| \\ \bullet \text{If p>1:} \\ \frac{1}{p} \cdot \left(\frac{d}{\cos(\mu)}\right)^{p-1} \cdot \sqrt{\left(\frac{d}{\cos(\mu)}\right)^2 + z^2} - \frac{p-1}{p} \cdot z^2 \cdot F_{p-2}(\mu) \end{cases}$$

Unfortunately the expression (B) has not analytical resolution but is a C^{∞} function. Then we can calculate it using a Gauss-Legendre rule too.

- *Singular integration technique:*

With this technique we succeed in remove de singularity of the kernel, hence the name of method. The integral that we have to compute then takes the form:

$$I(0) = \frac{d^{p+1}}{p+1} \int_{-\alpha}^{\Phi_2 - \alpha} \frac{\cos^m(\mu+\beta) \cdot \sin^n(\mu+\beta)}{\cos^{p+1}(\mu)} \cdot d\mu$$

This integral has analytical resolution which has the form:

$$I(0) = \frac{d^{p+1}}{p+1} \cdot \sum_{i=0}^{m} \sum_{j=0}^{n} (-1)^i \cdot \binom{m}{i} \cdot \binom{n}{j} \cdot A^{i+j} \cdot B^{m+n-i-j} \cdot F_k$$

Where:

$$F_k = \int_{-\alpha}^{\Phi_2 - \alpha} \frac{\sin^k(\mu)}{\cos^{k+1}(\mu)} \cdot d\mu$$

The above expression has analytical resolution. We have to compute the next recursion:

$$F_k = \begin{cases} \bullet \text{For k=0:} \\ \dfrac{1+\tan(\frac{\mu}{2})}{1-\tan(\frac{\mu}{2})} \\ \bullet \text{For k=1:} \\ \dfrac{1}{\cos(\mu)} \\ \bullet \text{For k>1:} \\ \dfrac{1}{\mathrm{k}} \cdot \dfrac{\sin^{k-1}(\mu)}{\cos^k(\mu)} - \dfrac{k-1}{k} F_{k-2} \end{cases}$$

Now we have formulation to do numerical experiments.

3 EXPERIMENTS WITH MONOMIAL CHARGE DENSITIES

First we have tested the method only with the problem of the kernel's singularity. The interpolated charge density obtained for a monomial $x^1 \cdot y^0$ is showed in the next figure:

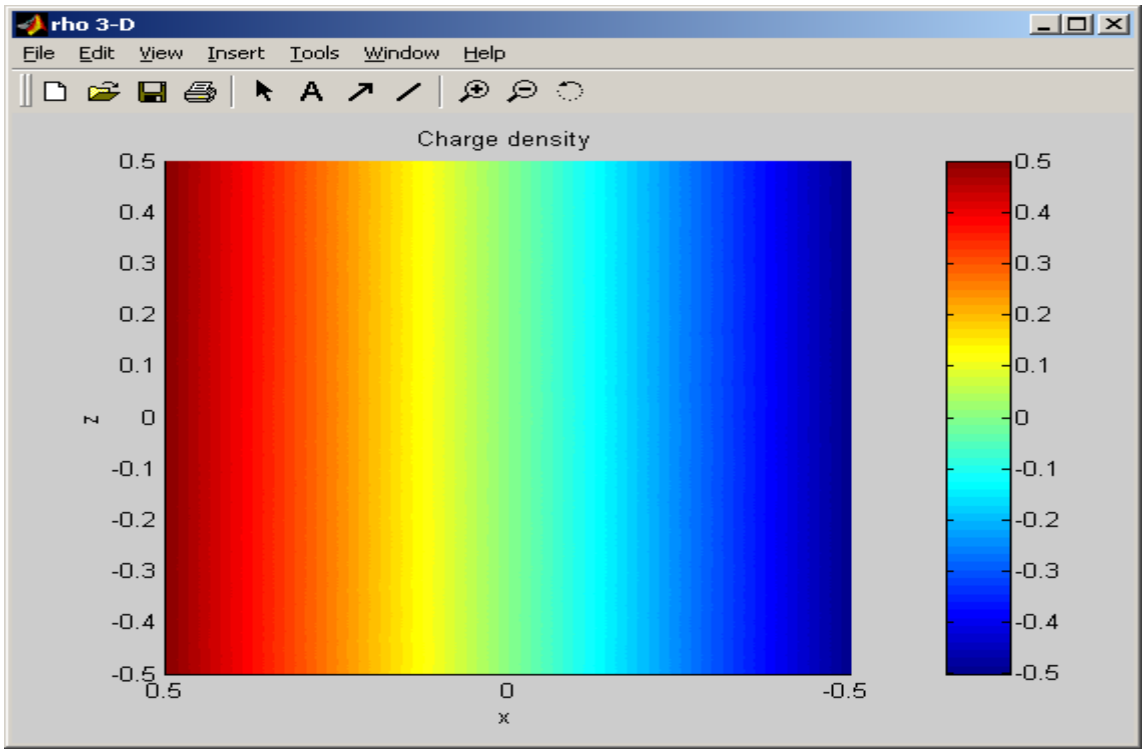

We can see that in this case the method perform well. The charge density is perfectly interpolated. If we make a study on the convergence of the method we obtain the next behavior:

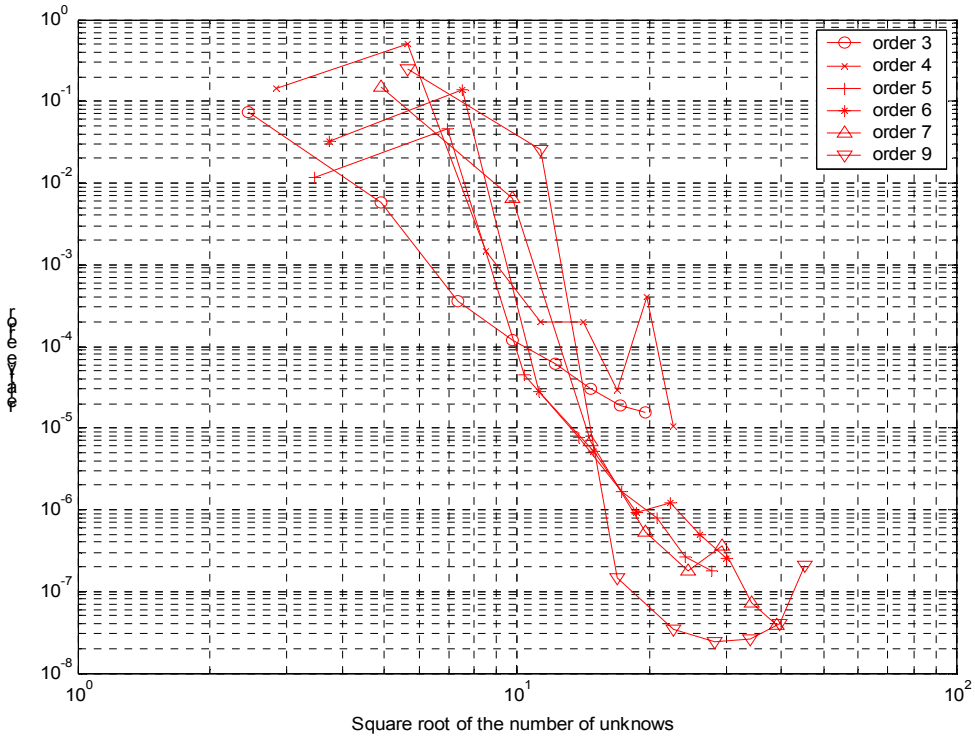

We can see that the method performs well because we can arrive to errors of the save order that the quadrature or cubature rule used.

4 EXPERIMENTS SINGULAR CHARGE DENSITIES

When we have proved to extract singular charge density we obtain results in the way showed in the next figure.

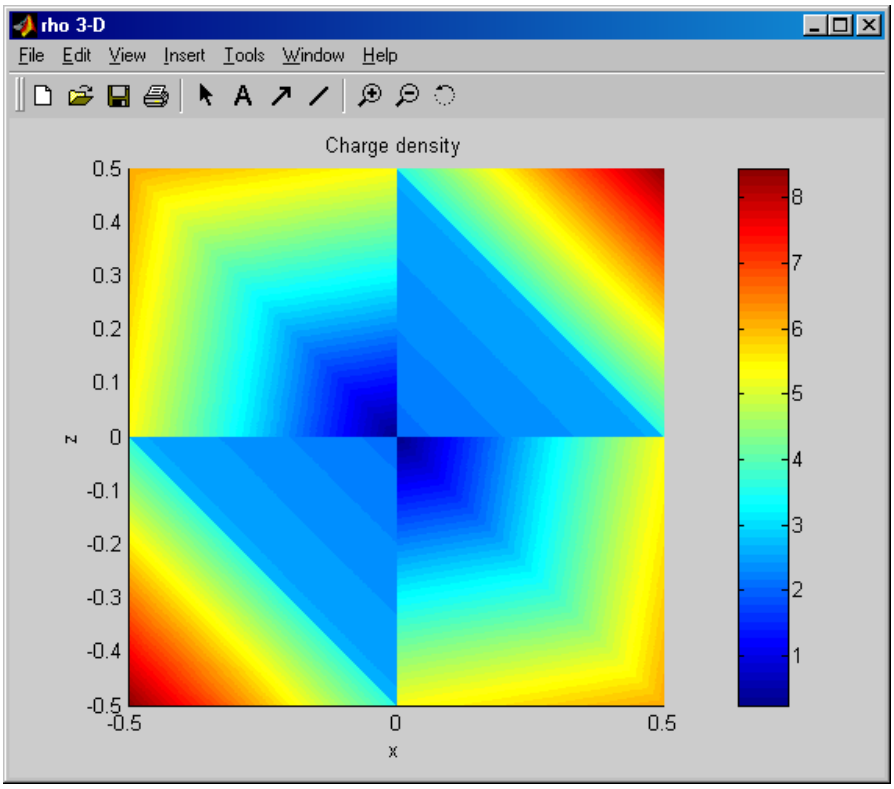

This figure corresponds to an experiment with three points in each triangle. We can see that the triangles which have a corner in the border of the planar structure perform wrong. This is due to the samples of this triangles are not enough close to the border and then the sample's valor extracted is not enough big as it would be. This due to we are using a method based monomial test functions instead of using a method based on singular test functions which does still not exists for our kind of singularity.

We have researched on methods which prove to maintain the properties of Gaussian quadratures using singular test functions with the same behavior of the charge density in edges and corners. This methods proves to remove analytically the kernel's singularity and test function singularity to obtain smooth integrands in order to apply a Gaussian quadrature, but we have still not arrive to a close formulation. This is a very hard problem which has still not solution and we have not found literature about it.

5 CONCLUSIONS

The results for planar objects are very bad, since the charge is singular at edges and corners. On the contrary, when the unknown charge is a monomial, Nyström method performs well. This is due to the method is based on rules that relay in a polynomial or monomial basis and the rapidly varying of the charge density near edges and corners can not be expanded by this kind of basis. Since the rapidly varying current and charge in pre-fractals structures cannot be expanded by a polynomial basis, Nyström method is not adequate to do it. Fortunately the method of moments do not have these problems and can be used to solve pre-fractal structures but without the theoretic advantages of the Nyström's method.

We have proved to solve the problems of the Nyström's method using singular test functions of the same kind that the charge distribution, but this line is still in the formulation phase.

DISCLAIMER

The work associated with this report has been carried out in accordance with the highest technical standards and the FRACTALCOMS partners have endeavoured to achieve the degree of accuracy and reliability appropriate to the work in question. However since the partners have no control over the use to which the information contained within the report is to be put by any other party, any other such party shall be deemed to have satisfied itself as to the suitability and reliability of the information in relation to any particular use, purpose or application.

Under no circumstances will any of the partners, their servants, employees or agents accept any liability whatsoever arising out of any error or inaccuracy contained in this report (or any further consolidation, summary, publication or dissemination of the information contained within this report) and/or the connected work and disclaim all liability for any loss, damage, expenses, claims or infringement of third party rights.

FRACTALCOMS

Exploring the limits of Fractal Electrodynamics for the future telecommunication technologies
IST-2001-33055

Meshing wire pre-fractal antennas

Author(s):	**Eduard Úbeda, Juan M. Rius**
Participant(s):	**UPC**
Workpackage and task:	**WP3, T3.1**
Security:	**Public**
Nature:	**Report**
Version and date:	**1.0, 19-12-2002**

Total number of pages: 15

Abstract:

Given the difficulties found in Task 3.2 with thin-wire modelling, the aim of this work is to find an alternative way to model pre-fractal wire antennas using surface formulation of the Electric Field Integral Equation (EFIE). An extrusion-strip model for pre-fractal wires is proposed. A numerical integration and mesh refinement convergence study has been done. The extrusion strip model shows good convergence with both refinement of mesh size and refinement of EFIE source and testing integration, for both the cases of electrically very small and self-resonant antennas.

Keyword list: Meshing, Electric Field Integral Equation, Method of Moments, wire antennas, pre-fractals

RELATED WP AND TASKS (FROM THE PROJECT DESCRIPTION)

WP3: Software simulation tool

Task 3.1: Advanced meshing of fractal structures

1 INTRODUCTION

Some difficulties arise in the modeling of pre-fractal wire antennas using Pocklington integral equation and the thin-wire approximations [Deliverable D6, Task 3.2 Final Report] and [Report - WP3 T3.2 UPC T0+12 Prefractal wire modeling]. For that reason, the aim of this work is to find an alternative way to model wire antennas using surface formulation of the Electric Field Integral Equation (EFIE) and to study the convergence of the surface meshing in linear triangular basis functions.

2 FORMULATION

The electromagnetic analysis of the pre-fractals is carried out with the EFIE surface formulation. In the MoM-EFIE formulation, the electric boundary condition is applied on the surface *S* of the pre-fractal as

$$\hat{n}\times\vec{E}\left(\vec{J}\right)\Big|_{\vec{r}\in S}=0 \qquad \hat{n}\times\vec{E}^{S}\left(\vec{J}\right)\Big|_{\vec{r}\in S}=-\hat{n}\times\vec{E}^{i}\Big|_{\vec{r}\in S} \tag{1}$$

where $\vec{J}$ and $\vec{E}$ stand for the current and the electric field. $\vec{E}^{i}$ and $\vec{E}^{S}$ denote, respectively, the incident and the scattered field. The current is discretized in terms of $\vec{f}_n\left(\vec{r}\right)$, the RWG basis functions, so that

$$\vec{J}_N\left(\vec{r}\right)=\sum_{n=1}^{N}c_n\vec{f}_n\left(\vec{r}\right) \tag{2}$$

where *N* denotes the number of edges of the geometry between triangles. The *RWG* basis functions are defined over two triangles sharing an edge as

$$\vec{f}_n\left(\vec{r}\right)=\begin{cases}\dfrac{l_n}{A_n^{+}}\left(\vec{r}-\vec{r}_{\mathrm{o},v}^{+}\right), & \vec{r}\in T_n^{+}\\[2ex] -\dfrac{l_n}{A_n^{-}}\left(\vec{r}-\vec{r}_{\mathrm{o},v}^{-}\right), & \vec{r}\in T_n^{-}\end{cases} \tag{3}$$

being l_n the length of the edge and $A_n^{\pm}$, $\vec{r}_{\mathrm{o},v}^{\pm}$ the areas and the opposite vertices at the triangles at both sides $T_n^{\pm}$ (see Fig. 1).

The system in (1) can be expressed in matrix form as

$$[E_m^i]=-[z_{mn}][c_n] \qquad m=1..N,\ n=1..N \tag{4}$$

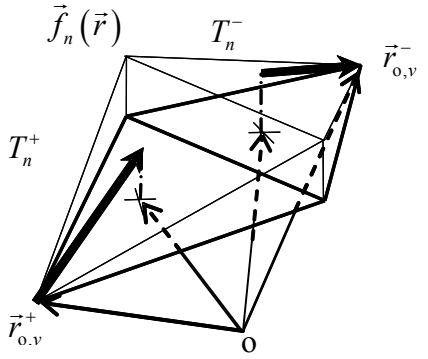

Fig. 1.- RWG basis function.

In view of (3), the vector of current coefficients $[c_n]$ is the normal components of the current across each edge of the geometry. The right-hand side vector $[E_m^i]$ results from the inner-product of the weighting functions *RWG* with the electric field generated by the coaxial feed without the presence of the pre-fractal; that is,

$$[E_m^i] = \left\langle \vec{f}_m, \vec{E}^i \right\rangle = \iint\limits_{T_m^+ \cup T_m^-} \vec{f}_m(\vec{r}) \vec{E}^i(\vec{r}) dS \tag{5}$$

Similarly, the impedance elements of the matrix $[z_{mn}]$ come from the weighting of the expanded scattered electric field by the testing *RWG* set

$$z_{mn} = \left\langle \vec{f}_m, \vec{E}^S\left(\vec{f}_n\right) \right\rangle \qquad m = 1..N,\ n = 1..N \tag{6}$$

In accordance with the surface equivalence theorem, the scattered field is the contribution to the total field due to the electric currents induced over the surface of the pre-fractal. The expression of $\vec{E}^S$ in terms of the vector and scalar potentials lets the previous expression as

$$\begin{aligned} z_{mn} = & -jk\eta \iint\limits_{T_m^+ \cup T_m^-} \vec{f}_m(\vec{r}) dS \iint\limits_{T_n^+ \cup T_n^-} G(\vec{r},\vec{r}') \vec{f}_m(\vec{r}) dS' \\ & + j\frac{\eta}{k} \iint\limits_{T_m^+ \cup T_m^-} \nabla \cdot \vec{f}_m(\vec{r}) dS \iint\limits_{T_n^+ \cup T_n^-} G(\vec{r},\vec{r}') \nabla' \cdot \vec{f}_n(\vec{r}) dS' \end{aligned} \tag{7}$$

where $G(\vec{r},\vec{r}')$ stands for the free-space Green´s function.

3 WIRE MODELING WITH CYLINDRICAL SURFACES

The cylindrical surface of the wire has to be discretized into very small triangles (see Fig. 2).

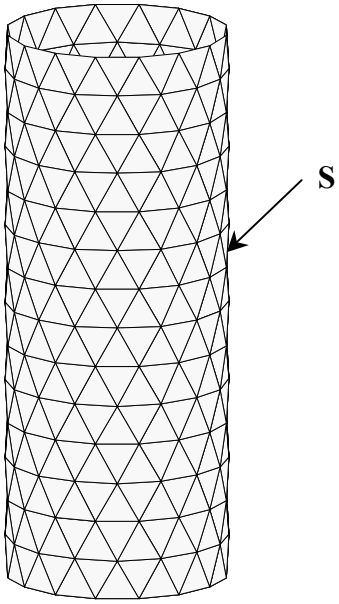

Fig. 2.- Cylindrical surface of a wire meshed with triangles.

In theory, one can achieve any degree of accuracy through the fine meshing of the surface and the choice of sufficient integrating source and field points. In practice, though, the use of very small triangles raises dramatically the number of unknowns and therefore the CPU and memory requirements. Also, as it is well-known, the use of very fine grids in terms of the wavelength with the EFIE operator yields very badly-conditioned systems, with unstable solutions, very sensitive to round-off errors. Furthermore, the automatic CAD aided modeling of such pre-fractal geometries, especially those with a high number of iterations, becomes rather complicated because many surface-surface intersections between cylindrical portions have to be considered (see Fig. 3).

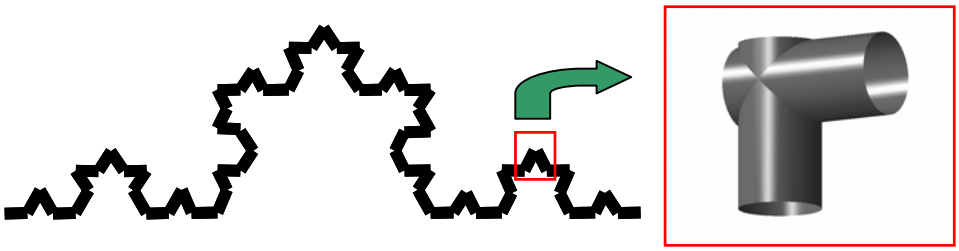

Fig. 3.- Koch pre-fractal with 3 iterations.

The effect of the accuracy of the EFIE integral operator for a dipole of λ/2 with a radius for the cylindrical surface of λ/500 has been checked by increasing the number of source-integrating points and the number of triangles. As shown in Fig. 4, the increase on the number of triangles is much more effective in refining the accuracy of the results. This makes sense because it reverts in a more accurate expansion of the current –which is modeled in terms of linear segments– and in a more precise modeling of the curvature of the wire. The increase on the number of source-integrating points is less critical. Indeed, for segments lower than λ/320, the performance with three or more source-integrating points is very similar (see Fig. 5).

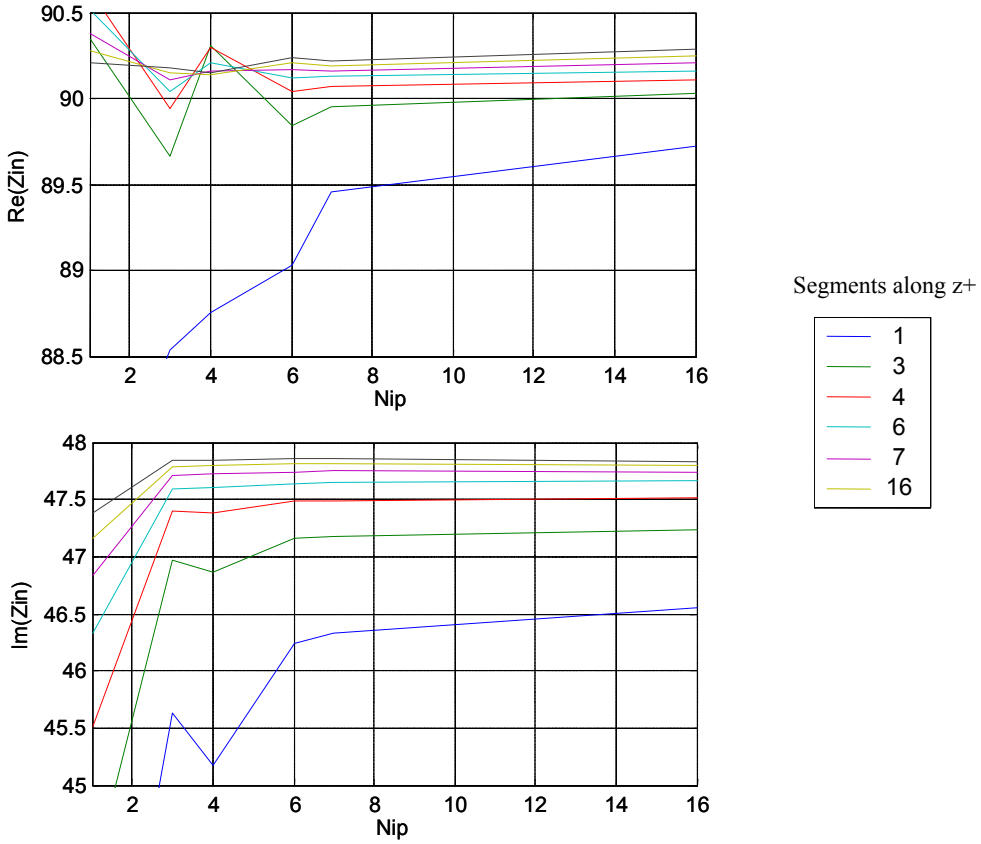

Fig. 4.- Input impedance for a dipole of λ/2 and radius 0.002 λ

The accuracy for a Yagi antenna with the active and parasite dipoles of length λ/2 and radius λ/500 separated 0.05λ has also been tested (Fig. 6). In Fig. 7, the input impedance for increasingly fine discretizations is presented with 7 source-integrating points. It can be seen how the triangular meshing does not converge to a definite value. In consequence, it cannot be inferred a rule-of-thumb criterion to use the results from the thin-wire, which was the original purpose.

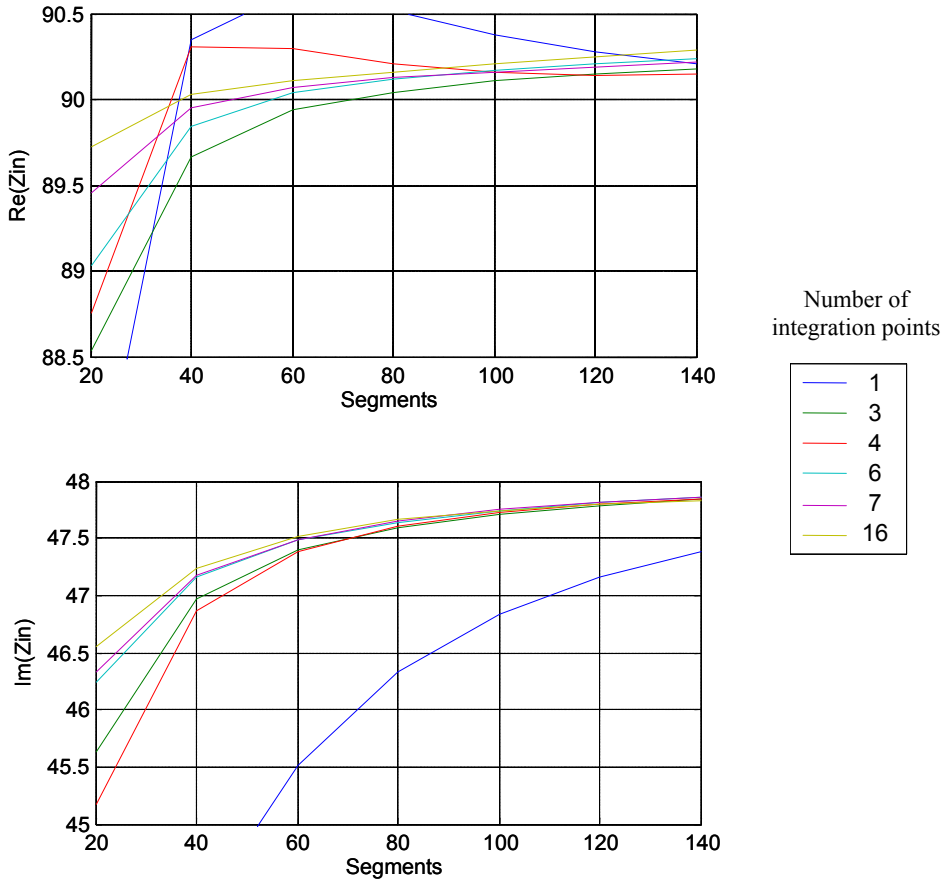

Fig. 5.- Input impedance for a dipole of λ/2 and radius 0.002 λ

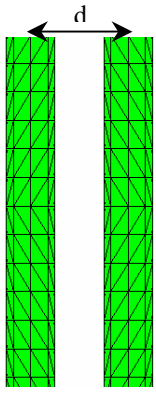

Fig. 6.- Active and parasite dipoles of λ/2 and radius 0.002 λ and d=0.05λ

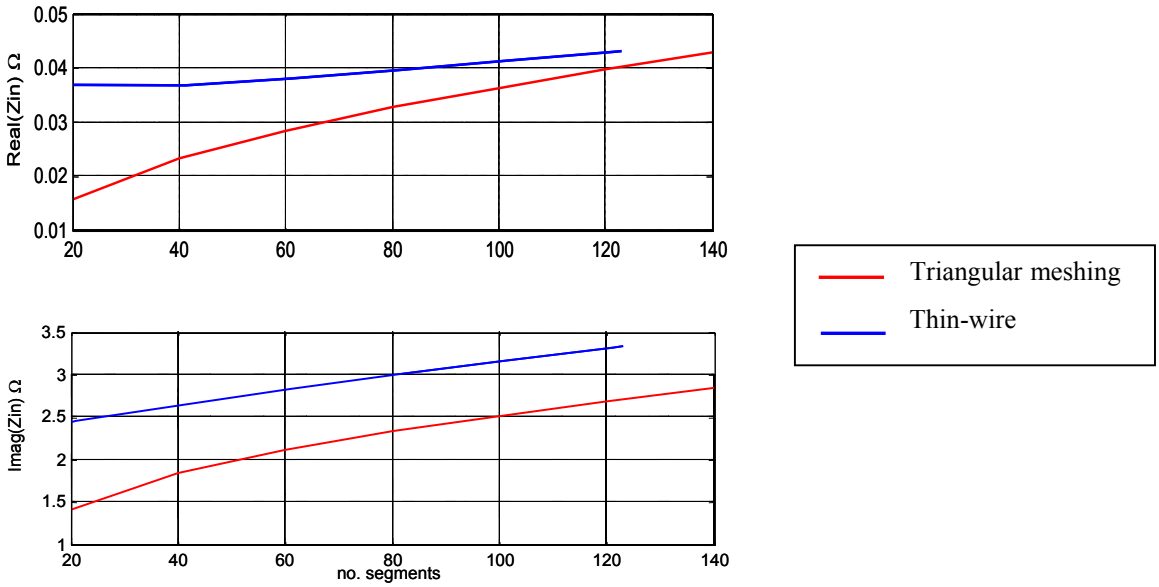

Fig. 7.- Input impedances of two dipoles of λ/2 –one active and one parasite– and radius 0.002 λ and d=0.05λ

4 WIRE MODELING WITH STRIPS

Another option is to model the wire as a narrow strip. The wire modeling with strips can be carried out in two manners: planar strip and extrusion strip.

- **Planar strips:** The practical interest of the printed technology makes the modeling with planar strips interesting. However, the automatic modeling of these pre-fractals is not trivial since the corners between the strip-strip intersections have to be considered (see Fig. 8a). Furthermore, these microstrip planar antennas cannot work as omnidirectional monopoles.
- **Extrusion strip:** This approach stands for a wire extrusion in the direction perpendicular to the plane of the wire (see Fig. 8b). Although such modeling of antennas has little practical interest, in this case the automatic meshing becomes trivial. Furthermore, this tool is useful to simulate electromagnetic effects such as the "corner coupling" or the "shortcut effect" in non-physical pre-fractals with segments wider than long. [Report - WP3 T3.2 UPC T0+12 Pre-fractal wire modeling] shows that the extrusion strip is the best option to model pre-fractal wire antennas. Most simulations in FRACTALCOMS have been made with these extrusion-strip antennas.

In Fig. 9, the resonant frequencies and the radiation resistances obtained with both models, wire-strip and planar strip, for Koch pre-fractals of 1, 2, 3, 4 and 5 iterations with height 6 cm are shown. In view of these results, the resonant frequencies and the radiation resistances are the same, respectively, for 1, 2 and 3 iterations and for 2 and 3 iterations for both models. The pre-fractal with 4 iterations leads to a segment dimension of 0.75mm. Since the strip width is taken to be 2 mm, the pre-fractal becomes very distorted, whereby, in practice, it cannot be built.

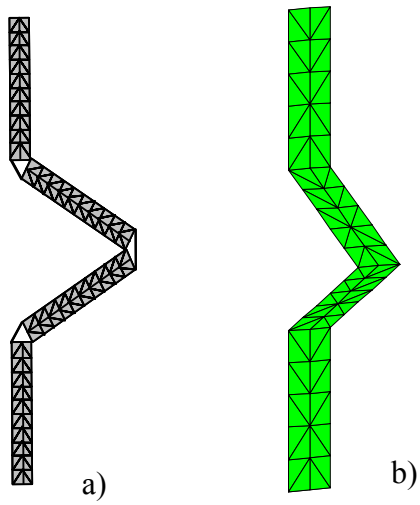

Fig. 8.- Koch pre-fractal monopole of 1 iteration modeled as planar strip (a) and an extrusion strip (b).

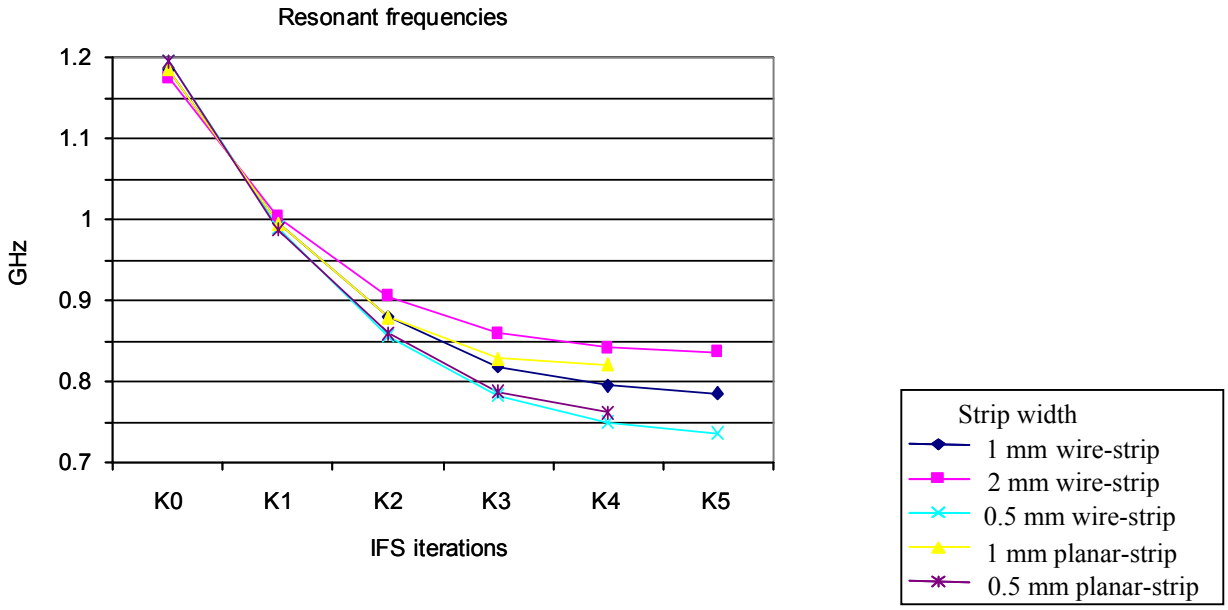

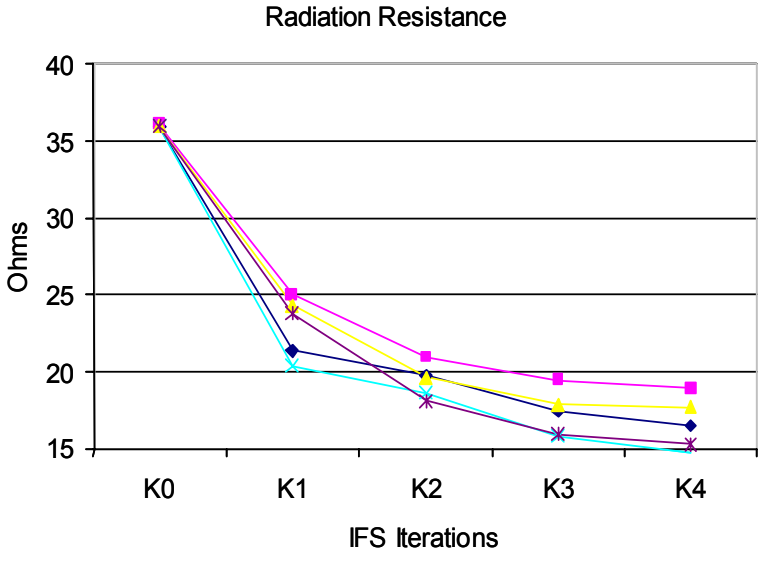

Fig. 9.- Resonant frequencies and radiation resistance of the Koch pre-fractals with 1,2,3,4 and 5 iterations with the extrusion-strip and planar-strip models.

5 CONVERGENCE OF NUMERICAL INTEGRATION AND MESH REFINEMENT

A systematic convergence analysis of numerical integration and mesh refinement has been performed for extrusion-strip pre-fractal antennas models. Then the antennas are electrically small, this problem needs to be solved at low frequencies and with very fine meshing grids. This makes the linear systems very badly-conditioned and therefore the iterative solvers cannot be used. The solution of such system must then be obtained by directly inverting the matrix. Thanks to our algorithm of inversion [2], which resorts to the block-decomposition of the matrix and to the temporary storage in disk, the memory requirements are kept adjusted to the available resources regardless of the dimensions of the matrix.

Since the distances between source and field triangles are very small, the electric field varies steeply between neighboring triangles and therefore accurate integration may be required in the EFIE formulation. For the self-interactions, the source-integration has been made analytically and a field-integration with 4 points has been used. For interactions between different triangles, three different strategies have been followed. The Operator 1 carries out a numerical source-integration with 4 points and numerical field-integration with 1 point. The Operator 2 carries out the source-integration analytically for the highest order term 1/R and it uses again 4 points for the source-integration of the remaining smooth part. The field-integration is made with one point. The operator 3 excels as the most accurate one because it develops the source-integration as in Operator 2 and for the field-integration four points are taken. Logically, the operators 2 and 3 require more CPU time than the Operator 1. Indeed, they turn out 3 and 20 times, respectively, slower than the Operator 1.

The aim of the study is to find the best trade-off between accuracy and number of unknowns by testing the Operators 1, 2 and 3 for different pre-fractals derived from the Koch-monopole. The Koch-monopoles of 1 iteration (K1) and of 4 iterations (K4), with long and short segments, respectively, are analyzed. The different types of meshing employed for each case are presented in Fig. 10 (K1) and in Fig. 11 (K4), respectively. For both cases, the width of the strip is 0.37 mm and the height of the strip is a=6 cm.

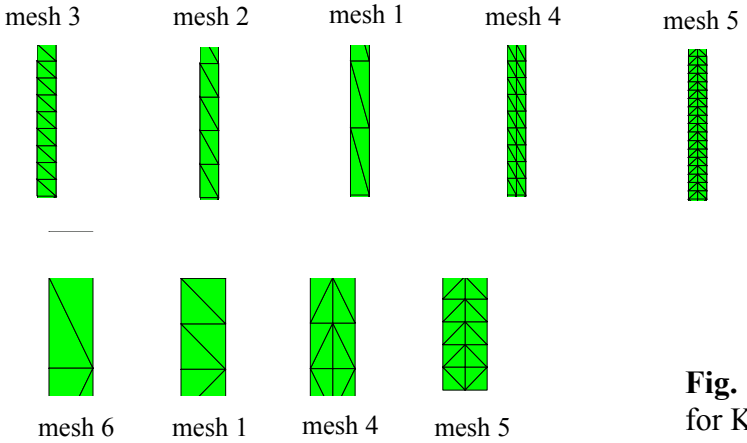

Fig. 10.- Types of meshing for K1 pre-fractal.

Fig. 11.- Types of meshing for K4 pre-fractal.

The input impedance and the quality factor at *ka=0.3* and at the frequency of resonance is shown for both cases in Fig. 12 and in Fig. 15. The errors of the results with respect to the most accurate Operator (Operator 3) and the finest mesh (mesh 5) are shown, respectively, in Fig. 13 and Fig. 14 for K1 and in Fig. 16 and Fig. 17 for K4.

Mesh refinement:

For K1 and K4, as it is shown in Fig. 13 and in Fig. 16, the finer the meshing and the less distorted the aspect ratio of meshing triangles, the more accurate the results become.

Numerical integration refinement:

In view of Fig. 14, for K1 and with fine meshes, such as mesh 1, mesh 4 and mesh 5, Operator 2 is slightly better than Operator 1, whereas for the coarse meshing (mesh 2) there is no gain in using Operator 2. For K4 (see Fig. 17), with fine meshings such as mesh 4 and mesh 5, the performances of Operator 2 and Operator 1 are comparable, meanwhile for the medium density mesh 2 Operator 2 behaves better. With the coarse meshing mesh 6, Operator 2 behaves even worse than Operator 1. In view of the results for both pre-fractals, K1 and K4, it is clear that the accurate field-integration (Operator 3) improves more the accuracy than the analytical source integration (Operator 2).

		mesh 3	mesh 2	mesh 1	mesh 4	mesh 5
	Mesh size (mm)	1.526	0.827	0.523	0.413	0.262
	λ / mesh size at ka=0.3	823.8	1519.5	2402.7	3042.7	4803.7
	Unknowns	239	479	959	2398	4798
R_{in} (Ω) for ka=0.3	Operator 1	0.932	0.900	0.894	0.893	0.892
	Operator 2	0.929	0.900	0.895	0.893	0.892
	Operator 3	0.930	0.901	0.895	0.894	0.892
X_{in} (Ω) for ka=0.3	Operator 1	-879.8	-866.0	-872.9	-865.8	-869.1
	Operator 2	-850.4	-865.5	-876.4	-866.1	-875.9
	Operator 3	-869.5	-879.4	-882.2	-875.8	-875.7
Q for ka=0.3	Operator 1	992.6	1012.1	1026.3	1019.9	1025.2
	Operator 2	962.5	1011.5	1030.1	1020.2	1026.9
	Operator 3	982.5	1026.4	1036.4	1030.5	1032.5
Resonant freq. (GHz)	Operator 1	0.988	0.988	0.988	0.986	0.985
	Operator 2	0.989	0.988	0.987	0.985	0.984
	Operator 3	0.988	0.987	0.987	0.984	0.984
R_r (Ω) at resonance	Operator 1	23.71	23.79	23.76	23.68	23.64
	Operator 2	23.84	23.79	23.74	23.67	23.63
	Operator 3	23.76	23.72	23.71	23.61	23.58
Q at resonance	Operator 1	11.80	11.58	11.69	11.66	11.74
	Operator 2	11.34	11.57	11.74	11.68	11.77
	Operator 3	11.64	11.79	11.84	11.84	11.87

Fig. 12.- Input impedance and quality factor at *ka=0.3* and at the frequency of resonance for K1.

		mesh 3	mesh 2	mesh 1	mesh 4	mesh 5
	Mesh size (mm)	1.526	0.827	0.523	0.413	0.262
	λ / mesh size at ka=0.3	823.8	1519.5	2402.7	3042.7	4803.7
	Unknowns	239	479	959	2398	4798
R_{in} (Ω) for ka=0.3	Operator 1	4.52%	0.90%	0.30%	0.13%	0.00%
	Operator 2	4.15%	0.88%	0.31%	0.13%	0.00%
	Operator 3	4.27%	0.97%	0.32%	0.18%	0.00%
X_{in} (Ω) for ka=0.3	Operator 1	1.23%	0.35%	0.44%	0.38%	0.00%
	Operator 2	2.90%	1.18%	0.06%	1.11%	0.00%
	Operator 3	0.71%	0.42%	0.74%	0.01%	0.00%
Q for ka=0.3	Operator 1	3.18%	1.28%	0.11%	0.52%	0.00%
	Operator 2	6.27%	1.51%	0.31%	0.66%	0.00%
	Operator 3	4.84%	0.59%	0.38%	0.19%	0.00%
Resonant freq. (GHz)	Operator 1	0.32%	0.37%	0.31%	0.09%	0.00%
	Operator 2	0.50%	0.39%	0.31%	0.09%	0.00%
	Operator 3	0.47%	0.39%	0.36%	0.08%	0.00%
R_r (Ω) at resonance	Operator 1	0.30%	0.61%	0.50%	0.18%	0.00%
	Operator 2	0.88%	0.66%	0.48%	0.18%	0.00%
	Operator 3	0.77%	0.62%	0.57%	0.15%	0.00%
Q at resonance	Operator 1	0.50%	1.36%	0.44%	0.65%	0.00%
	Operator 2	3.61%	1.67%	0.22%	0.78%	0.00%
	Operator 3	1.93%	0.66%	0.29%	0.25%	0.00%

Fig. 13.- Error with respect to mesh 5 for K1.

		mesh 3	mesh 2	mesh 1	mesh 4	mesh 5
	Mesh size (mm)	1.5255	0.827	0.523	0.413	0.2616
	λ / mesh size at ka=0.3	823.8	1519.5	2402.7	3042.7	4803.7
	Unknowns	239	479	959	2398	4798
R_{in} (Ω) for ka=0.3	Operator 1	0.16%	0.15%	0.09%	0.13%	0.08%
	Operator 2	0.18%	0.15%	0.06%	0.12%	0.06%
	Operator 3	0.00%	0.00%	0.00%	0.00%	0.00%
X_{in} (Ω) for ka=0.3	Operator 1	1.18%	1.52%	1.06%	1.14%	0.76%
	Operator 2	2.19%	1.59%	0.66%	1.11%	0.01%
	Operator 3	0.00%	0.00%	0.00%	0.00%	0.00%
Q for ka=0.3	Operator 1	1.03%	1.39%	0.97%	1.03%	0.71%
	Operator 2	2.03%	1.45%	0.61%	1.00%	0.54%
	Operator 3	0.00%	0.00%	0.00%	0.00%	0.00%
Resonant freq. (GHz)	Operator 1	0.03%	0.09%	0.06%	0.12%	0.11%
	Operator 2	0.12%	0.09%	0.04%	0.09%	0.09%
	Operator 3	0.00%	0.00%	0.00%	0.00%	0.00%
R_r (Ω) at resonance	Operator 1	0.21%	0.26%	0.20%	0.30%	0.27%
	Operator 2	0.32%	0.26%	0.12%	0.25%	0.22%
	Operator 3	0.00%	0.00%	0.00%	0.00%	0.00%
Q at resonance	Operator 1	1.31%	1.84%	1.29%	1.54%	1.14%
	Operator 2	2.59%	1.89%	0.82%	1.42%	0.89%
	Operator 3	0.00%	0.00%	0.00%	0.00%	0.00%

Fig. 14.- Error with respect to Operator 3 for K1.

		mesh 6	mesh 1	mesh 4	mesh 5
	Mesh size (mm)	0.827	0.523	0.413	0.262
	λ / mesh size at ka=0.3	1519.5	2402.7	3042.7	4803.7
	Unknowns	1023	2044	5118	10238
R_{in} (Ω) for ka=0.3	Operator 1	0.881	0.878	0.878	0.877
	Operator 2	0.885	0.879	0.878	0.877
	Operator 3	0.881	0.879	0.879	0.878
X_{in} (Ω) for ka=0.3	Operator 1	-612.9	-614.3	-610.2	-610.4
	Operator 2	-610.6	-614.8	-609.6	-610.8
	Operator 3	-615.1	-615.6	-612.4	-612.0
Q for ka=0.3	Operator 1	762.6	765.8	761.7	762.5
	Operator 2	760.0	766.6	761.0	763.0
	Operator 3	765.0	767.8	764.2	764.6
Resonant freq. (GHz)	Operator 1	0.727	0.732	0.729	0.730
	Operator 2	0.728	0.729	0.729	0.728
	Operator 3	0.727	0.726	0.726	0.725
R_r (Ω) at resonance	Operator 1	13.64	13.83	13.73	13.75
	Operator 2	13.68	13.73	13.73	13.70
	Operator 3	13.65	13.62	13.61	13.57
Q at resonance	Operator 1	21.30	20.88	21.00	20.96
	Operator 2	21.12	21.14	20.99	21.10
	Operator 3	21.34	21.43	21.36	21.44

Fig. 15.- Input impedance and quality factor at *ka=0.3* and at the frequency of resonance for K4.

		mesh 6	mesh 1	mesh 4	mesh 5
	Mesh size (mm)	0.827	0.523	0.413	0.2616
	λ / mesh size at ka=0.3	1519.513	2402.748	3042.705	4803.658
	Unknowns	1023	2044	5118	10238
R_{in} (Ω) for ka=0.3	Operator 1	0.46%	0.12%	0.08%	0.00%
	Operator 2	0.84%	0.15%	0.04%	0.00%
	Operator 3	0.37%	0.13%	0.07%	0.00%
X_{in} (Ω) for ka=0.3	Operator 1	0.40%	0.63%	0.03%	0.00%
	Operator 2	0.03%	0.66%	0.20%	0.00%
	Operator 3	0.50%	0.58%	0.05%	0.00%
Q for ka=0.3	Operator 1	0.01%	0.43%	0.10%	0.00%
	Operator 2	0.39%	0.48%	0.26%	0.00%
	Operator 3	0.05%	0.42%	0.05%	0.00%
Resonant freq. (GHz)	Operator 1	0.34%	0.39%	0.06%	0.00%
	Operator 2	0.02%	0.18%	0.11%	0.00%
	Operator 3	0.40%	0.24%	0.15%	0.00%
R_r (Ω) at resonance	Operator 1	0.84%	0.58%	0.14%	0.00%
	Operator 2	0.13%	0.20%	0.20%	0.00%
	Operator 3	0.54%	0.33%	0.26%	0.00%
Q at resonance	Operator 1	1.61%	0.41%	0.19%	0.00%
	Operator 2	0.12%	0.22%	0.48%	0.00%
	Operator 3	0.49%	0.06%	0.39%	0.00%

Fig. 16.- Error with respect to Operator 3 for K4.

		mesh 6	mesh 1	mesh 4	mesh 5
	Mesh size (mm)	0.827	0.523	0.413	0.2616
	λ / mesh size at ka=0.3	1519.513	2402.748	3042.705	4803.658
	Unknowns	1023	2044	5118	10238
R_{in} (Ω) for ka=0.3	Operator 1	0.03%	0.13%	0.11%	0.12%
	Operator 2	0.38%	0.07%	0.12%	0.09%
	Operator 3	0.00%	0.00%	0.00%	0.00%
X_{in} (Ω) for ka=0.3	Operator 1	0.36%	0.22%	0.35%	0.26%
	Operator 2	0.73%	0.13%	0.46%	0.21%
	Operator 3	0.00%	0.00%	0.00%	0.00%
Q for ka=0.3	Operator 1	0.32%	0.26%	0.33%	0.28%
	Operator 2	0.65%	0.15%	0.43%	0.21%
	Operator 3	0.00%	0.00%	0.00%	0.00%
Resonant freq. (GHz)	Operator 1	0.06%	0.84%	0.47%	0.69%
	Operator 2	0.10%	0.43%	0.44%	0.49%
	Operator 3	0.00%	0.00%	0.00%	0.00%
R_r (Ω) at resonance	Operator 1	0.07%	1.58%	0.91%	1.32%
	Operator 2	0.27%	0.81%	0.88%	0.94%
	Operator 3	0.00%	0.00%	0.00%	0.00%
Q at resonance	Operator 1	0.19%	2.60%	1.69%	2.25%
	Operator 2	1.02%	1.35%	1.72%	1.63%
	Operator 3	0.00%	0.00%	0.00%	0.00%

Fig. 17.- Error with respect to mesh 5 for K4.

6 CONCLUSIONS

Modeling highly-iterated pre-fractal wire antennas is a challenging problem. On the one hand, it has been shown in [Report - WP3 T3.2 UPC T0+12 Prefractal wire modeling] that several difficulties arise with Pocklington integral equation and thin-wire models, even with the extended kernel. On the other, modeling the wire cylindrical surface with a triangle mesh is not practical do to cylinder intersections at corners, the huge computational cost required and, in difficult problems, there is no convergence with mesh refinement.

For that reason, we propose here to model pre-fractal wires using a narrow strip. Two strip models are considered: the planar and the extrusion strip. Both lead to similar results for low-iteration pre-fractals, but the extrusion strip, unlike the planar one, can model highly iterated pre-fractals in which the strip width is comparable to the pre-fractal segment length.

For both kinds of strips, the discretization in triangles of size much smaller than the wavelength makes the linear system very badly-conditioned. For that reason, iterative solvers fail, even with huge pre-conditioners. A direct solver can be used with more than 10,000 unknowns thanks to the block-solution algorithm developed at UPC.

A numerical integration and mesh refinement convergence study has been done. The extrusion strip model shows good convergence with both refinement of mesh size and refinement of EFIE source and testing integration, for both the cases of electrically very small and self-resonant antennas.

REFERENCES

[1] Sadasiva M. Rao, Donald R. Wilton and Allen W. Glisson, "Electromagnetic Scattering by Surfaces of Arbitrary Shape", *IEEE Transactions on Antennas and Propagation*, vol. ap-30, no. 3, pp. 409-418, May 1982

[2] A. Heldring, Juan M. Rius and Leo Ligthart, "New block-ILU preconditioner scheme for numerical analysis of very large electromagnetic problems", *IEEE Tranactions on Magnetics,* vol. 38 no.2, march 2002

DISCLAIMER

The work associated with this report has been carried out in accordance with the highest technical standards and the FRACTALCOMS partners have endeavoured to achieve the degree of accuracy and reliability appropriate to the work in question. However since the partners have no control over the use to which the information contained within the report is to be put by any other party, any other such party shall be deemed to have satisfied itself as to the suitability and reliability of the information in relation to any particular use, purpose or application.

Under no circumstances will any of the partners, their servants, employees or agents accept any liability whatsoever arising out of any error or inaccuracy contained in this report (or any further consolidation, summary, publication or dissemination of the information contained within this report) and/or the connected work and disclaim all liability for any loss, damage, expenses, claims or infringement of third party rights.

FRACTALCOMS

Exploring the limits of Fractal Electrodynamics for the future telecommunication technologies
IST-2001-33055

FractalComs problem-type for GiD

Author(s):	**Jorge Suit Pérez Ronda, Miguel A. Pasenau de Riera, Gabriel Bugeda Castelltort**
Participant(s):	**CIMNE**
Work package and task:	**WP3 T3.1**
Security:	**Public**
Nature:	**Report**
Version and date:	**3.5, 06.11.2002**

Total number of pages: 21

Abstract:

Creation of the GiD problem type 'FractalComs' which adds an 'Antenna' menu to GiD. From this menu three types of fractal antennas can be automatically created: 'general, Koch's, Hilbert's and Peano's line antennas', 'Sperpinski triangle antennas' and based on Networked MRCMs Fractals (Multiple Reduction Copy Machines).

Keyword list: Line and triangle fractal antennas, GiD, Kock, Hilbert, Peano, networked MRCMs

FractalComs problem-type for GiD

WP3: SOFTWARE SIMULATION TOOL

TASK 3.1: ADVANCED MESHING OF FRACTAL STRUCTURES

1 INTRODUCTION

The main objective of Task 3.1 is the development of advanced meshing facilities for fractal domains. These facilities should allow meshing a wide range of fractal geometries in the most automatic and adaptive way with while keeping the user interaction to a minimum.

Fractal geometries posses a high degree of complexity due to the very high number of segments that naturally appear when standard geometrical recursive generation algorithms are used. Due to this fact, the generation of these type of geometries by hand needs a lot of user intervention and can consume a tremendous amount of user and computer time.

The starting point of this task has been the commercial pre and post-processing software package named GiD that has been developed at CIMNE. This software has been developed for giving support to all the necessary operations for the preparation of data for numerical analysis involving any type of geometrical discretization of the analysis domain, like in the case of the numerical algorithms used in the FRACTALCOMS project. In particular, it accepts geometrical definitions coming from any CAD system by using standard CAD files (IGES, VDA, DXF, etc.). Nevertheless, standard CAD systems are not prepared for the generation of fractal geometries.

The original development of GiD didn't take into account the possibility of generating fractal geometries in an automatic way and the generation of meshes specially adapted for these types of geometries. Due to that, the main activity in Task 3.1 has consisted in providing GiD with new software facilities for the automatic generation and meshing of fractal geometries. In addition, special adaptive mesh facilities have been added to the software in order to allow enhancing the quality of the numerical results in certain areas of the analysis domain.

At the starting point of the project, the main interest of the different analysis tools for fractal geometries was focused in wire antennas. Due to that, and following the initial work plan, at the end of the first year period, a tool for the automatic generation and meshing of wire antennas based on general fractal geometries was already available. In particular, Koch-, Hilbert- and Peano- line geometries were contemplated within GiD in an automatic way. For this type of geometries minor improvements have been developed during the second year of the project but, basically, these tools were considered as finished.

In addition, during the first year of the project an increasing interest in the use of planar fractal geometries like the Serpinski-triangle was detected. Some advances in the generation and meshing of these types of geometries were already developed and

reported in the six months report. Anyway, even taking into account that in the initial work plan Task 3.1 was supposed to be finished after the first year period, the project consortium agreed in developing new software facilities for the treatment of the planar fractal geometries during the second year. Due to that, Task 3.1 has been extended over the second year of the project in order to allow for these new developments that were not contemplated at the beginning of the project.
During the evolution of the project, many more different fractal antenna types were used, so that a new type of fractal definition was needed inside this tool: the networked Multiple Reduction Copy Machines, MRCMs, fractals.

2 TECHNICAL ASPECTS RELATED WITH THE GENERATION OF WIRE FRACTAL ANTENNAS

The main technical aspect of the new tools added to GiD for the generation and meshing of fractal geometries is the recursive definition of the fractal geometry. Following the indications from UPC, this definition is based in the use of a geometrical Initiator and a geometrical Generator. The generation of the fractal geometry is based on a recursive process in which each segment of the Initiator is substituted by the Generator. Both the Initiator and the Generator can be selected from an existing list or manually defined by the user. The geometrical generation process can be stopped here if the numerical model used for the analysis is based on a thin wire approximation.

If the thin wire approximation is not used, the recursive definition of the fractal geometry produces a wire antenna that needs to be widened in order to get a strip. This process is produced by widening each linear segment of the obtained geometry. Special care has to be taken in order to avoid overlapping between strips from consecutive segments at the corner points. This process is executed automatically after defining the width of the strip antenna. Examples of this process are provided in next sections of this report.

With a relatively low number of recursion levels the generation of the geometry of a trip antenna produces an extremely large number of geometrical nodes and patches. This process can consume a considerable amount of computational time unless special data management tools are used. The initial trials with these types of geometries demonstrated that the existing data base of GiD was not well suited for this type of geometrical definitions. This drove to some improvements in the data base structure that allowed the reduction of the computational time from minutes to seconds. This improvement has been done in the kernel of the GiD software.

In addition, depending on the geometry, overlapping between strips coming from non consecutive segments are also possible. At this moment this type of overlapping is not eliminated because it corresponds with the situation in which an antenna is fabricated using different layers that are not in electrical contact avoiding the circulation of electrical currents between the overlapped parts. Nevertheless, during the second year of the project it was planned to add the facility of eliminating this overlapping for considering a different typology of antennas.

The next step is the generation of the mesh for the numerical analysis of the fractal antenna. This process is performed in a completely automatic way after defining the size and the type (triangular or quadrilateral) of the elements. In addition, it is also possible to generate adapted meshes with a non uniform distribution of sizes after some manual definition of the desired size at each part of the domain.

Once the mesh is completely generated the data file for the numerical analysis code is automatically generated.

3 GRAPHIC USER INTERFACE (GUI)

GiD provides the Graphic User Interface that provides control over all the facilities mentioned for the generation and meshing of fractal geometries. GiD has been added with the corresponding menus asking for the necessary information and controlling all the process. This new menus are invoked through a new Problem Type in GiD, called 'Antennas':

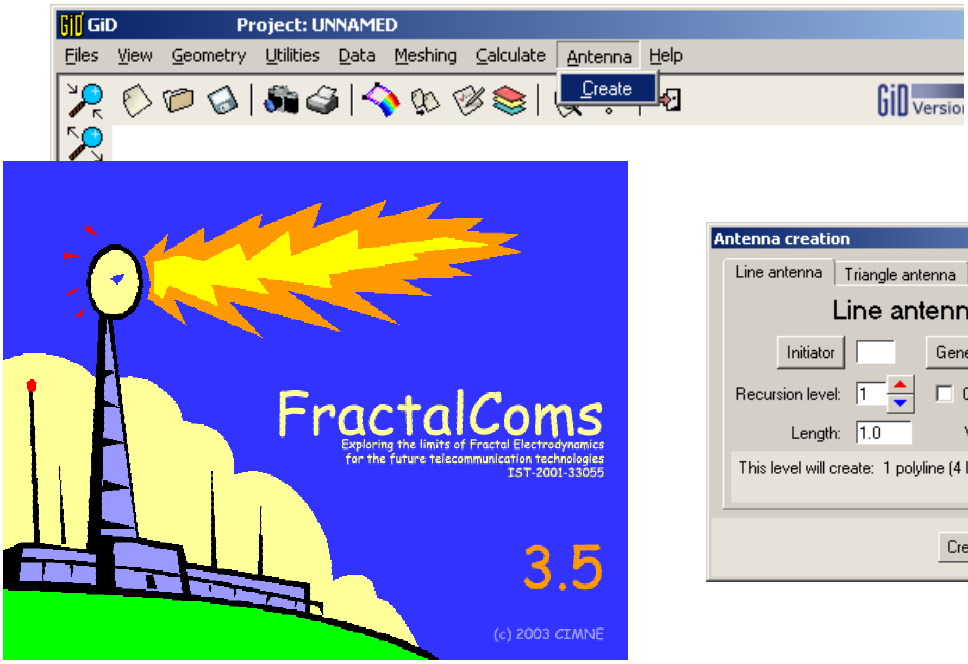

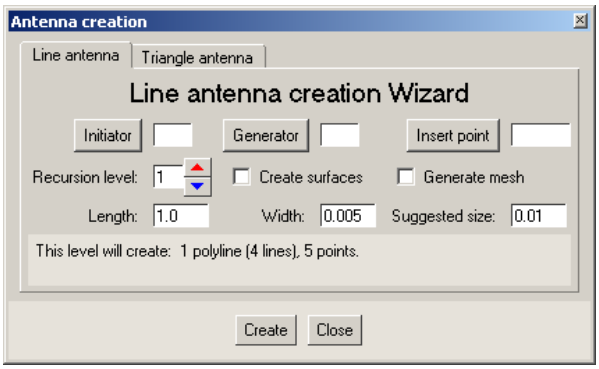

The procedure for generating a fractal wire antenna is as follows:

- First, the **Initiator** and **Generator** geometries have to be defined from a predefined list or from geometries defined by the user.
- After defining the **recursion level** the wire geometry can be generated.
- The strip fractal geometry can be generated after defining the desired **width**.
- The mesh can be generated after selecting the element **size**.

- Adapted meshes can be generated manually once the geometry has been automatically generated.

In line antennas the length of the antenna is the length of the **Initiator.** The path width can be adjusted. The potential problems that can be related to the path/strip width are solved automatically, when possible.

The strip of the 'Line antennas' is created just extruding a line along the **Initiator** curve of the fractal. If this line width is too big then the strip can hide some elevations of the lines, and create intersected surfaces.

4 LINE ANTENNAS: KOCH FRACTAL EXAMPLE

Selecting the following options:

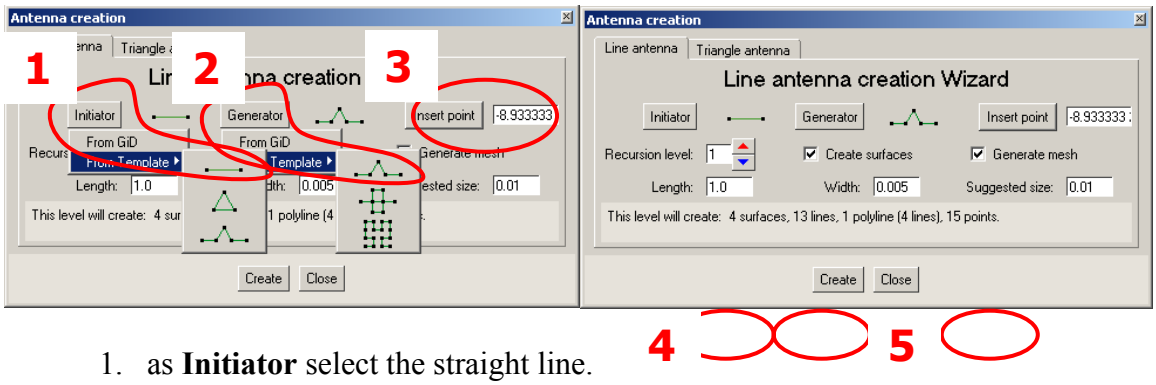

1. as **Initiator** select the straight line.
2. as **Generator** the Koch curve,
3. as **insert point** click the desired staring point of the antenna,
4. select the desired **recursion level**,
5. check the **create surface** and the **create mesh** options if wanted.

By increasing the recursion level the following set of geometries are obtained:

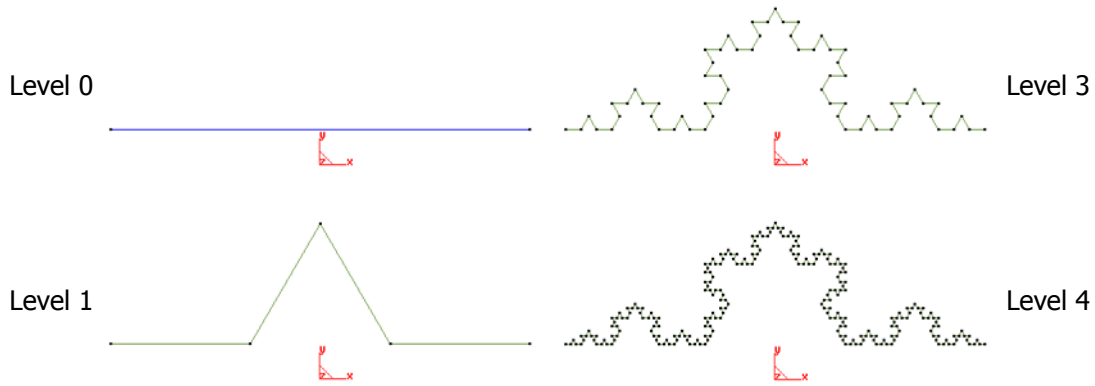

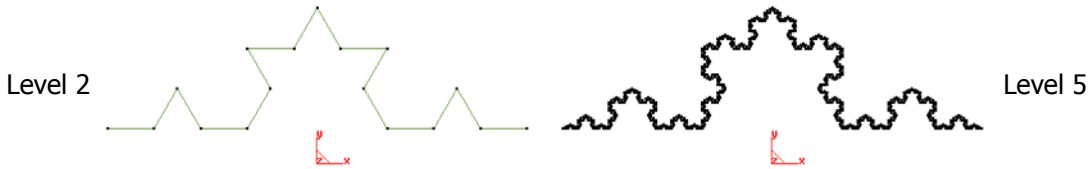

First the guideline (polyline) of the antenna is created. To create the strip, a small line is created at one end of the 'path' and extruded through the path.

The maximum level of recursion is fixed at 10, which creates round a million surfaces, three million lines and another three million points.

The corresponding strip antennas for each level of recursion are the following:

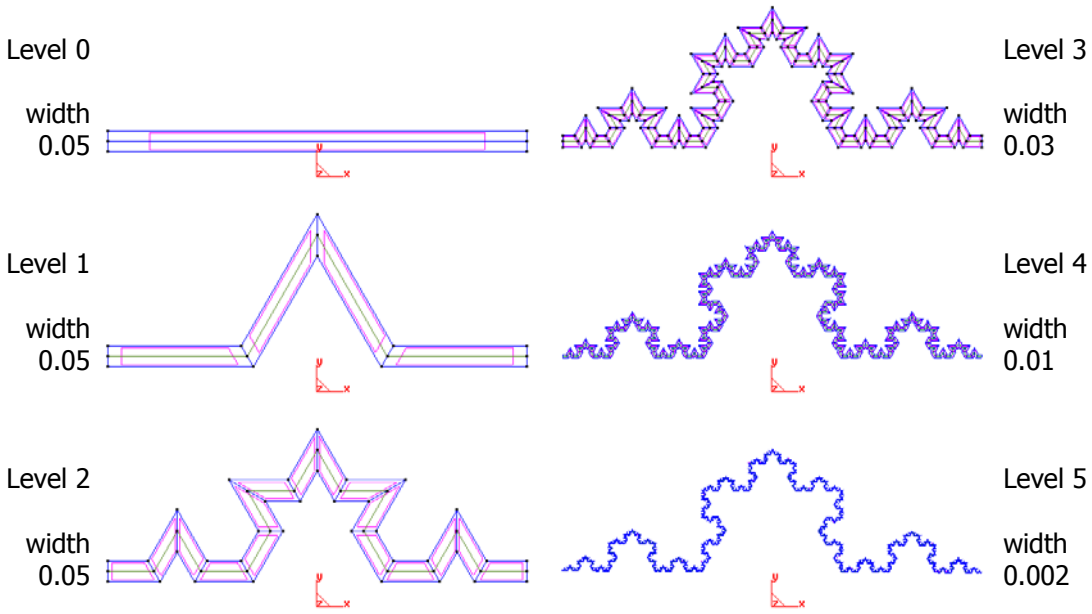

The wizard also warns the user when the path width entered in the window is bigger than elevations. If this width is too big, some line elevations will be masqueraded by the strip, and some surfaces will intersect when doing the extrapolation.

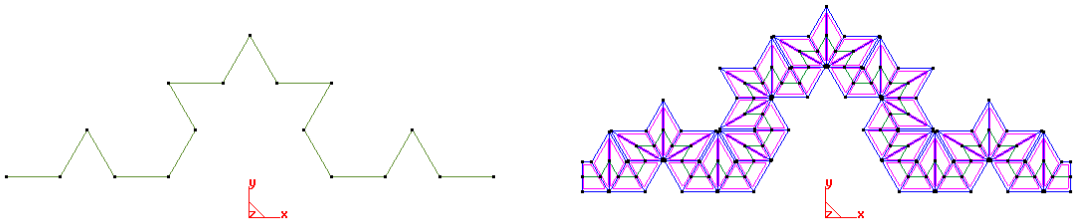

The high of the smallest elevation is 0.032 and the width used to create the strip is 0.06

The 'suggested size' of the elements for the meshing process is also changed when the user changes the 'width' entry.

The following sequence shows the different geometries and meshes corresponding to the Koch antenna when increasing the recursion level.

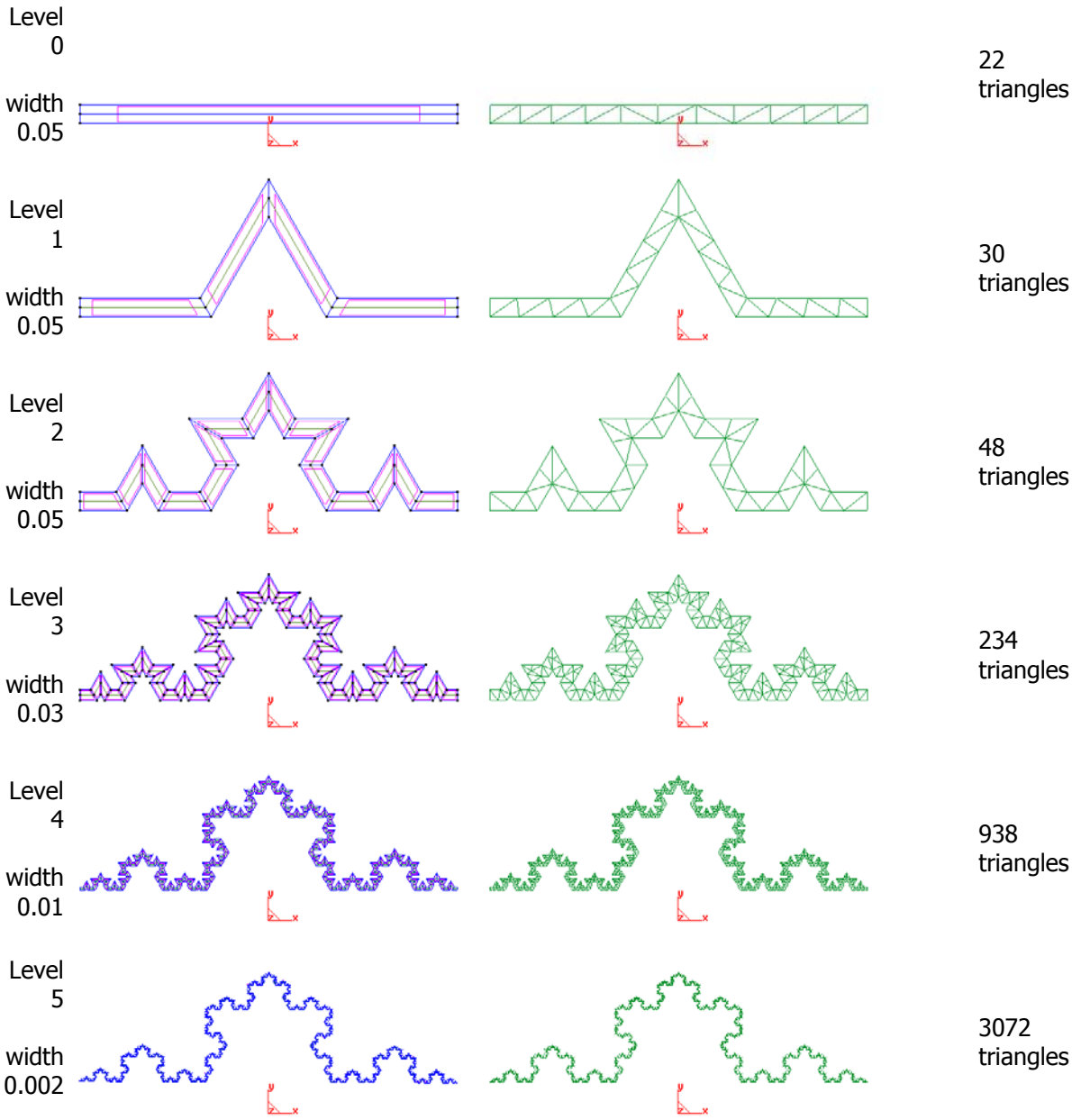

The next two figures show adapted meshes corresponding to recursion levels 2 and three where it is intended to increase the accuracy of the numerical results in the left part of the geometry.

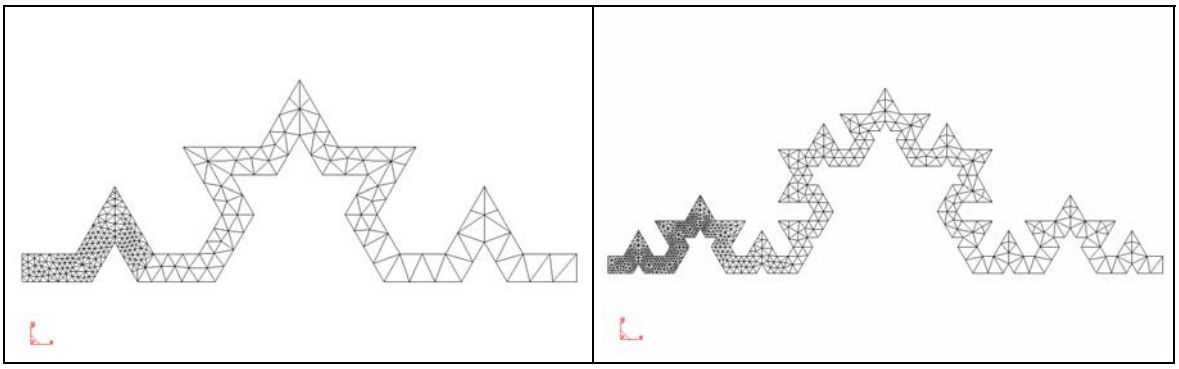

5 LINE ANTENNAS: EXAMPLE WITH ARBITRARY GEOMETRIES

To create using an Initiator and a Generator with arbitrary geometries we should select one line (marked with blue colour), or polyline (marked with green colour), as **Initiator**, and another line, or polyline, as **Generator**. The length of the antenna will be the length of the **Initiator** line.

So if we use these lines:

- one polyline which defines an hexagon (which contains the six lines) as **Initiator**,
- and another polyline, a 'pseudo-Koch' curve, as **Generator**.

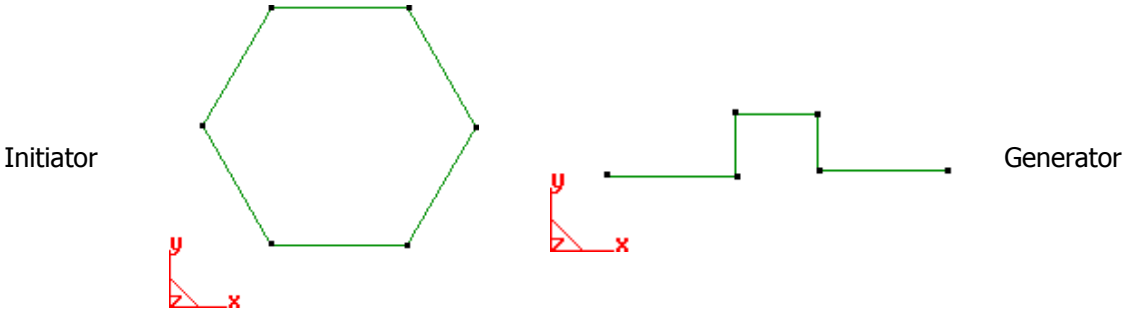

GiD draws polylines as green lines. Other lines are drawn blue, and surfaces, magenta.

We will get following antennas, depending on the recursion level:

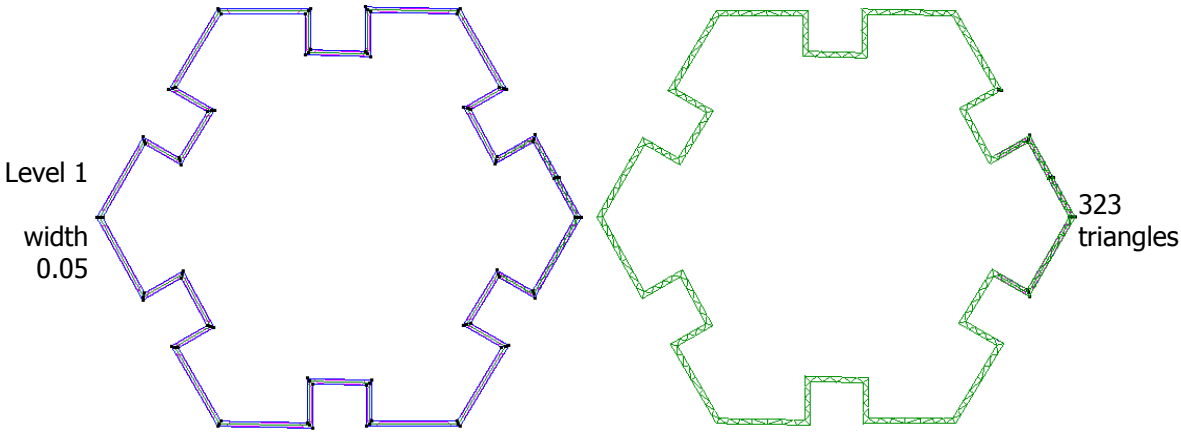

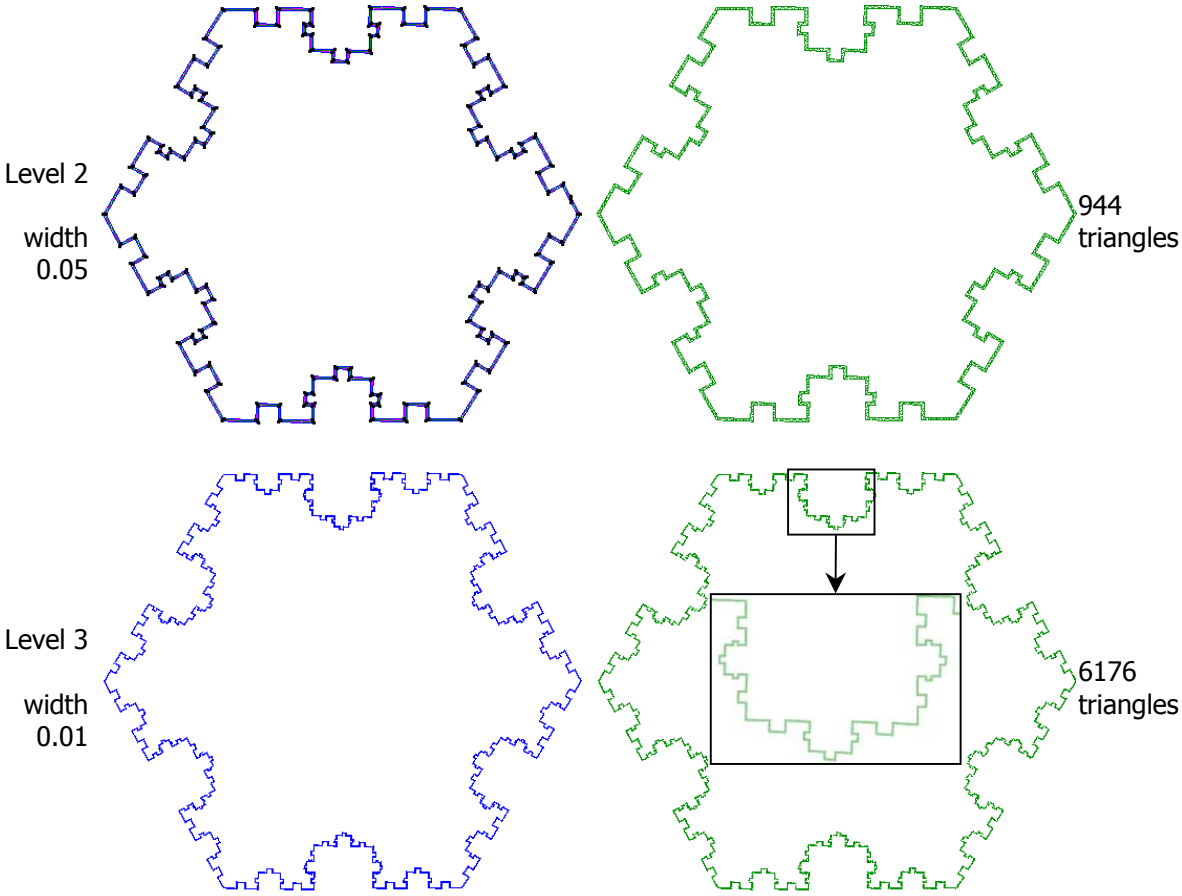

6 PLANAR ANTENNAS: SERPINSKI TRIANGLE

As mentioned in the Introduction, some preliminary work with planar geometries was already developed during the first year of the project. The first considered case was the Serpinski triangle.

For this geometry the level 0 of recursion is just a triangle. In the next levels of recursion the triangle(s) created in the previous level(s) are scaled and translated three times to create the Serpinski triangle.

So we get this table:

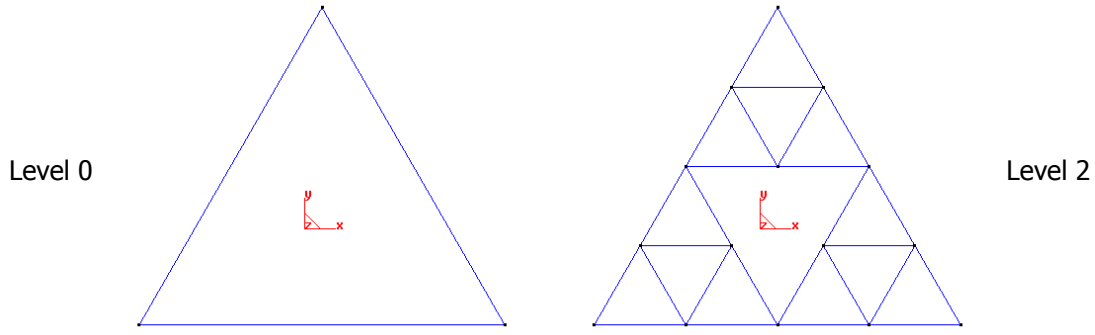

Level 1

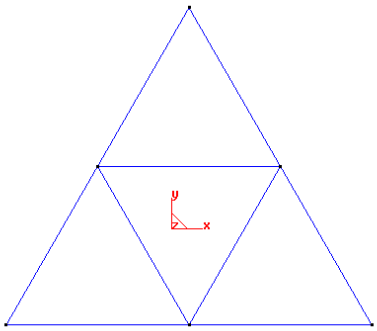

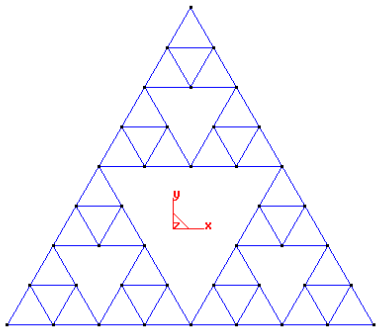

Level 3

Once the triangle surfaces are created, the connection paths between triangles are done in four steps: creating the lines of connection between the triangles, intersect them against the Serpinski triangle, creating the surfaces and deleting the orphan lines and points:

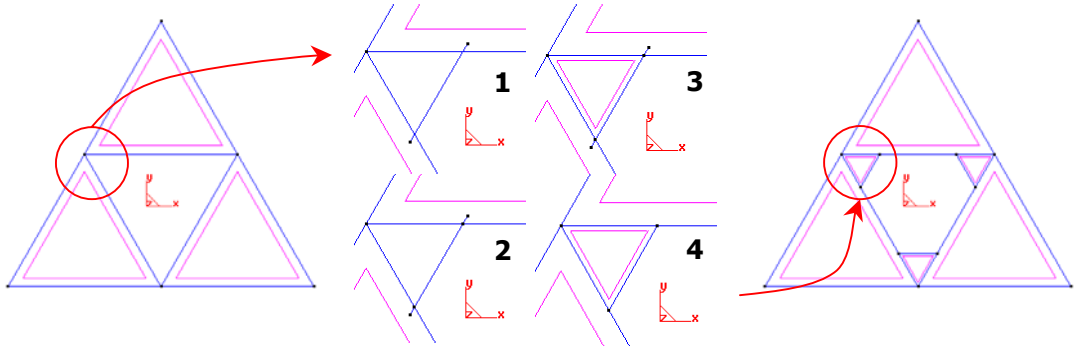

The maximum level of recursion is fixed at 10, which creates 147,621 surfaces, 177,147 lines, and 177,147 points.

Three layers are created in GiD: ‘TriangleAntenna’ which holds the lines of the Serpinski triangle, ‘Antenna’ which contains the Serpinski triangle surfaces and ‘AnchoAntenna’ which holds the connection paths between triangles.

The ‘suggested size’ of the elements for the meshing process is also changed when the user changes the ‘recursion level’ entry.

Level 0

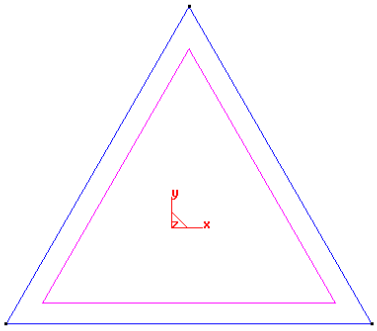

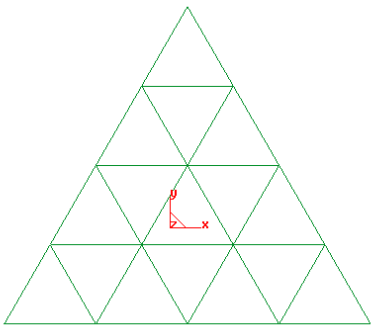

16 triangles

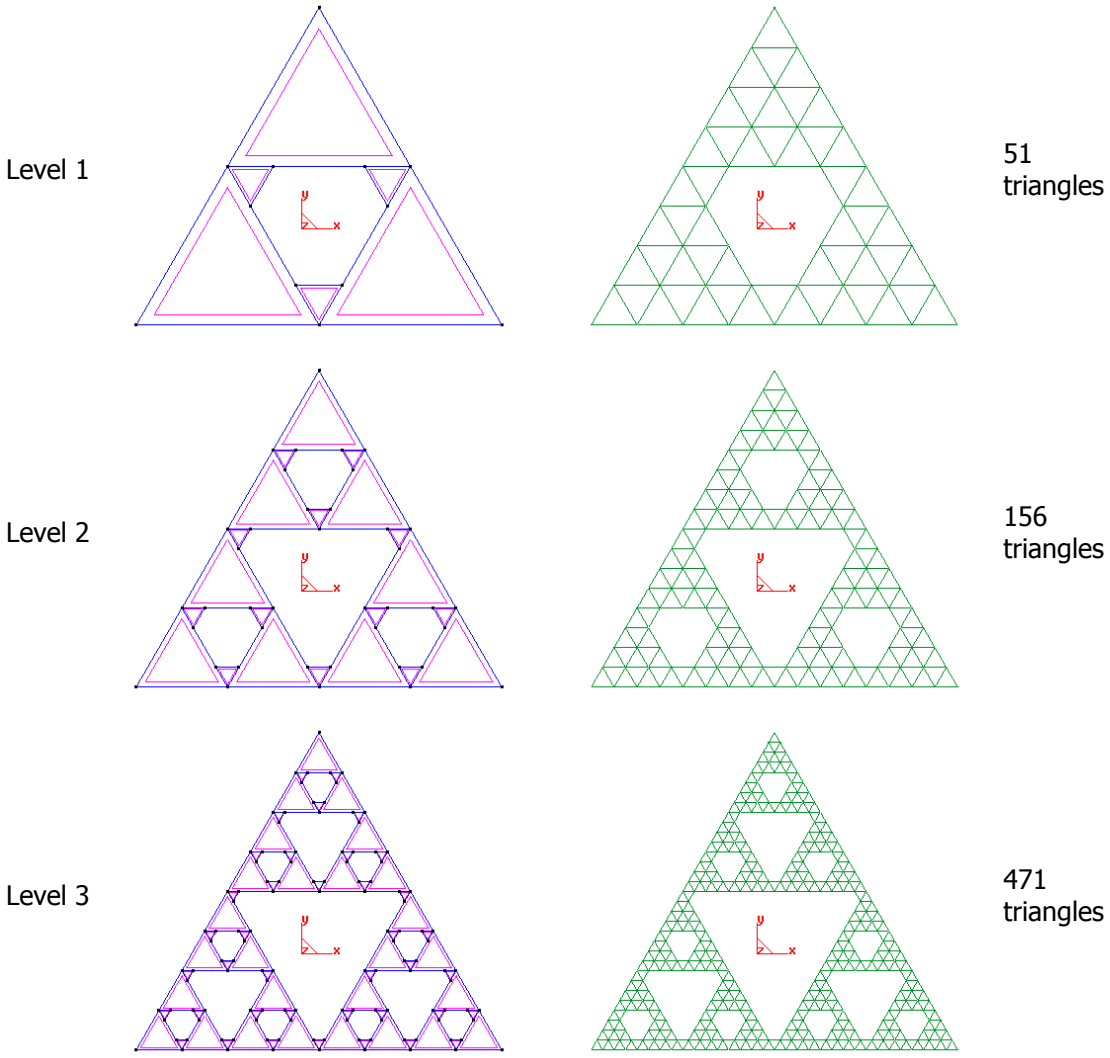

The wizard also warns the user when the connection path width entered in the window is bigger than littlest hole of the triangle. If this width is too big, some holes will be collapsed, i.e. the recursion process will stop.

7 NETWORKED MRCMS FRACTALS

During the second year of the project GiD has been provided with a new way of generating fractal geometry inside GiD. The implemented procedure follow the descriptions given in section 7.5 of **[1]**. As described **[1]**, a networked MRCM is defined by three components: the initial images, the set of transformations and the machines definitions.

In this way an initial image is a line, or polyline, of straight segments; each transformation is defined as an affine transformation, a combination of scale, rotation and translations; and a machine is the application of the transformations to the images. Every machine produces its own image, operating not only on its own image, but also on all images of the other machines in the network.

The initial images are defined as lines inside GiD, if an image has more than one point a polyline should be defined. Here we also call '**generators**' to the machines.

7.1 GiD Interface

This kind of fractal is defined in the page "`Networked antenna`" where the user can find another three pages: **Geometry** (for the initial images and global parameters), **Transformations** (to define affine transformation), **and Generators** (to define the machines).

`Geometry`

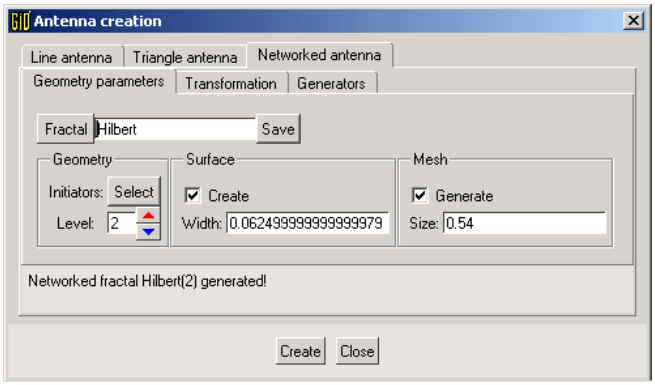

In this page the user selects or defines a new fractal. When an existing fractal is selected the corresponding definition fills the content of the pages `Transformations` and `Generators`. Also a new fractal can be defined selecting **New networked** in the button **Fractal**. The initial images are selected pressing the **Select** button. The images selected (lines or polylines) are labelled with the pattern **Path<id>** where **<id>** is the identifier of the line inside GiD (see `Utilities --> List --> Lines`).

The parameters of **Surface** and **Mesh** are similar to the ones appeared in the previous versions of the problem type for `Line antenna` and `Triangle antenna` pages. **Level** is the level of recursion when applying the definition of the machines and is constrained to be >= 0 and <=10.

`Transformations`

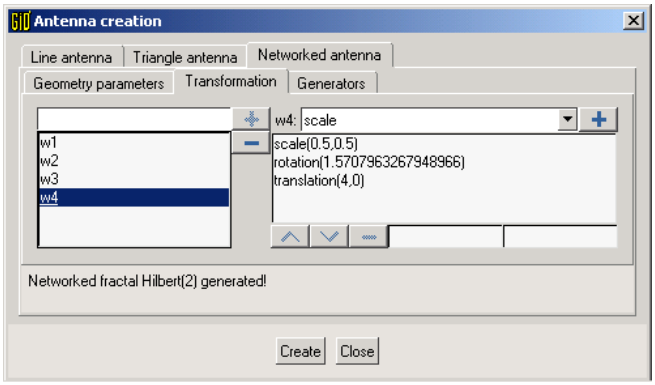

The set of affine transformations used in the definitions of the machines is defined on this page. On the left panel the user enters the names of the transformations whilst on the right the composition of each transformation is defined.

In order to make easier the definition of an affine transformation, this is defined as a composition of the elementary transformations: **scale**, **rotation**, **reflection**, and **translation**. The order in which the elementary transformations are entered is the order in which they are applied. The angle for the transformation rotation can be given in radians or degree, for instance: 5, 10 d or pi means 5 radians, 10 degrees or pi radians respectively. Besides pi, the constant pi_2, pi_3, pi_4, pi_6 can also be used as argument for rotation which corresponds to pi/2, pi/3, pi/4 and pi/6.

Generators

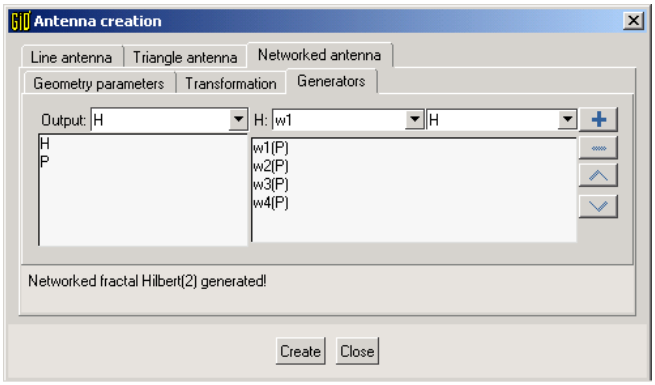

Every machine or generator is defined as the union of the transformations applied to the previous images of the machines/generators. For every machine name entered on the left panel of the **Generator** page the user defines its transformation combinations on the right panel.

The **Output machine** is the one that will be created, and meshed, into GiD after the generation process finished for the required level.

7.2 Networked MRCM file description

Here we describe the format of the file used to keep the definition of the networked fractals.

A fractal is started with the sentence

`Fractal <Name>`

where <Name> is the name identifying the fractal, if there is another fractal with the same name then this fractal is redefined

After this sentence, one or more path definition using a Path sentence appears:

`Path <ID> <list-of-coordinates>`

where <ID> is an identifier of the path which must be unique within the fractal. The rest of the arguments is the list of coordinates for the path and must be an even number of coordinates (X and Y), for instance:

```
Path H 0 1 1 1 1 3 3 3 3 1 4 1
```

defines the path H as a sequence of 6 points.

The block **Transformation** is used to start the definition of a new affine transformation, the syntax is:

`Transformation <ID>`

where **<ID>** is the identifier of the transformation and must be unique within a fractal.

After the Transformation sentence, the set of elementary transformations, which defines it, is written. The elementary transformations are:

```
scale <sx> <sy>
translation <dx> <dy>
rotation <angle>
reflect-x
reflex-y
```

Finally the generator or machines is defined. A machine is defined with the **Machine** sentence. The "Machine" sentence finishes the last Transformation block. The syntax of a "Machine" is:

```
Machine <PathID> <TransID> <PathID> [<TransID> <PathID>]
```

where <PathID> is the identifier of an existing path, <TransID> is the identifier of an existing transformation. The <PathID> after every <TransID> is the identifier of an existing path to which the transformation will be applied, for instance:

```
Machine H w1 P w2 P w3 P w4 P
```

defines the machine

$$H = w_1(P) \cup w_2(P) \cup w_3(P) \cup w_4(P)$$

The **Output** sentences specify the output image, for instance:

```
Output H
```

For example, the definition of the Hilbert fractal will be this:

```
Fractal Hilbert
Path H 0 1 1 1 1 3 3 3 3 1 4 1
Path P 1 0 1 3 3 3 3 1 4 1
Transformation w1
scale 0.5 0.5
rotation pi_2
reflect-y
Transformation w2
scale 0.5 0.5
translation 0 2
Transformation w3
scale 0.5 0.5
reflect-y
translation 4 2
Transformation w4
scale 0.5 0.5
rotation pi_2
translation 4 0
Machine H w1 P w2 P w3 P w4 P
Machine P w1 H w2 P w3 P w4 P
Output H
```

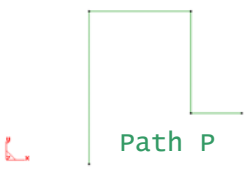

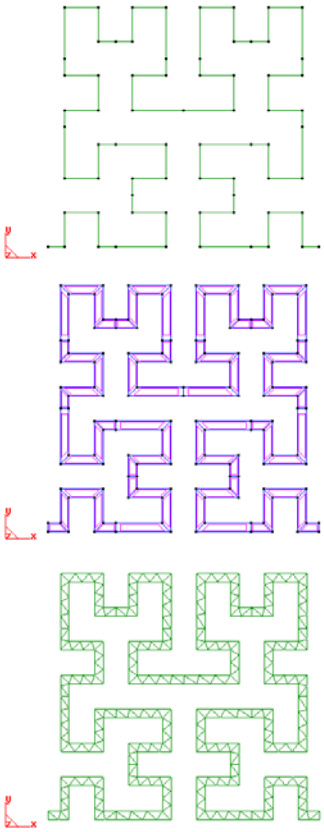

8 MRCMS FRACTALS EXAMPLE: CREATING THE PEANO FRACTAL

First: let's define a new fractal: **Peano**

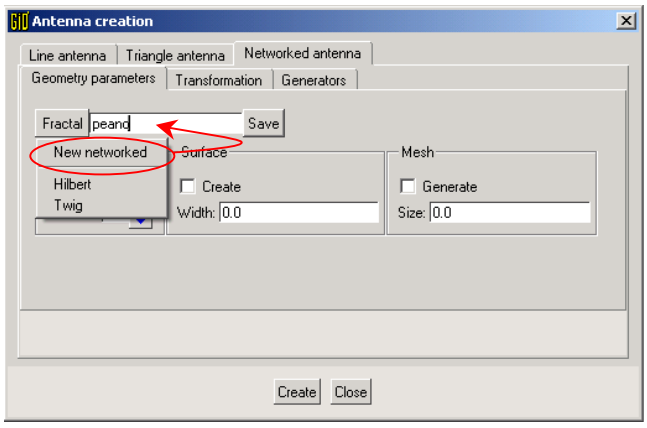

The machines, transformations and initial images needed to create the Peano Fractal are these:

Initial image **S**

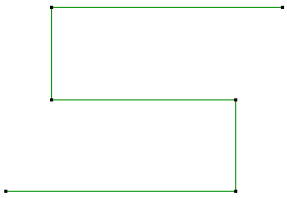

Initial machine **S**

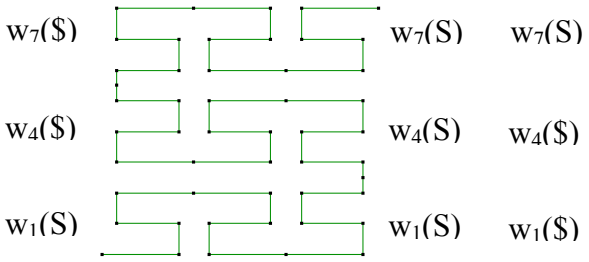

Initial image **$**

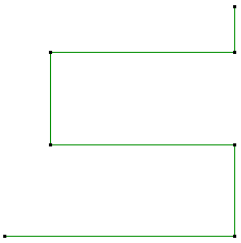

Initial machine **$**

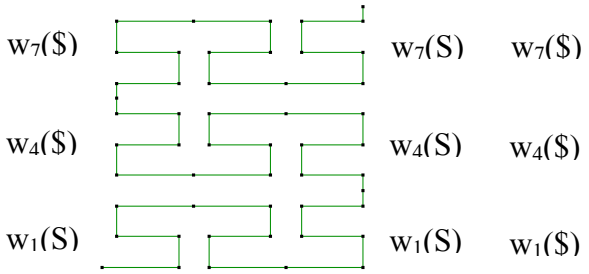

Second: to create the initial machine '**S**' in GiD, just click on the 'create line' icon, or 'Geometry->Create->Line' menu, and enter following points in the command line:

```
0,1 5,1 5,3 1,3 1,5 6,5
```

then 'escape' and then create a polyline selecting the just created lines.

To create the initial machine '**$**' in GiD, the same procedure, but with following points:

```
0,1 5,1 5,3 1,3 1,5 5,5 5,6
```

then ‘escape’ and then create a polyline selecting the just created lines.
So we can see that we are working in the area `[ 0, 0]` to `[ 6, 6]`. This is important for the later transformations.

Third, now we can select these two polylines as **Initiators**.

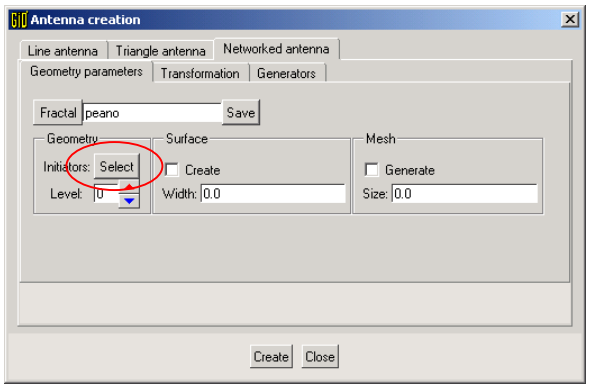

Fourth: following the above pictures of the generators, we can enter the transformations in the **Transformation** panel. Let’s define the sets of transformations from `w1` until `w9`. And for each one of these transformations sets, its elementary transformations:

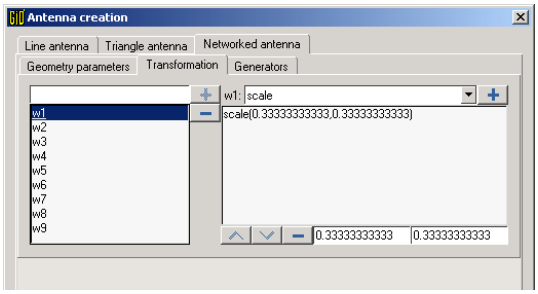

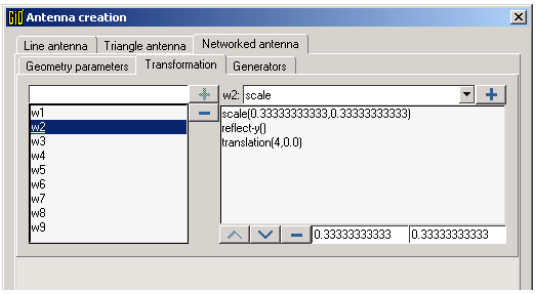

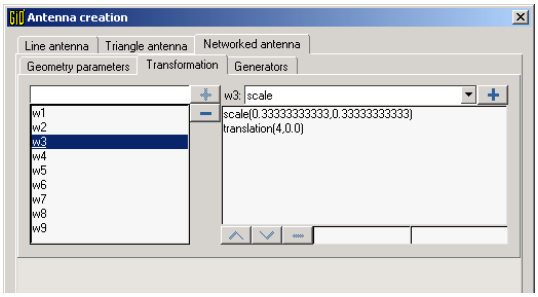

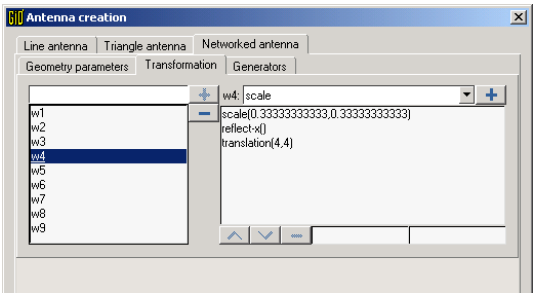

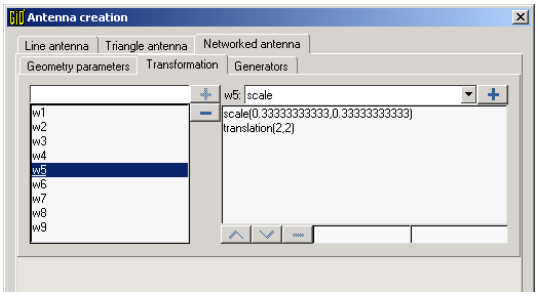

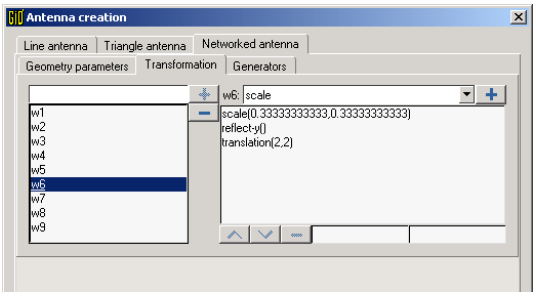

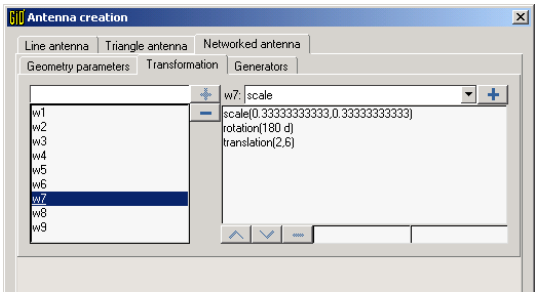

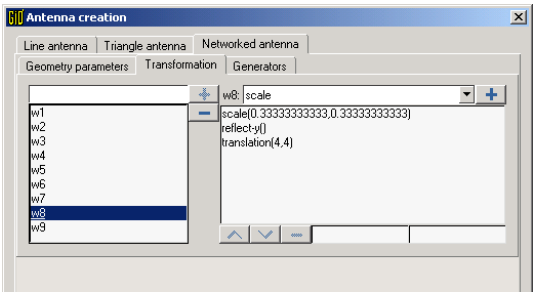

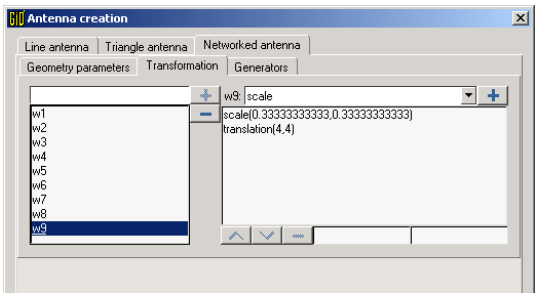

Note that the translations parameters are based on the working area defined by the initial images, which ranges from [0,0] to [6,6].

Fifth: after defining the transformations let's begin with the machines / **generators**.

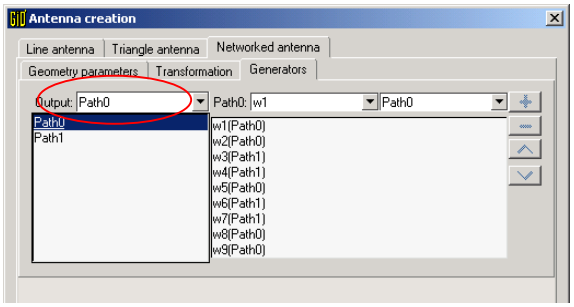

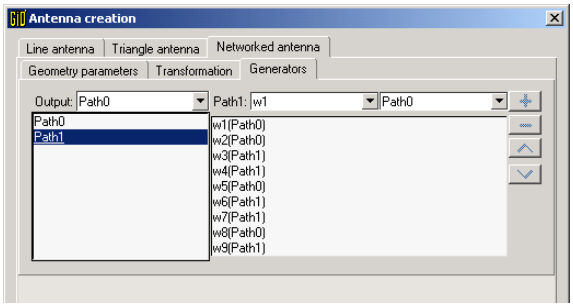

Here we define two machines, note that the last transformation is applied to different images on each machine.
In the **output** combo box we select which one is our valid final image.

Sixth: now we can save it. This fractal definition is stored together with the GiD project, so we have to save the GiD project, because the user normally does not have write permissions on the problem type's directory. An import / export option is added to the tool, so fractals can be exchanged. The fractals imported are saved inside the GiD project.

And finally, selecting the level we want, we can generate the fractal:

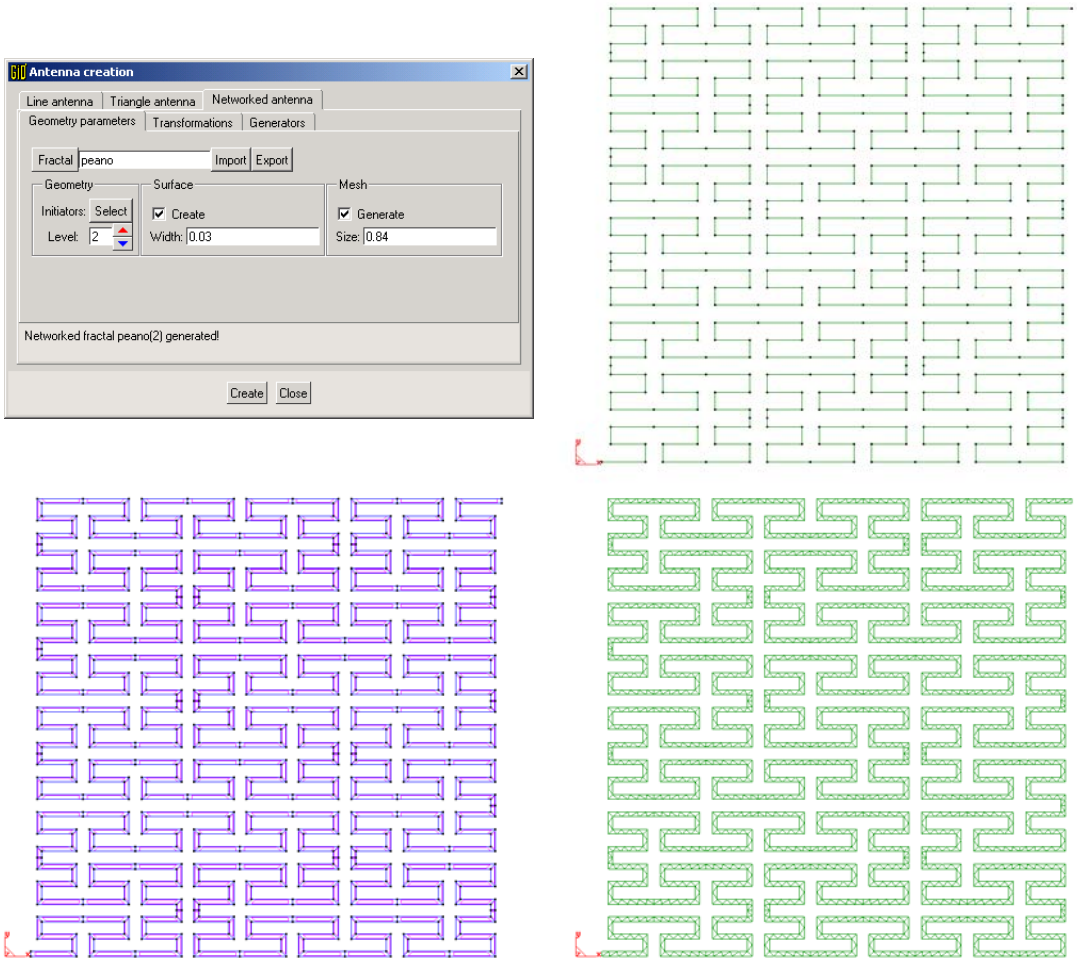

9 MRCMS FRACTALS EXAMPLE: THE TWING FRACTAL

One of the enhancements of the interface with GiD was to create surfaces for fractals with more than two ends. The scheme followed is based on Grafs and can be used to create the surfaces of following grafs:

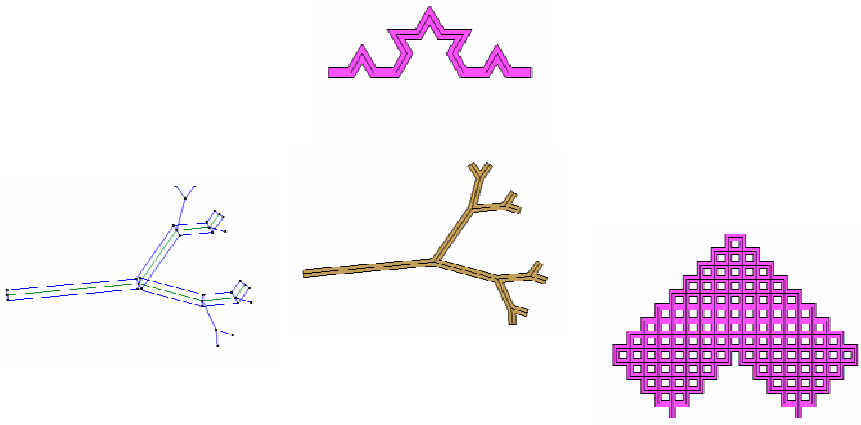

Using the conventions described below on the left, the algorithm to create the surfaces is the one listed on the right:

Notations

$G=(V,E)$

$V=\{v_1, v_2, \ldots, v_n\}$

$E=\{e_k=\{v_i, v_j\} : v_i, v_j \in V\}$

$Nbr_i=\{v_k : e_k^i=\{v_i, v_k\} \in E\}$

$SNbr_i=(v_i^1, v_i^2, \ldots v_i^k), \alpha_i^1=\widehat{v_i^1, v_i^2}, \alpha_i^1<\alpha_i^2<\ldots\alpha_i^k$

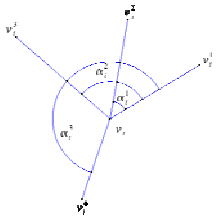

Algorithm

- Sort the neigborhoods
- Split every edge
- Offset every edge
- Connect edges
- Build surfaces

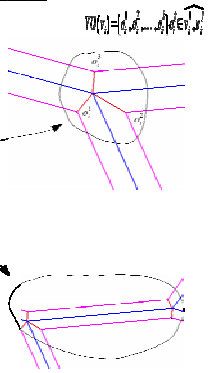

The resulting graph has the following properties:

Facts

- $G'=(V',E'), |V'|=\sum_{v \in V} d(v)+n, |E'|=2|E|+n$

- Every node of the offset graph has degree 2
- If G is a tree (aciclic graph) then the resulting graph offset is a closed path
- If G is not a tree then we obtain $|E|-|V|+2$ closed path

Examples

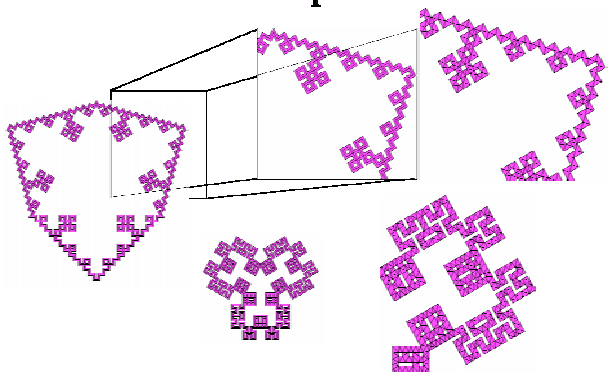

Using this new feature for the twig fractal with recursion level 1, 2 and 3:

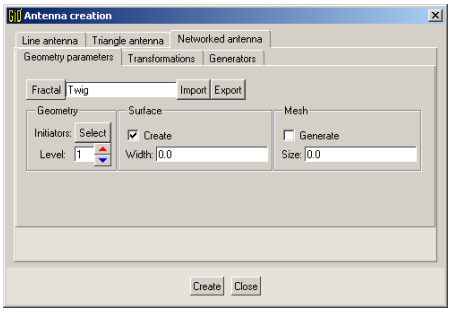

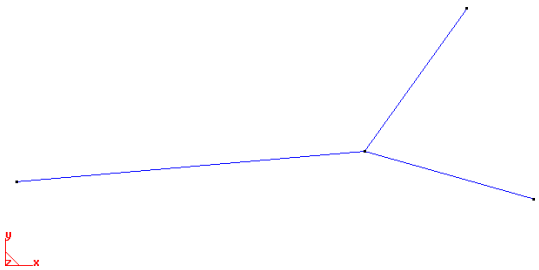

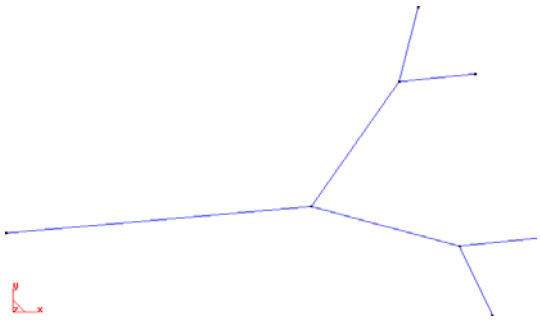

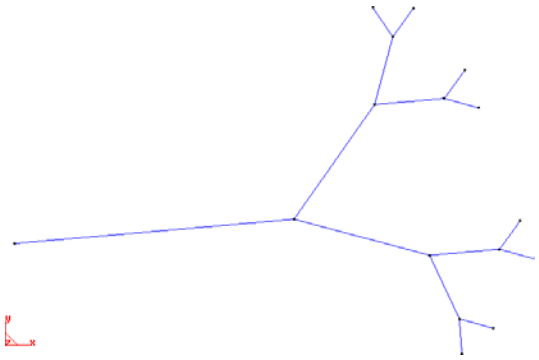

We get following surfaces and meshes:

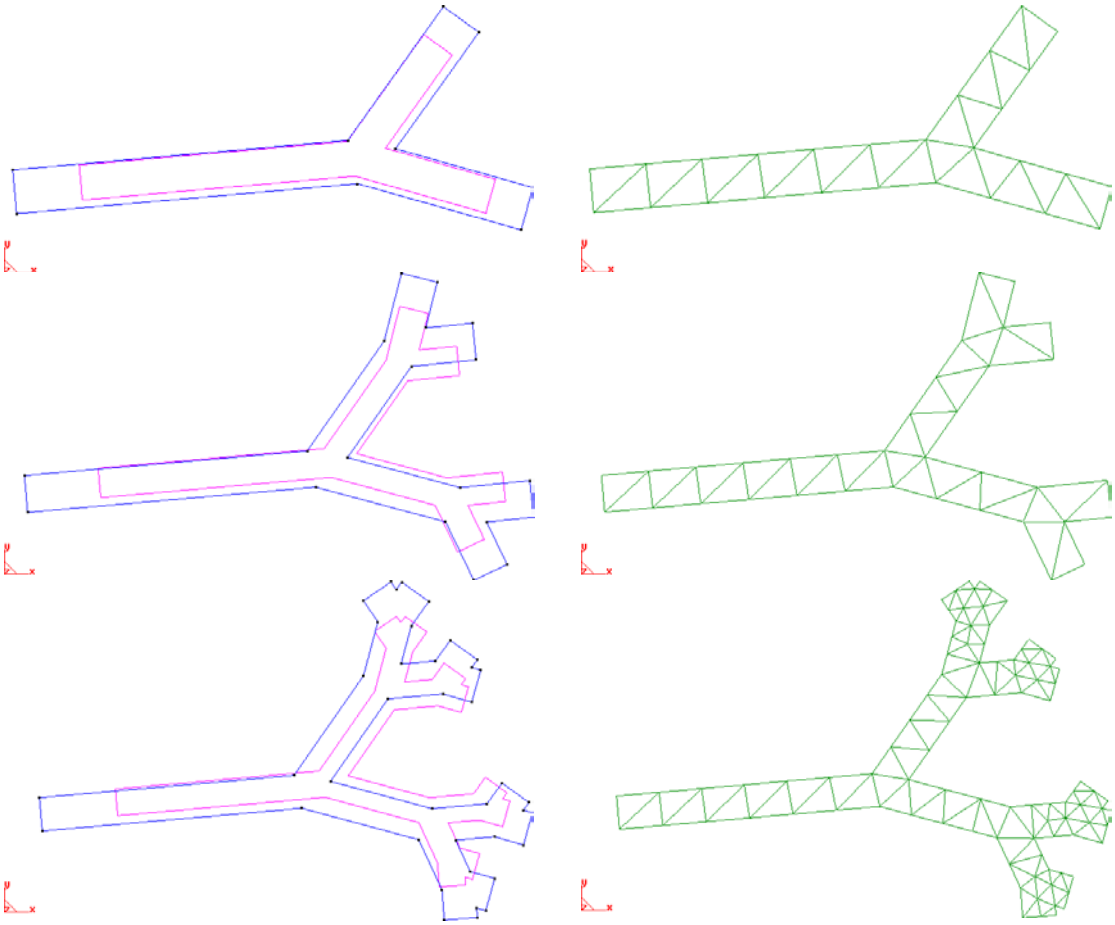

10 CONCLUSIONS

As initially planned, after the first year of the project an automatic tool for the generation and meshing of geometries for the analysis of fractal wire antennas was developed and fully tested. Following the indications of UPC, the geometries are obtained through a recursive algorithm where a geometrical Generator is replicated at each segment of the geometrical Initiator. This simple scheme allows to reproduce most of the wire fractal geometries providing a completely automatic way of producing the necessary data files for the numerical analysis if wire antennas. In addition, tools are provided for the generation of meshes adapted to the necessities of the numerical analysis. From this point of view it was considered that the initial objectives of Task 3.1 were fully accomplished.

During the first year of the project an increasing interest in antennas created from planar fractal geometries was detected. This suggested enlarging the software capabilities developed during the first year in order to deal with this alternative type of geometries. Even taking into account that in the initial project work plan Task 3.1 was supposed to be active only during the first year of the project CIMNE, together with the rest of the FRACTALCOMS consortium, agreed in maintaining this task active for the second year in order to allow for the mentioned software improvements. This allowed to introduce the generation of planar geometries in GiD and, also, to introduce some minor improvements in the treatment of the wire geometries. This expansion of the activity in

Task 3.1 has been carried out by CIMNE using some remaining man months that had not been completely consumed during the first year project. This allowed developing this additional activity without any additional budget. An example of this is the twing fractal surface creation.

11 REFERENCES

[1] H.O. Peitgen, H. Jürgens, D. Saupe: **Chaos and Fractals: New Frontiers of Science**, Springer-Verlag, New York, 1992.

DISCLAIMER

The work associated with this report has been carried out in accordance with the highest technical standards and the FRACTALCOMS partners have endeavoured to achieve the degree of accuracy and reliability appropriate to the work in question. However since the partners have no control over the use to which the information contained within the report is to be put by any other party, any other such party shall be deemed to have satisfied itself as to the suitability and reliability of the information in relation to any particular use, purpose or application.

Under no circumstances will any of the partners, their servants, employees or agents accept any liability whatsoever arising out of any error or inaccuracy contained in this report (or any further consolidation, summary, publication or dissemination of the information contained within this report) and/or the connected work and disclaim all liability for any loss, damage, expenses, claims or infringement of third party rights.

FRACTALCOMS

Exploring the limits of Fractal Electrodynamics for the future telecommunication technologies
IST-2001-33055

Study of quadrangular basis functions and their applications to fractal structures.

Author(s):	**Eugenia Cabot and Juan Mosig.**
Participant(s):	**EPFL**
Workpackage and task:	**WP3, T3.1**
Security:	**Public**
Nature:	**Report**
Version and date:	**1.0, 10-6-2002**

Total number of pages: 25

Abstract:

A new type of basis function defined over quadrangular domains has been studied. Some numerical test have been made to evaluate if they are adequate to solve some numerical problems encountered in electromagnetic simulations of pre-fractal structures.

Keyword list: MoM, basis functions.

RELATED WP AND TASKS (FROM THE PROJECT DESCRIPTION)

WP3: Software simulation tool. Task: 3.1: New basis functions for vertex-connected structures, specific treatment of T-junctions and similar complex connectors.

1 INTRODUCTION

When simulating fractal shaped antennas with a MoM (Method of Moments) [1] code, some problems appear due to modeling restrictions. We have tried to develop some tools to improve the quality of results.

2 FRACTAL GEOMETRIES AND MOM

There are mainly three numerical problems in electromagnetic simulations of pre-fractal structures.
The first of them is connectivity. Some surface fractal structures have differentiated parts connected between them only by a point (see for instance the Sierpinski Gasket, where triangles and subtriangles are connected by a vertex). In EM problems, when solving the integral equation to find the coefficients of the expanded currents (unknowns in the MoM), some discretization is needed. This discretization is made in general by couples of triangular and/or rectangular cells [4]. The condition to form a couple of these cells is that they have a common edge. That is, there is no way of defining connectivity with only one point, it is defined by a line. So when making the discretization of the fractal structure some additional cells must be put in order to assure connection between the different parts. As far as we don't have a numerical model in which vertex connection is possible, the rate in which the additional connector affects to the performance of the antenna will not be determined.
The second problem is some localized modes found on the surface of some fractal structures. An efficient way to model them should be found.
Meander shapes that appear in wire fractal cases cause also some trouble. High coupling between segments of wire is due to wire bending. For this reason current instead of flowing following the fractal shape "jumps" following the shortest path. So which is the real efficient equivalent length from the electromagnetic point of view? And also we have to think about the complicated meander bending modeling, because the number of unknowns in the MoM method is highly increased by the fact that a high number of unknowns is needed for the modeling of these sudden changes of direction (see the Koch monopole even in the lowest iterations).

3 BASIS FUNCTIONS DEFINED OVER QUADRANGULAR REGIONS [2]

3.1 A new set of basis functions

In order to address the first problem, we have developed a new type of basis functions defined over quadrangular domains. The quadrangles are defined by four arbitrary vertex and by analogy with widely used rooftop basis functions defined over rectangles, current is allowed to flow from one side c_1 to the opposite one c_3 remaining tangential to the other two sides c_2 and c_4.

But if full freedom can be exerced defining the four vertexes, the new basis functions should become the standard RWG rooftop on a triangular domain [3] if $P_1 = P_4$ and a new basis allowing flow of current through connecting points when $P_2 = P_3$.
Here follows the mathematical theory of these new basis functions.

3.2 Definition of quadrangular regions

An arbitrary quadrangle on a plane is defined by a set of four ordered points P_i, i=1...4, or equivalently by four 2D vectors $\overrightarrow{OP_i}$ where *O* is an arbitrary origin of coordinates.

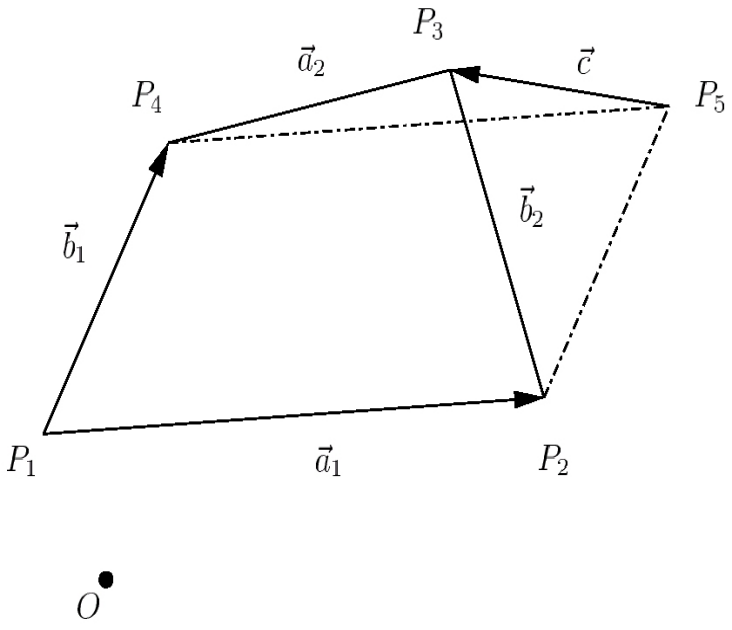

Figure 1. Definition of quadrangular region.

In practice, the origin *O* can be always selected as the point P_1 (local coordinates) and the quadrangle is better defined by the four vectors $\vec{a}_1 = \overrightarrow{P_1P_2}$, $\vec{a}_2 = \overrightarrow{P_4P_3}$, $\vec{b}_1 = \overrightarrow{P_1P_4}$, $\vec{b}_2 = \overrightarrow{P_2P_3}$. These vectors aren't independent, since obviously $\vec{a}_1 + \vec{b}_2 = \vec{a}_2 + \vec{b}_1$ and hence $\vec{a}_2 - \vec{a}_1 = \vec{b}_2 - \vec{b}_1$. Here we suggest to define an arbitrary quadrangle by three independent vectors, $\vec{a}$, $\vec{b}$, $\vec{c}$, given by:

$\vec{a} = \vec{a}_1$

$\vec{b} = \vec{b}_1$

$\vec{c} = \vec{a}_2 - \vec{a}_1 = \vec{b}_2 - \vec{b}_1$

While $\vec{a}$ and $\vec{b}$ correspond to two sides of the quadrangles the third vector $\vec{c}$ has an interesting geometrical interpretation since it gives the "distance" between the farthest vertex P_5 on an auxiliary parallelogram constructed on $\vec{a}$, $\vec{b}$ and the actual vertex P_3. It can be somewhat said that $\vec{c}$ measures the "degree of irregularity" of the quadrangle.

3.3 Particular cases

We will assume always $\vec{a} \neq \vec{0}$. Then $\vec{b}$ and $\vec{c}$ cannot be simultaneously zero for the quadrangle to exist.
Acceptable particular cases are:

1. $\vec{c} = \vec{0} \Rightarrow$ Parallelogram.
2. $\vec{b} = \vec{0} \Rightarrow$ Triangle.
3. $\vec{c} = -\vec{b} \Rightarrow$ Triangle.

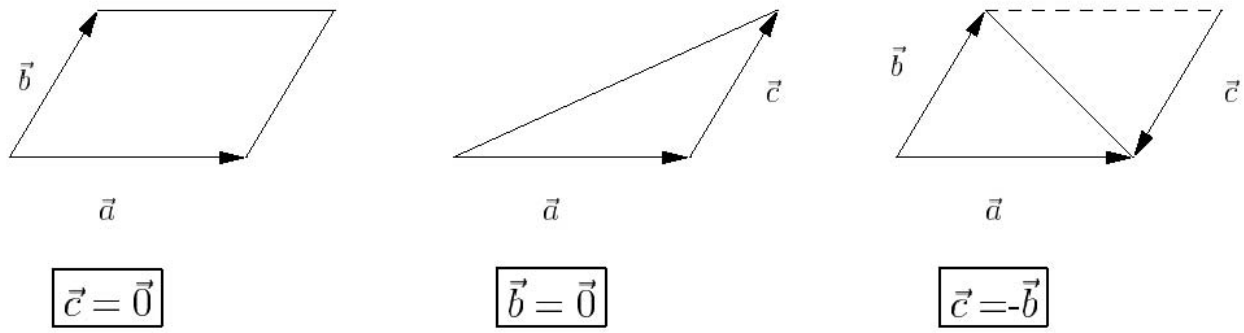

Figure 2. Particular cases.

3.4 Skew coordinates

Any quadrangle defined on the *xy* plane can be put into a biunivocal correspondence with an unit square in an auxiliary *uv* plane by the relationship:

$$\vec{r} = u\vec{a} + v\vec{b} + uv\vec{c}$$

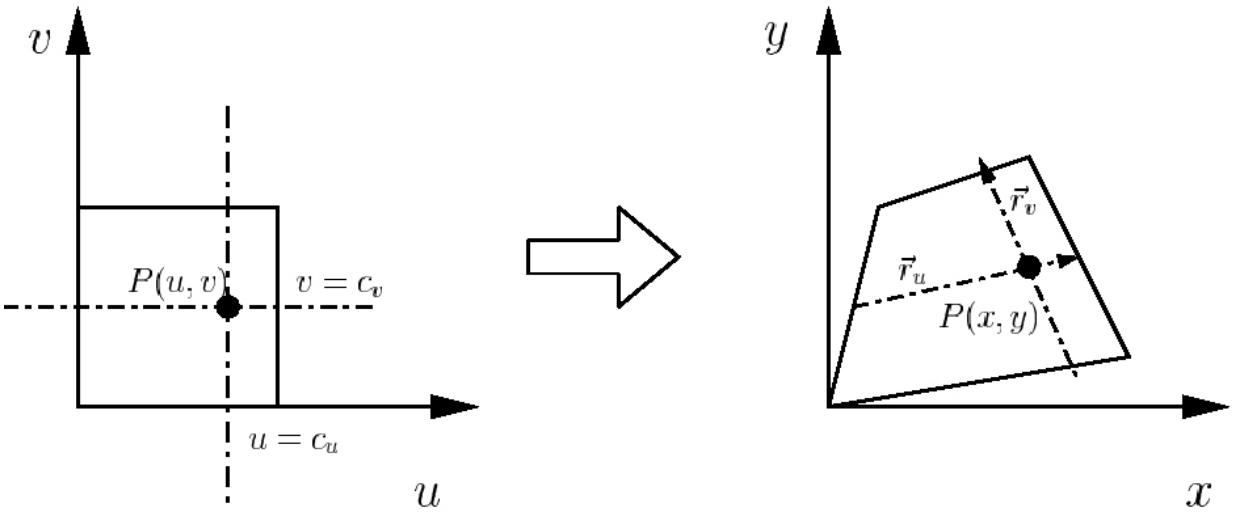

Figure 3. Plane (u,v) and plane (x,y).

It must be pointed out that in the general case (arbitrary quadrangle, $\vec{c} \neq \vec{0}$) the coordinate transformation is a nonlinear one.

The perpendicular lines $u = c_u$ and $v = c_v$, where c_u and c_v are constants, defining the point $P(u,v)$ correspond to, respectively,

$$\vec{r} = u(\vec{a} + v\vec{c}) + v\vec{b} = u\vec{r}_u + v\vec{b}$$

and

$$\vec{r} = v(\vec{b} + u\vec{c}) + u\vec{a} = v\vec{r}_v + u\vec{a}$$

where the auxiliary vectors

$$\vec{r}_u = \vec{a} + v\vec{c}$$

$$\vec{r}_v = \vec{b} + u\vec{c}$$

intersect at the point $P(x,y)$. These vectors will play an essential role in the following developments.

3.5 The Jacobian

In the general case

$$\vec{r} = u\vec{a} + v\vec{b} + uv\vec{c}$$

derivation respect *u* and *v* gives:

$$\frac{\partial \vec{r}}{\partial u} = \vec{a} + v\vec{c} = \vec{r}_u$$

$$\frac{\partial \vec{r}}{\partial v} = \vec{b} + u\vec{c} = \vec{r}_v$$

The Jacobian of the coordinate transformation is defined in general as

$$J = \begin{vmatrix} \frac{\partial x}{\partial u} & \frac{\partial x}{\partial v} \\ \frac{\partial y}{\partial u} & \frac{\partial y}{\partial v} \end{vmatrix} = \hat{e}_z \cdot \left(\vec{r}_u \times \vec{r}_v \right)$$

This can be viewed as the z-directed component of the vector product $\vec{r}_u \times \vec{r}_v$. Using the shorthand notation $S_{pq} = \hat{e}_z \cdot (\vec{p} \times \vec{q})$ we get

$J = S_{r_u r_v}$

or developing this expression

$J = S_{ab} + uS_{ac} + vS_{cb}$

In particular, when $\vec{c} = \vec{0}$ (parallelogram) we get a constant value for the Jacobian $J = S_{ab}$, which is equal to the area of the parallelogram. For the triangular cases $\vec{b} = \vec{0}$ or $\vec{c} = -\vec{b}$, we get a Jacobian showing a linear dependence on the *u*-coordinate.

3.6 Generalization of RWG basis for surface current distributions to quadrangular domains

It is desirable that quadrangular basis functions have the same good properties as rectangular or triangular ones. These properties are:

1) $\vec{J}(0,v) \cdot \hat{n}_1 = 0$

2) $\vec{J}(u,0) \cdot \hat{n}_2 = 0$

3) $\vec{J}(1,v) \cdot \hat{n}_3 = \frac{1}{l}$

4) $\vec{J}(u,1) \cdot \hat{n}_4 = 0$

5) $div\,(\vec{J}) = \frac{1}{S}$, with $S =$ surface.

For a couple of cells current is supposed to be maximum at the common edge and zero in the opposite one, so basis function must accomplish property number 1, which ensures that the normal component of current is zero in the edge opposite to the common edge. Properties number 2 and 4 ensure that current is tangential to the other two edges. Property number three refers to current density continuity in the boundary of the cells forming the couple, whereas property number 5 postulates that the divergence of the current density, that is, the charge, is constant on a cell.

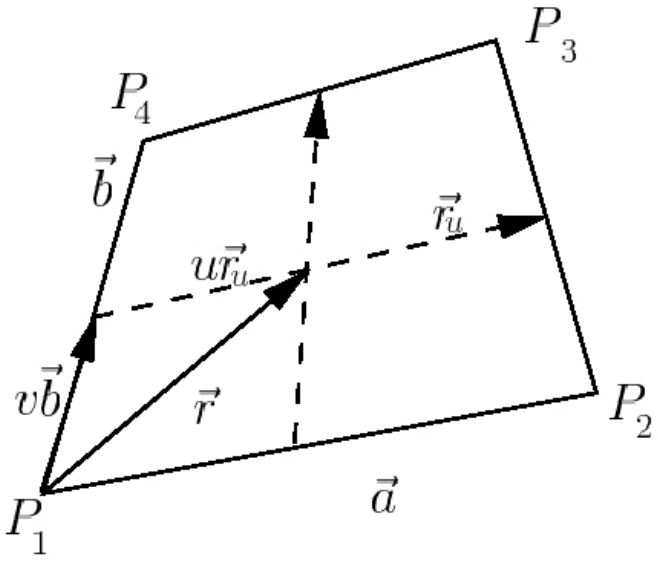

Figure 4. Parameters on a quadrangle useful for current definition.

3.6.1 Basis function ensuring continuity of normal current but not constant charge

The first obvious idea is to consider the definition:
$\vec{J}(\vec{r}) = \vec{r} - v\vec{b} = u\vec{a} + uv\vec{c} = u(\vec{a} + v\vec{c}) = u\vec{r}_u$
Let us check if this functions accomplishes the properties mentioned before.
It is obvious that on the $\overline{P_1P_4}$ side, $u = 0$ and $\vec{J} = \vec{0}$.
On the sides $\overline{P_1P_2}$ and $\overline{P_4P_3}$, $\vec{J}$ remains tangential by definition:

- On $\overline{P_1P_2}$, $v = 0$ and $\vec{J} = \vec{r} = u\vec{a}$.
- On $\overline{P_4P_3}$, $v = 1$ and $\vec{J} = \vec{r} - \vec{b} = u(\vec{a} + \vec{c})$

But if we want to have $\vec{J} \cdot \hat{n}\big|_{u=1} =$ constant we have to introduce a slight modification

$$\vec{J} = \frac{u\vec{r}_u}{\vec{r}_u \times \vec{b} + \vec{a} \times \vec{c}}$$

because this way all the properties we checked before are still fulfilled and we obtain now
$\vec{J} \cdot \hat{n}\big|_{u=1} = \dfrac{1}{\left|\vec{b} + \vec{c}\right|}$.

And as $dl = \left|\vec{b} + \vec{c}\right| dv$ and $\hat{n} = \dfrac{(\vec{b} + \vec{c}) \times \hat{e}_z}{\left|\vec{b} + \vec{c}\right|}$ we obtain that the current flowing out the side $\overline{P_2P_3}$ is
$I = \int_{P_2P_3} \vec{J} \cdot \hat{n}\, dl = 1$

It remains to check property number 5.

After some mathematical developments we get an expression for divergence in skew coordinates,

$$div(\vec{J}) = \frac{1}{S_{r_u r_v}} \left[\begin{bmatrix} \vec{r}_v(2) & -\vec{r}_u(2) \end{bmatrix} \begin{bmatrix} \frac{\partial}{\partial u} \\ \frac{\partial}{\partial v} \end{bmatrix} J_x + \begin{bmatrix} -\vec{r}_v(1) & \vec{r}_u(1) \end{bmatrix} \begin{bmatrix} \frac{\partial}{\partial u} \\ \frac{\partial}{\partial v} \end{bmatrix} J_y \right].$$

The divergence of function $\vec{J}$ is then,

$$div(\vec{J}) = \frac{1}{\vec{r}_u \times \vec{b} + S_{ac}} + \frac{uS_{ac}}{S_{r_u r_v}\left(\vec{r}_u \times \vec{b} + S_{ac}\right)}.$$

So the divergence of the current depends on the *u,v* coordinates in the general case (for the parallelogram ($\vec{c} = \vec{0}$) $div(\vec{J}) = 1/S$ and for the triangle ($\vec{b} = \vec{0}$) $div(\vec{J}) =$ constant).

$\vec{J} = \dfrac{u\vec{r}_u}{\vec{r}_u \times \vec{b} + \vec{a} \times \vec{c}}$ fulfills conditions 1) to 4) but not 5).

3.6.2 Basis function ensuring constant charge but not continuity of normal current

A quadrangular basis function with constant charge is

$$\vec{J} = \frac{S_{r_u r_v} - \frac{u}{2} S_{ac}}{S_{r_u r_v}} u\vec{r}_u = \eta_1 u\vec{r}_u$$

The divergence of this expression is constant and equal to 1.

Particular cases include the parallelogram $\vec{c} = \vec{0}$, $\vec{J} = u\vec{a}$, the normal triangle $\vec{b} = \vec{0}$, $\vec{J} = \dfrac{u}{2}\left(\vec{a} + v\vec{c}\right)$, and also the inverted triangle.

For $u = 1$ we have:

$$\vec{J}(u=1, v) = \frac{S_{ab} + \frac{1}{2} S_{ac} + vS_{cb}}{S_{ab} + S_{ac} + vS_{cb}} \vec{r}_u$$

so condition 4) is not fulfilled because in the $u = 1$ side $\hat{n} = \dfrac{(\vec{b} + \vec{c}) \times \hat{e}_z}{\left|\vec{b} + \vec{c}\right|}$ and since $\vec{J} = \eta_1 u\vec{r}_u$

$$\vec{J} \cdot \hat{n} = \eta_1 u \frac{\vec{r}_u \times \vec{b} + \vec{a} \times \vec{c}}{\left|\vec{b} + \vec{c}\right|}.$$

So

$$\vec{J} \cdot \hat{n}\big|_{u=1} = \eta_1 (u=1) \frac{\vec{r}_u \times \vec{b} + \vec{a} \times \vec{c}}{\left|\vec{b} + \vec{c}\right|},$$

and this cannot be matched in both sides of the common edge.

3.6.3 Basis function ensuring both constant charge and continuity of normal current

The augmented expression $\vec{J}(u,v) = F_u(u)\frac{u\vec{r}_u}{S_{uv}} + v(1-v)F_v(v)\frac{\vec{r}_v}{S_{uv}}$ still fulfills conditions 1) to 4) if

$F_u(0) \neq \infty$
$F_u(1) = 1$
$F_v(0) \neq \infty$
$F_v(1) \neq \infty.$

We therefore postulate simple linear expressions,
$F_u = Au + B$
$F_v = Cv + D$

and try to obtain $div(\vec{J}) = \frac{1}{S}$. After some developments we get

$$\vec{J} = \frac{\left(S_{ab} + \frac{S_{ac}}{2}u + \frac{S_{cb}}{2}\right)u\vec{r}_u - \frac{Scb}{2}v(1-v)\vec{r}_v}{S\,S_{r_u r_v}}$$

This expression accomplishes properties 1) to 5).

3.7 Surface current distribution over different geometries.

In the following tables we can find the representation of current distribution over different geometries mainly the general quadrangular case, the parallelogram case and the triangular particular cases. The representation of the three possible kind of functions has been made (the one ensuring continuity over the boundary edge, the one ensuring constant charge over every cell, and the one ensuring both properties).
The plots shown in the tables are the current density vector on a cell, the charge distribution over this cell and the normal component of current over the edge supposed to be connected to the other cell forming the couple for basis function definition.

	Current density vector	Charge	Normal component of current
Continuity of normal current	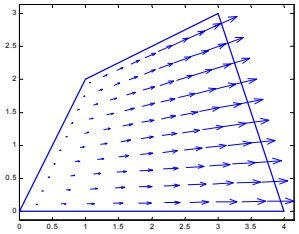	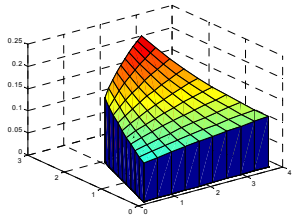	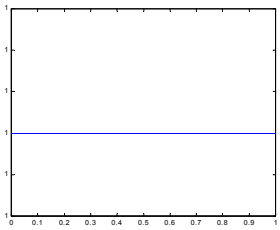
Constant charge	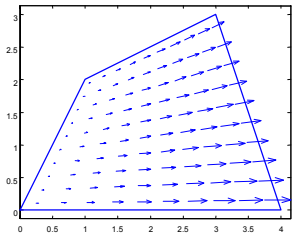	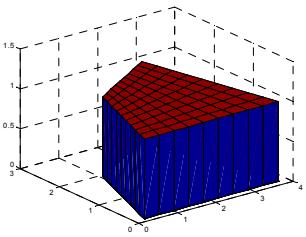	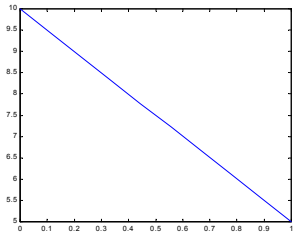
Both properties	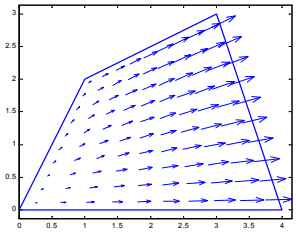	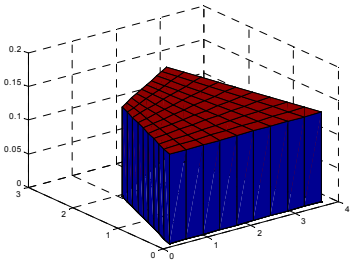	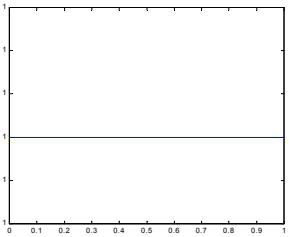

- Parallelogram case ($\vec{c} = \vec{0}$).

For this particular case the three functions give a constant charge and ensure continuity of current normal component.

	Current density vector	Charge	Normal component of current
Continuity of normal current	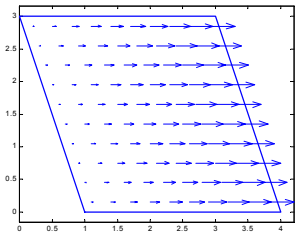	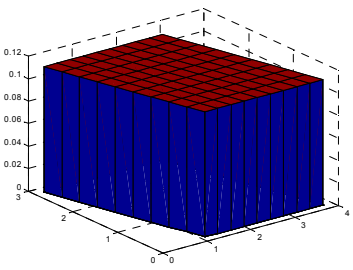	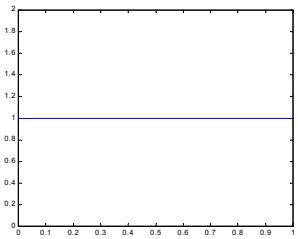

Constant charge	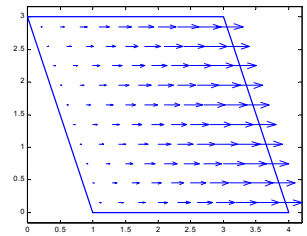	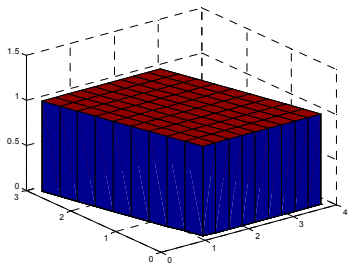	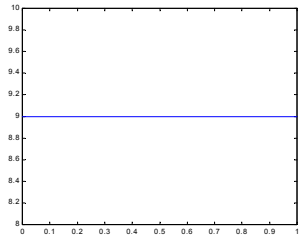
Both properties	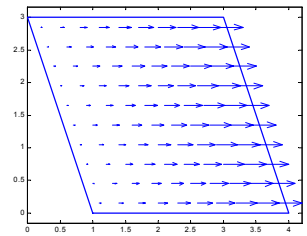	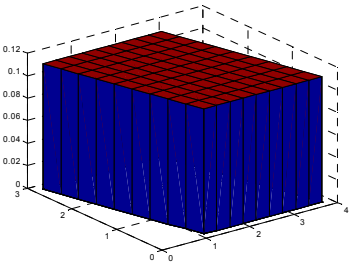	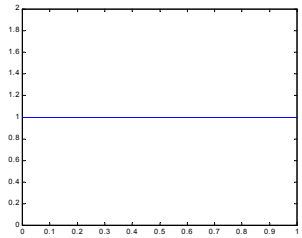

- Triangular case ($\vec{b} = \vec{0}$).

For the triangular case continuity of normal component of current and constant charge is assured with any of the three functions, as expected, because for this triangular case the general basis function defined over quadrangular domains becomes the classical definition for a RWG function.

	Current density vector	**Charge**	**Normal component of current**
Continuity of normal current	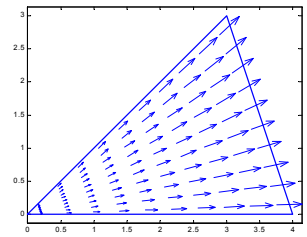	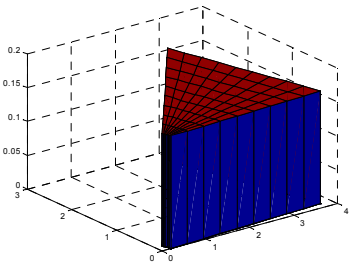	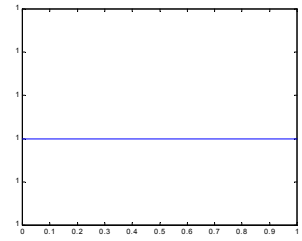
Constant charge	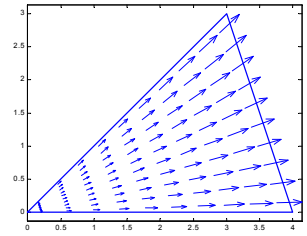	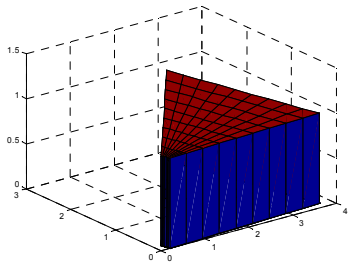	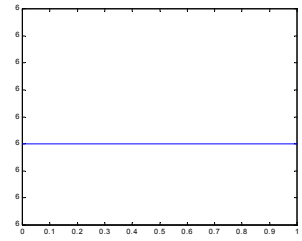

Both properties	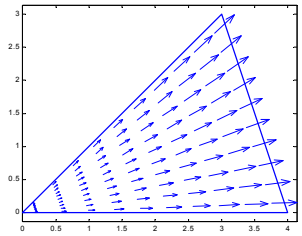	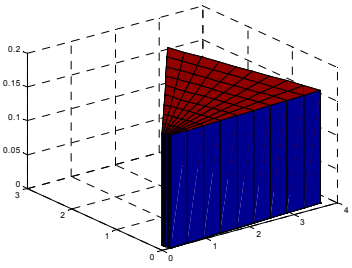	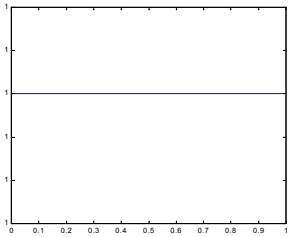

- Triangular case ($\vec{c} = -\vec{b}$).

	Current density vector	**Charge**
Continuity of normal current	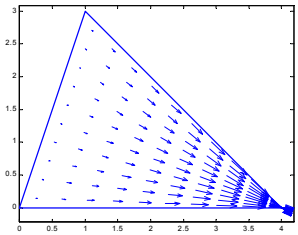	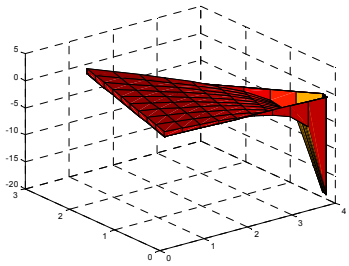
Constant charge	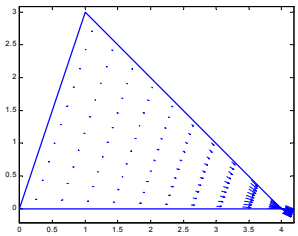	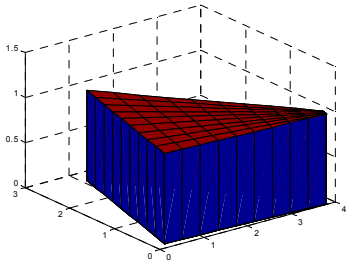
Both properties	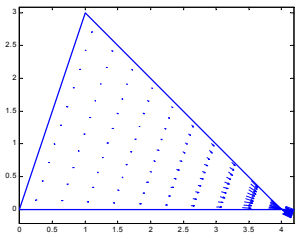	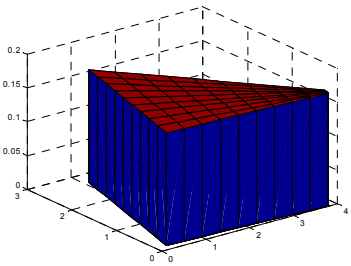

4 NUMERICAL TESTS

4.1 Representation of current density over strip scatterer

The first numerical test is made in order to check the smoothness of the current when approximated with a quadrangular basis function expansion. Is solution accurate even when the basis function doesn't assure continuity when the cells have an irregular shape?

There are some other functions used to represent currents that are not continuous, as the so called piece-wise sinusoidal.
The test consists in solving by the MoM a very simple structure, a strip scatterer, for two different meshes, a rectangular one and an irregular quadrangles one, with a plane wave excitation, as appeared in [6]. Results are in the following figures.

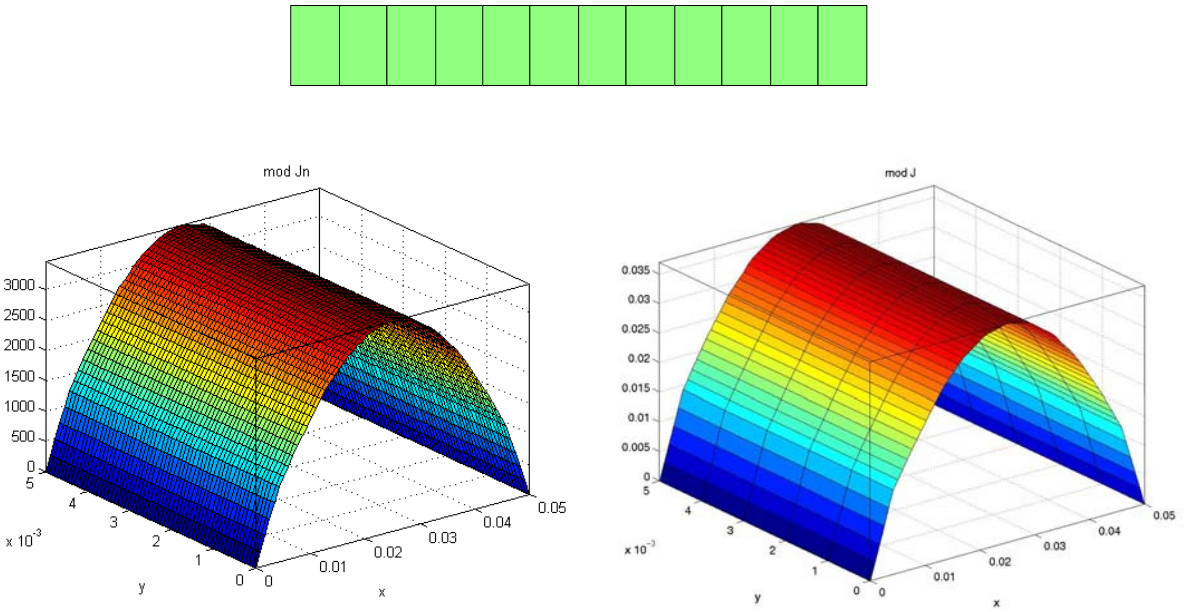

Figure 5. Magnitude of current density using a bf of constant divergence (left) and constant divergence+ ensured continuity (right).

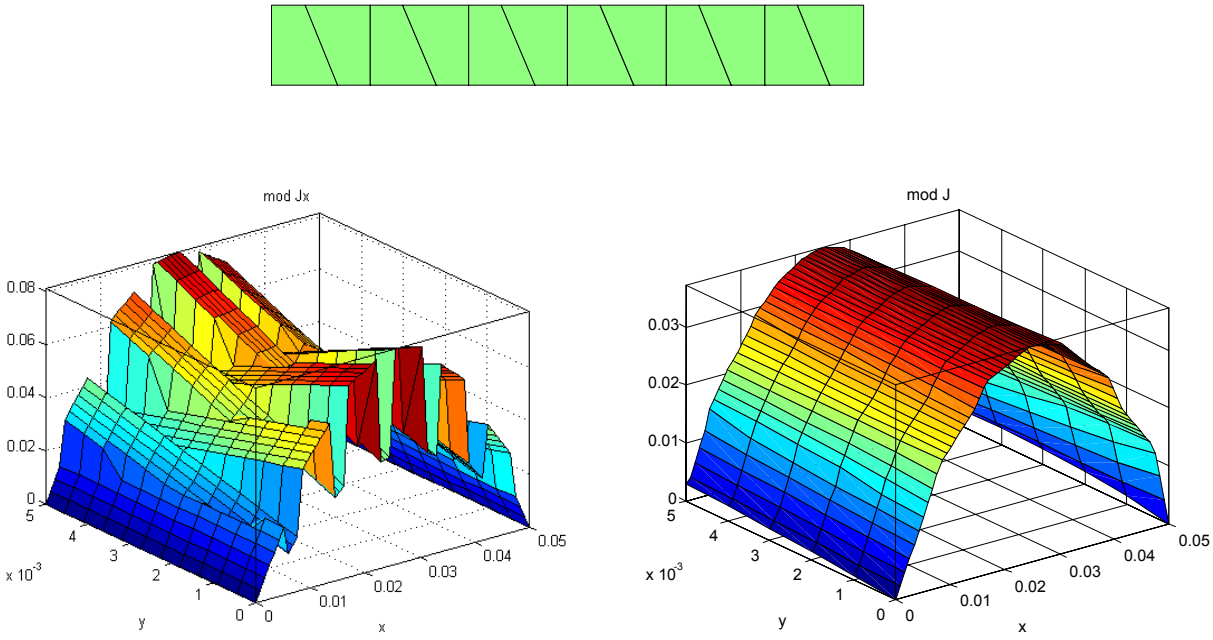

Figure 6. Magnitude of current density using a bf of constant divergence (left) and constant divergence+ensured continuity (right).

It can be seen that to get a smooth shape for the current a function ensuring continuity is needed. From now on all results will be only computed with basis function ensuring both continuity and constant charge.

4.2 Representation of current density over square scatterer

This test is basically the same as before, but in a 2-D structure [5]. Now there are x-connected and y-connected basis functions. The first mesh is a regular mesh (square) and the second one is an irregular quadrangular mesh. Excitation is again a x-directed plane wave.

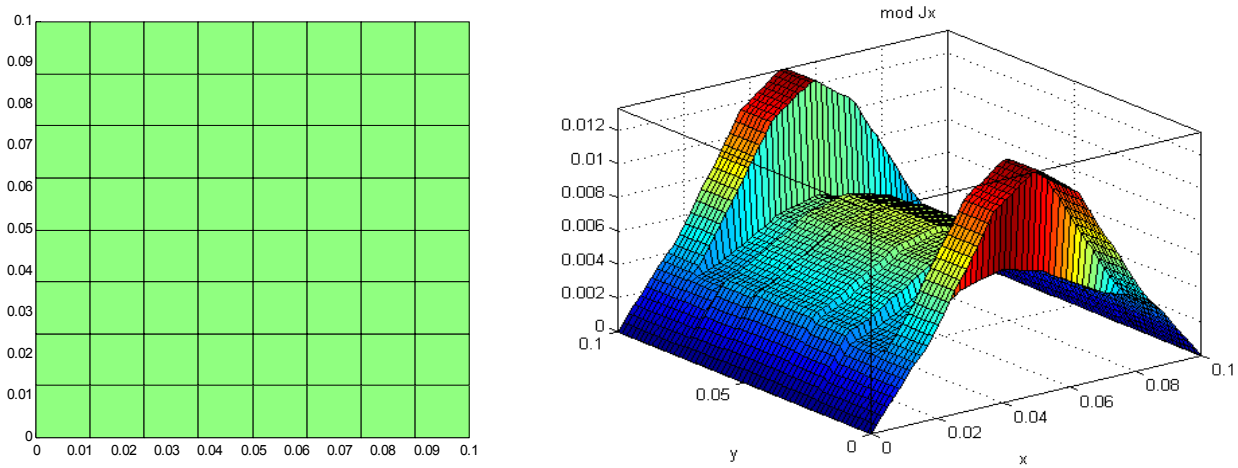

Figure 7. Current density on a square scatterer modeled with a regular mesh.

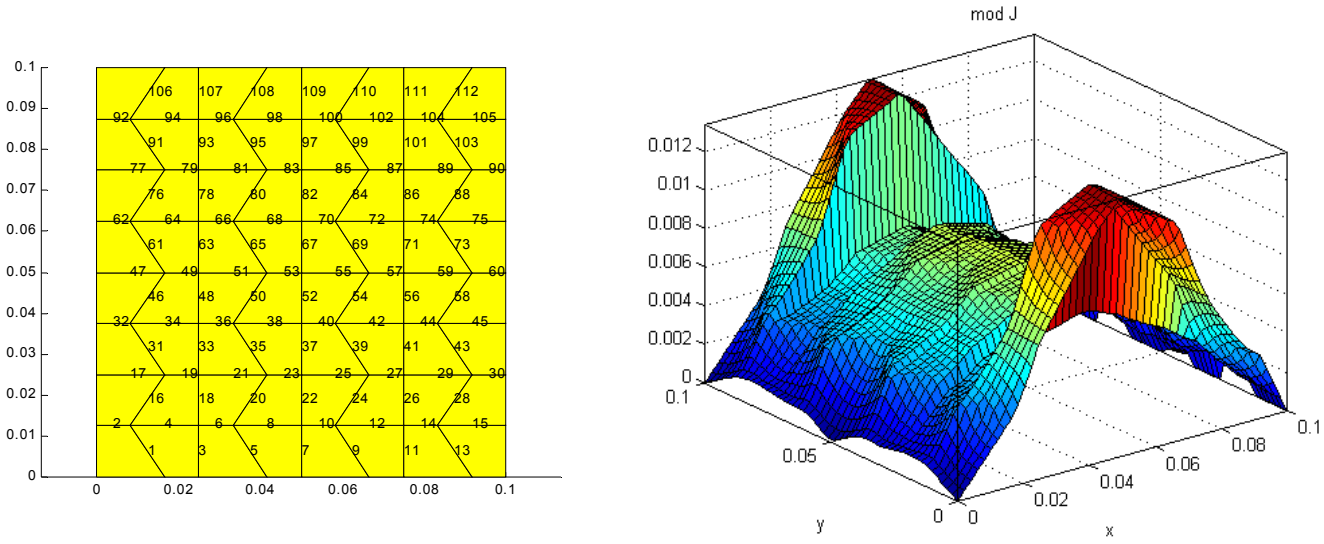

Figure 8. Current density on a square scatterer modeled with an irregular mesh.

It can be seen in Figure 7 and Figure 8 that results match for the two different meshes, particularly there is a good agreement in the level of current, as it can be checked looking at the maximum value of current density.

4.3 Stability study of quadrangular basis functions

In the following lines a test to check the stability of basis functions defined over quadrangular domains will be done. The test consists on computing the input impedance of a strip scatterer fed with a delta gap model and discretized in different ways. The discretization meshes go from the regular rectangular one to the triangular one, which are the two extreme cases, as it can be seen in Figure 9.

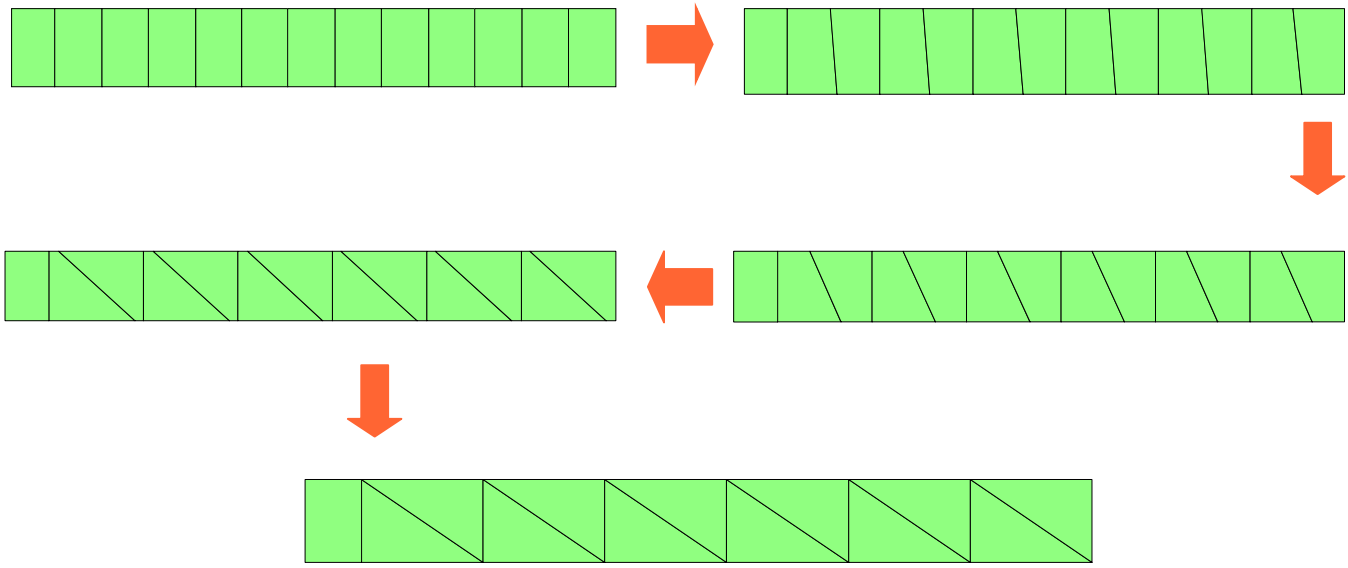

Figure 9. Evolution of the strip meshes from rectangular divisions to triangular ones.

If quadrangular basis functions are stable, the shape of the curve representing input impedance as a function of frequency must be the same.

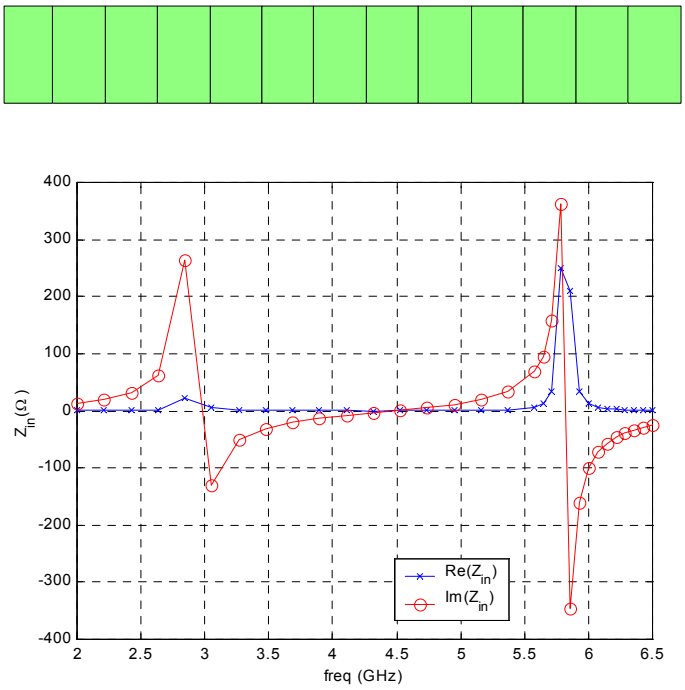

Figure 10. Input impedance: real part (blue, x) , imaginary part (red, o) for the rectangular case.

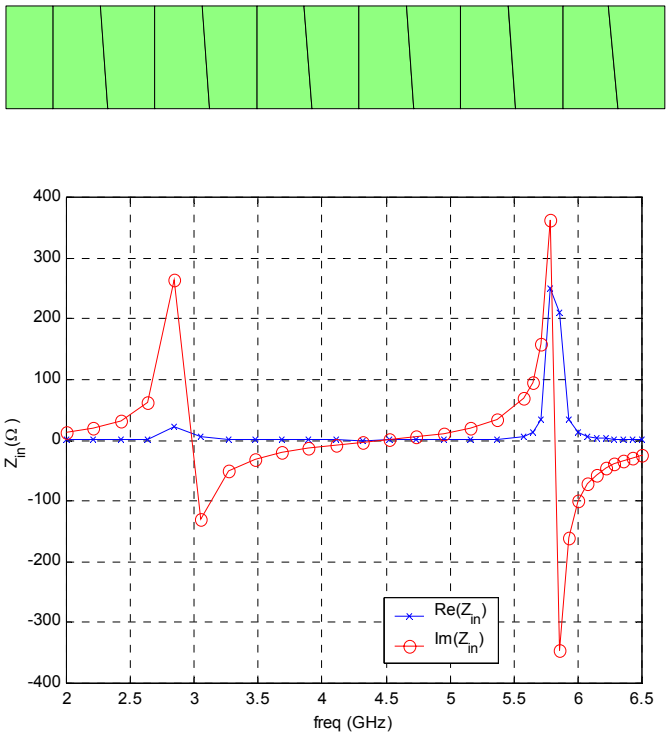

Figure 11. Input impedance: real part (blue,x) , imaginary part (red, o) for the first quadrangular case.

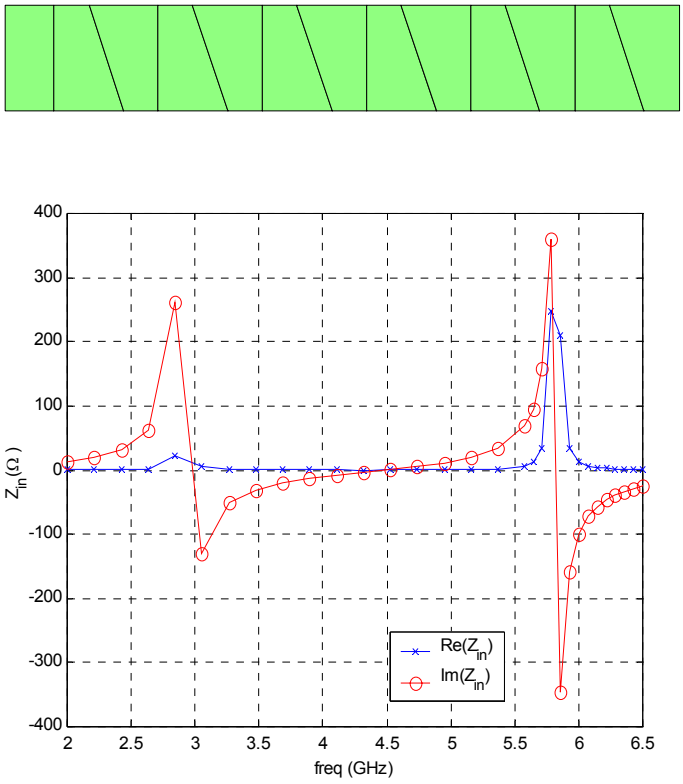

Figure 12. Input impedance: real part (blue,x) and imaginary part (red, o) for the second quadrangular case.

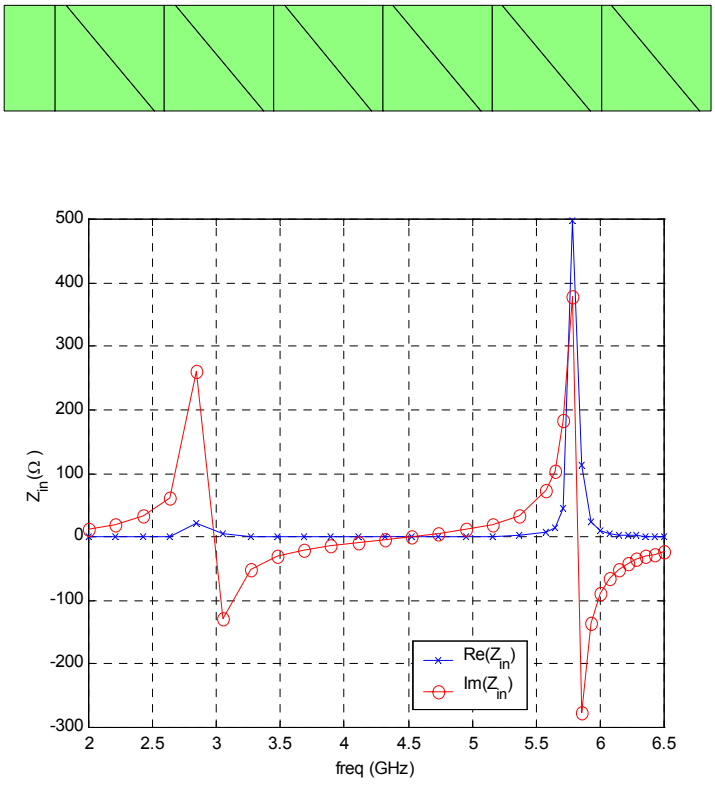

Figure 13. Input impedance: real part (blue,x) and imaginary part (red, o) for the degenerated quadrangular case.

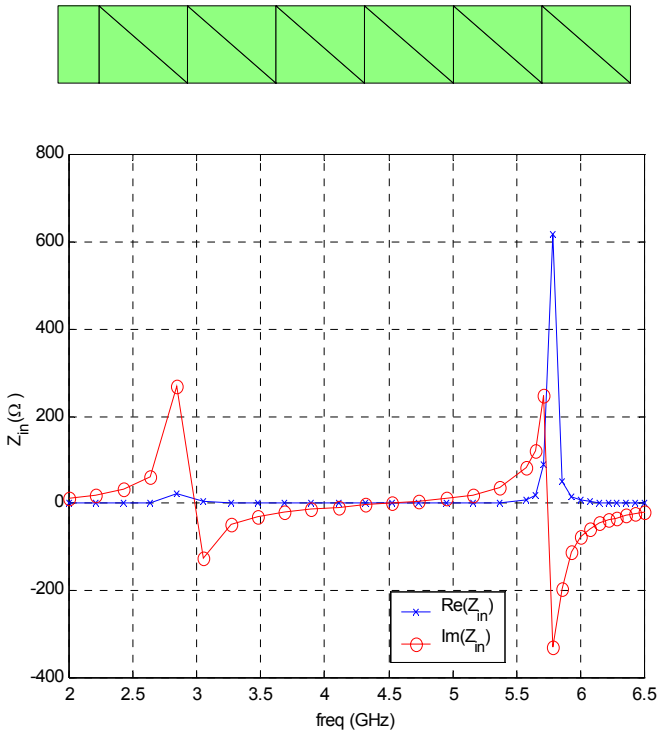

Figure 14. Input impedance: real part (blue, x) and imaginary part (red, o) for the triangular case.

In Figure 10 to Figure 14 it can be observed the same behaviour for the input impedance for all the different kind of meshes. In particular, when the differences in the mesh are minimum (Figure 10 and Figure 11, for instance) there is no difference at all in the results, but when differences in the mesh are notable (Figure 10, Figure 13 and Figure 14) there are some slight differences on the level. But it is the same for a traditional rectangular and triangular mesh, as structure is modeled in two different ways results cannot be exactly the same. The important thing to see here is that the frecuency behaviour remains the same for all the meshes, that is, resonances appear for the same frequencies. Hence, results converge and quadrangular basis functions are stable.

4.4 Quadrangular basis functions applied to bow-tie antenna.

A bow-tie antenna is a useful structure to test quadrangular basis functions, for mainly to reasons. The first reason for such an assertion is the fact of being a structure that suits perfectly a quadrangular mesh (up to now all the examples have been some rectangular/square structures forced to be meshed with quadrangular shapes, whereas they should have been 'naturally' meshed in rectangular/square subdivisions).

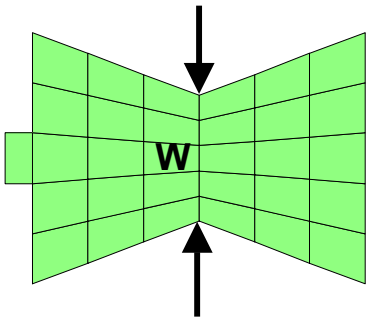

Figure 15. Structure under study.

The second reason is that when the connection between both sides of the antenna is only a point, the particular case of quadrangular basis function consistent on two triangles connected by a vertex, can be tested, as the antenna junction can be modeled with the help of these basis functions. This is an example that could be further implemented for the study of fractal structures, as the Sierpinski antenna, that has this kind of punctual connections.

The test is basically the study of input impedance of the antenna for different central widths (w), see Figure 15. Input impedance is computed numerically and compared with a commercial electromagnetic code (ADS). As our homemade code is not optimized, the amount of computation time is still quite high, and only eight points for each structure have been computed.

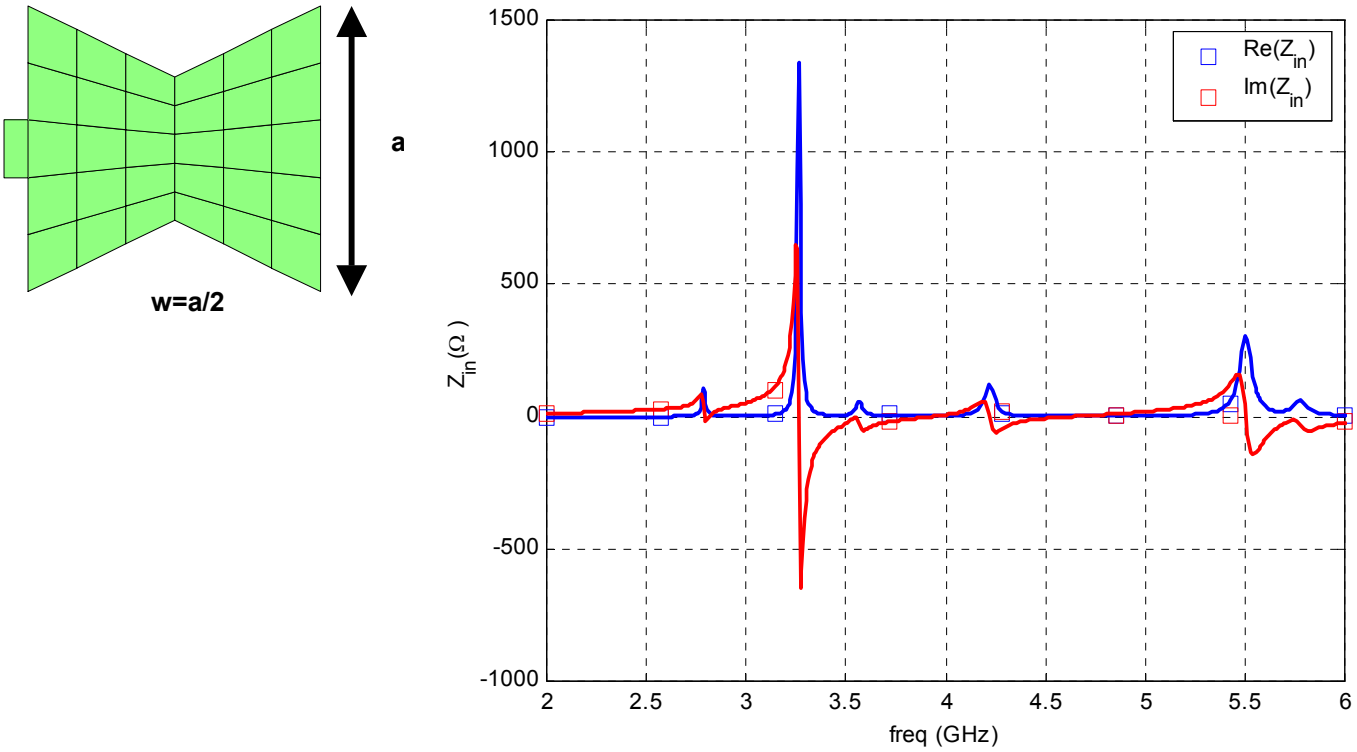

Figure 16. Input impedance: Solid line (ADS), squares (quadrangular basis functions). Real part (blue), imaginary part (red).

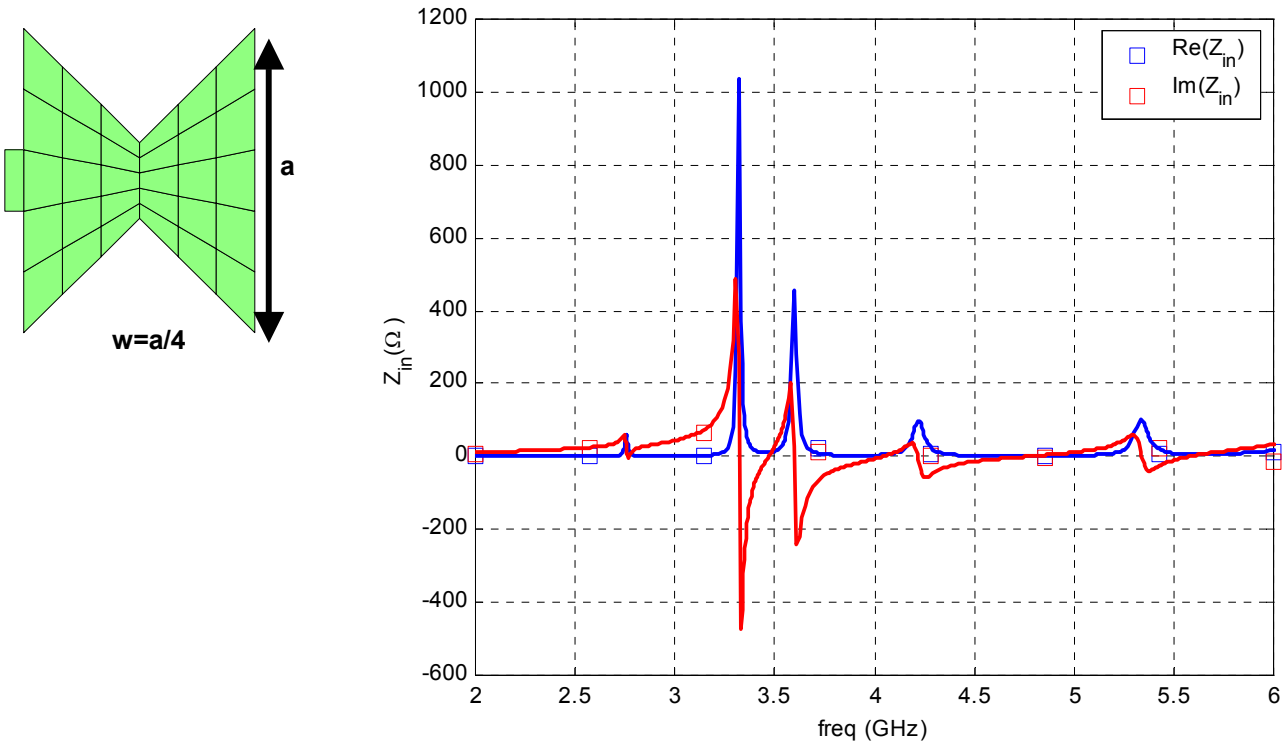

Figure 17. Input impedance: Solid line (ADS), squares (quadrangular basis functions). Real part (blue), imaginary part (red).

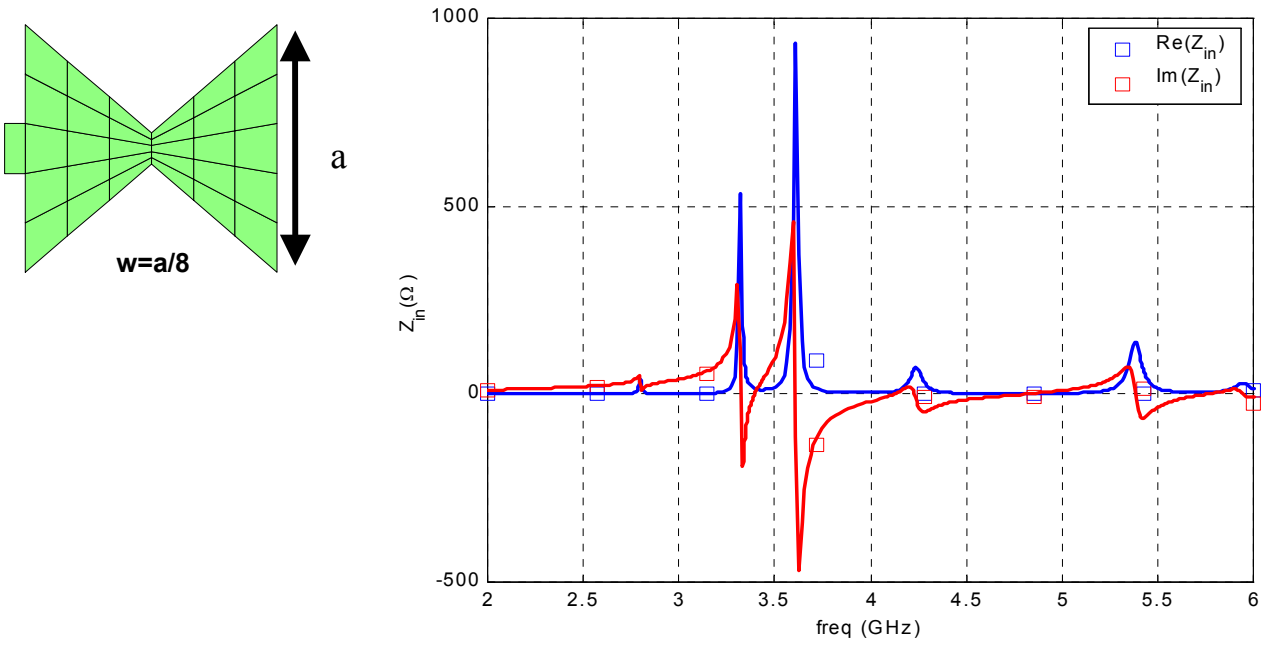

Figure 18. Input impedance: Solid line (ADS), squares (quadrangular basis functions). Real part (blue), imaginary part (red).

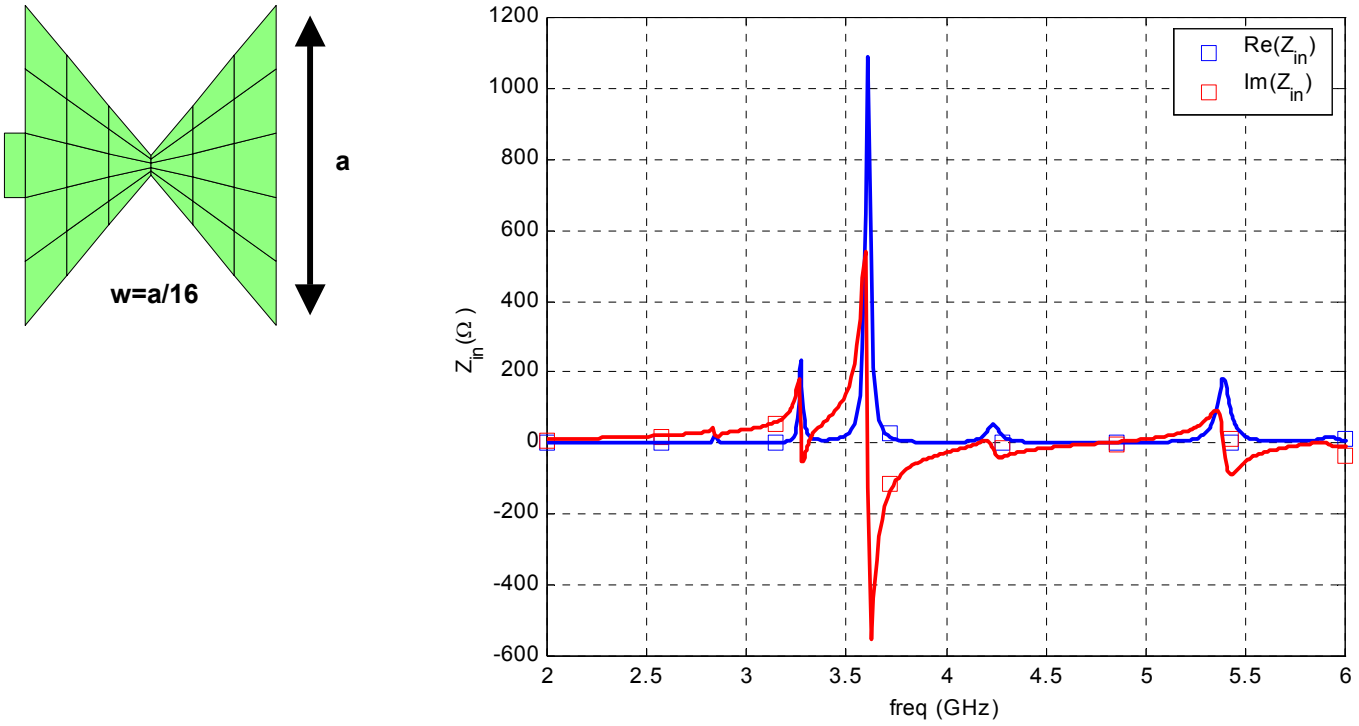

Figure 19. Input impedance: Solid line (ADS), squares (quadrangular basis functions). Real part (blue), imaginary part (red).

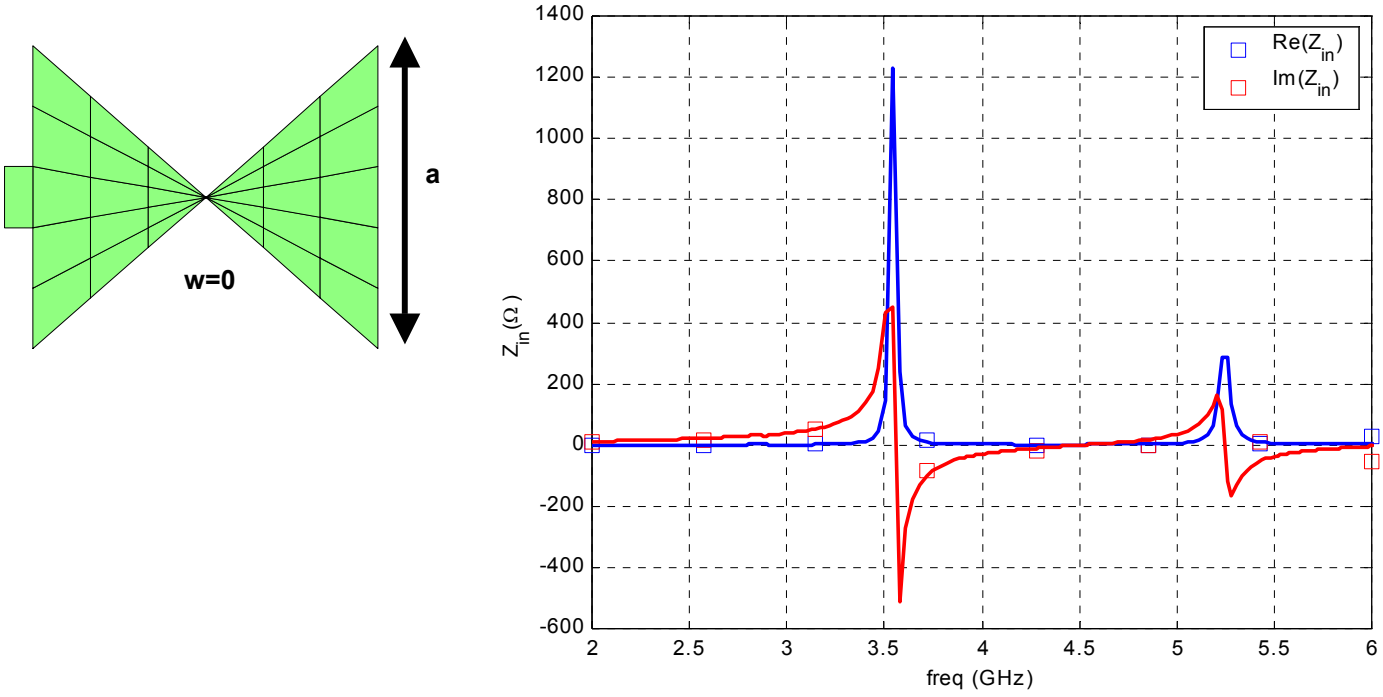

Figure 20. Input impedance: Solid line (ADS), squares (quadrangular basis functions). Real part (blue), imaginary part (red).

In general there is a good agreement in results comparing ADS results with the ones given by the code implementing quadrangular basis functions. For higher frequencies there is a slight mismatch, but it can be due to the fact that maybe mesh is not dense enough for these frequencies. In the last case, where the parts of the antenna are connected in a point, agreement is specially good, and this is really a clue to show that special basis function case with triangles connected in a vertex works. The next obvious step to do is the modelling of connections in a Sierpinski gasket antenna with this kind of function.
Another advantage of quadrangular basis functions is the simplicity of meshes. Traditional meshers have to model irregular shapes with the use of triangles as rectangles are not allowed due to the geometry of the problem, and this increases a lot the number of unknowns and the problem becomes cumbersome. Quadrangles produce a simpler mesh, with less number of unknowns, as where traditional meshes need two triangles for the modelling, we can now put a single quadrangle. Besides as the general expression for the function includes the particular cases of rectangular and triangular basis functions the use of mixed meshes is natural.

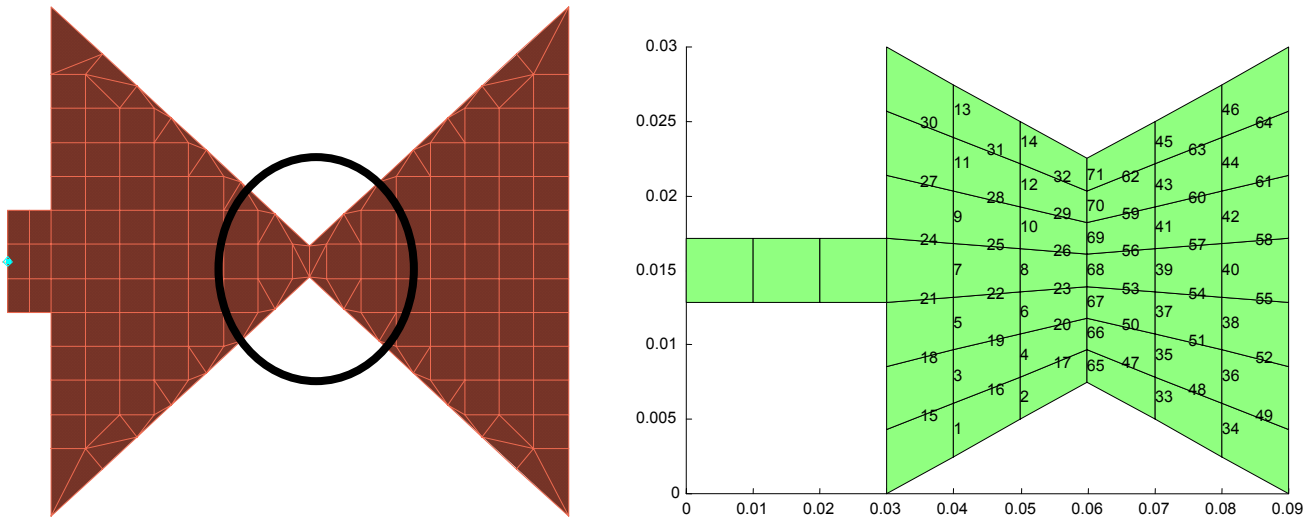

Figure 21. Examples of meshes: ADS (left) and quadrangular cells (right).

In some surface structures such as the Sierpinski Gasket shaped antenna the problem of connectivity appears. To model such a geometry with standard basis functions connected by an edge an artificial mesh has to be done, adding an additional cell making the connection between the two parts of the antenna.

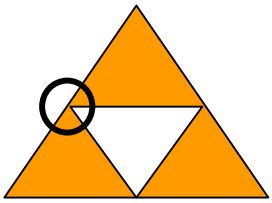

Figure 22. Problem of connectivity in the first iteration of a Sierpinski Gasket.

Here it has been tested a new method able to solve these connectivity problems in a bow-tie antenna. Whereas with a traditional mesh there is not connection in the central point as there are not standard basis functions connected in a point, with the new system there is a connection, as it can be seen in Figure 23, representing the surface density current on the antenna.

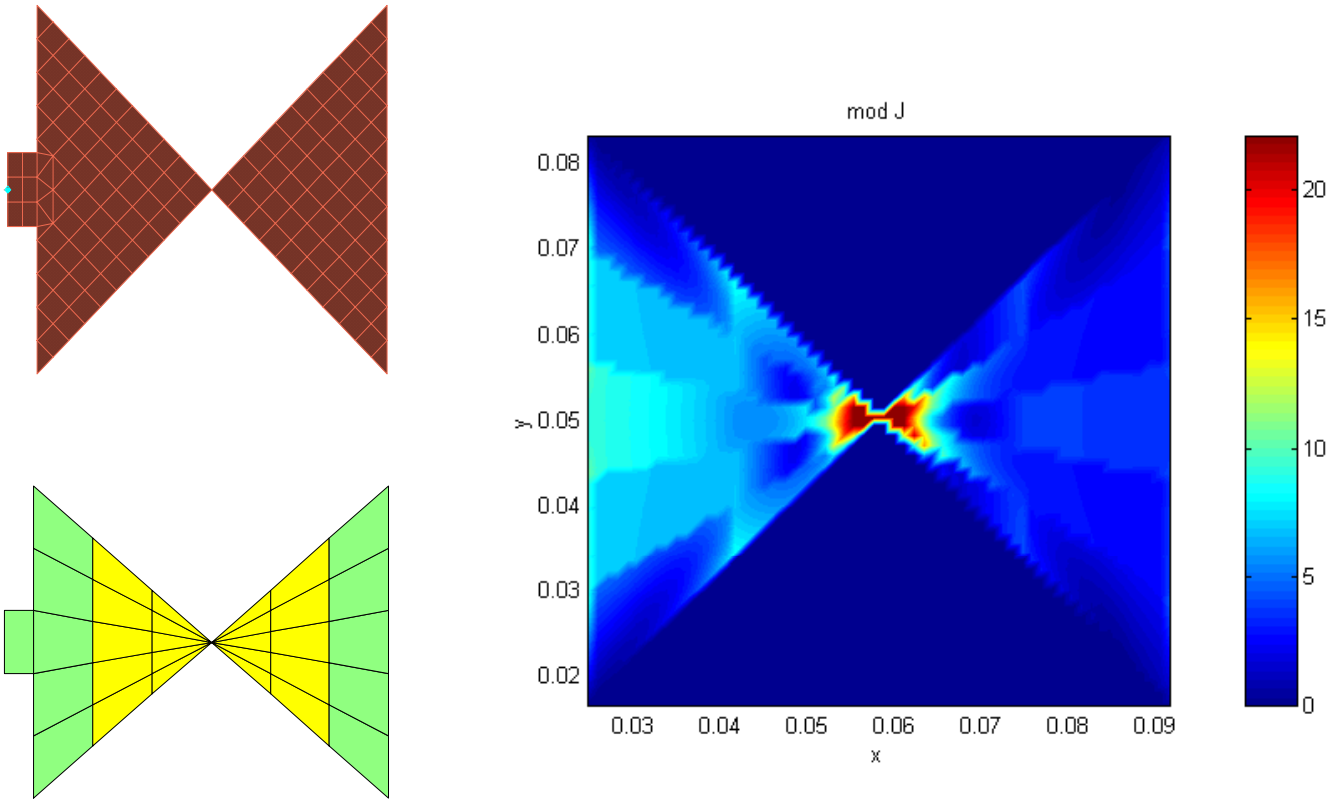

Figure 23. On the left ADS mesh (up) , quadrangular mesh (down) and on the right magnitude of surface density current obtained with quadrangular basis functions.

5 CONCLUSIONS

Quadrangular basis functions have been introduced and applied to the study of canonic structures (line and patch) and particular geometries including point connectivity (bow-tie antenna and Sierpinski triangles) and there is a good agreement with standard basis functions (rectangle and triangle).

6 REFERENCES

[1] Harrington R.F. “Field computation by Moment Methods”, IEEE Press 1993.

[2] Mosig J. “A new proposal for quadrangular basis functions in 2D implementations of MPIE”, internal report, LEMA-EPFL.

[3] Rao S.M., Wilton D.R., Glisson A.W., “Electromagnetic Scattering by Surfaces of Arbitrary Shape”, Antennas and Propagation, IEEE Transactions on , vol. 30 no. 3, May 1982.

[4] Mosig J.,Hall R.C., Gardiol F.E. “Numerical analysis of microstrip patch antennas”, in “Handbook of microstrip antennas”, Peter Peregrinus, IEE Electromagnetic Waves series, no. 28, London, 1989.

[5] Kolundzija B.M.,”Accurate solution of square scatterer as benchmark for validation of electromagnetic modeling of plate structures**”,** Antennas and Propagation, IEEE Transactions on , vol. 46, no. 7 , July 1998.

[6] Kolundzija B.M., “On the locally continuous formulation of surface doublets”, Antennas and Propagation, IEEE Transactions on, vol. 46, no. 12, December 1998.

7 DISCLAIMER

The work associated with this report has been carried out in accordance with the highest technical standards and the FRACTALCOMS partners have endeavoured to achieve the degree of accuracy and reliability appropriate to the work in question. However since the partners have no control over the use to which the information contained within the report is to be put by any other party, any other such party shall be deemed to have satisfied itself as to the suitability and reliability of the information in relation to any particular use, purpose or application.

Under no circumstances will any of the partners, their servants, employees or agents accept any liability whatsoever arising out of any error or inaccuracy contained in this report (or any further consolidation, summary, publication or dissemination of the information contained within this report) and/or the connected work and disclaim all liability for any loss, damage, expenses, claims or infringement of third party rights.

FRACTALCOMS

Exploring the limits of Fractal Electrodynamics for the future telecommunication technologies
IST-2001-33055

Currents and charges in printed T-junctions

Author(s):	**Eugenia Cabot, Juan Mosig**
Participant(s):	**EPFL**
Workpackage and task:	**WP3, T3.1**
Security:	**Public**
Nature:	**Report**
Version and date:	**1.0, 24-1-2003**

Total number of pages: 22

Abstract:

When building prefractal antennas of intricate shape (Koch, fractal tree) with microstrip or printed technology, discontinuities such as right-angle bends, T-junctions and crossings are encountered. In a boundary element discretisation, brute force approach would require an important computer effort and time for such complicated structures and would prevent us to analyse but the very first fractal iterations. Knowing the electromagnetic behaviour of these connections (mainly the distribution of currents and charges), a model could be created in order to substitute a brute force discretisation in the junctions. In the present work, a study of currents and charges in a T-junction is done in order to know which kind of global basis function would serve best as model for this type of junctions. This global basis should allow us to analyse pre-fractal antennas up to the iteration limit imposed by current technology.

Keyword list: microstrip discontinuities, T-junctions, pre-fractal structures and antennas, numerical methods, boundary elements, integral equations.

RELATED WP AND TASKS (FROM THE PROJECT DESCRIPTION)

WP3, T3.1.

1 INTRODUCTION

The electromagnetic description of junctions between conducting wires is a classical problem which can be solved in many different ways and with many degrees of approximation.
Traditionally, junctions are classified according to the number of arms or access, which define their topological properties. Then we have two-access (bends or L-junctions), three-access, (T- or Y-junctions), four access (X-junctions) and so on [1] . In this work we will always consider conductors printed in dielectric substrates backed by a ground plane (microstrip configuration). Figure 1 depicts the different junctions.

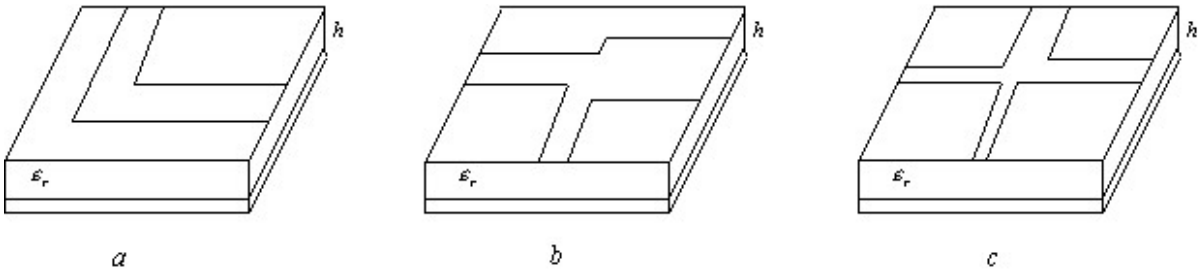

Figure 1. Different junctions: L-junction (a) , T- or Y-junction (b) and X-junction (c).

The interest of these elementary junctions is that they are the building blocks of many kinds of printed pre-fractal antennas whose study is the final goal of this project.
For instance in the Figure 2, L- and symmetric T-junctions are ubiquitous in the H fractal tree and in the Koch wire.

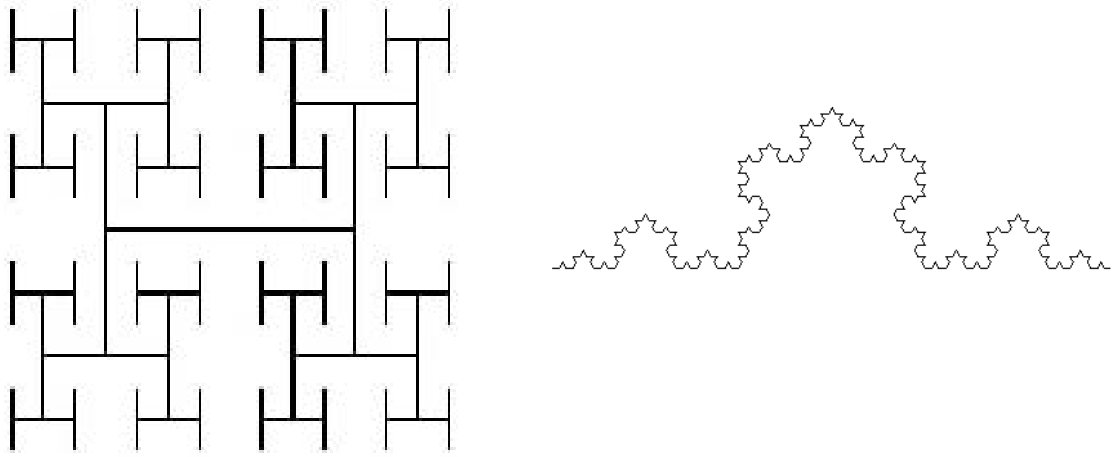

Figure 2. H-tree shape (left) and 4th Koch curve iteration (right).

According to the workplan of this project, we will concentrate here essentially on T-junctions. However the methods developed here could be applied to any other junction and some

alternative geometries will be considered when their study helps to clarify the sought-after properties of junctions.

2 RELEVANT PARAMETERS

We will consider essentially the case of printed "small junctions", i.e. junctions where all the relevant geometries and topological features can be enclosed by a circle whose diameter Φ is much smaller than the wavelength λ (Figure 3). Under this assumption, it is well known that the substrate parameters (permittivity ε_r and thickness h) are of minor relevance. In this study, we will essentially fix them to some reasonable values given by current technologies and no parametric study will be done on them.
The most relevant parameters in a small junction are the shape and topology, the ratio between different conductor strip widths and the excitation of the circuit. The frequency shouldn't have a major influence as far as the junction is out of resonance. However, it is judicious to perform full studies at different frequencies to confirm any general observed trend.
The main goal of our study is the analysis of the current and charge distribution in the junction. A detailed knowledge of these quantities is of paramount relevance to implement an efficient analysis of prefractal antennas, for instance by defining time-saving macrobasis functions with the correct current and charge distributions.

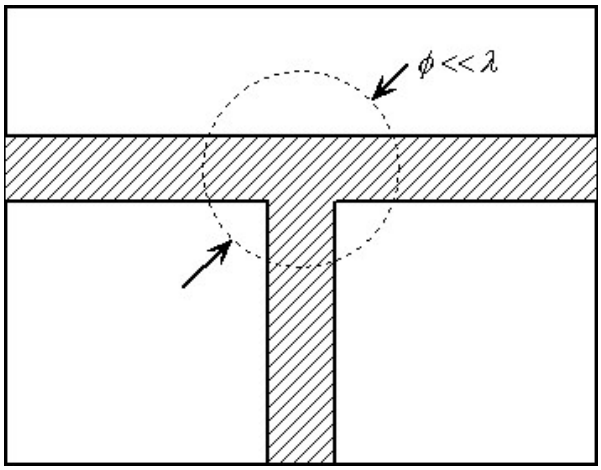

Figure 3. Dimensions of the junction.

3 ELECTROMAGNETIC MODELS FOR JUNCTIONS

The obvious model for analyzing printed junctions is a full-wave integral equation formulation numerically discretized with a boundary element method (or Method of Moments). It may be asked whether simpler models are useful, and we can think of quasistatic techniques and of the Transmission Line (TL) models. We will discuss now these models.

3.1 Static & Quasistatic models

For very low frequencies, displacement currents can be neglected and Maxwell equation

$$\nabla \times \vec{H} = \vec{J} + \frac{\partial \vec{D}}{\partial t}$$

becomes the Ampère theorem:

$$\nabla \times \vec{H} = \vec{J}$$

Consequently, the current distribution is solenoidal (divergenceless) since $\nabla \cdot \vec{J} = 0$ and continuity equation

$$\nabla \cdot \vec{J} + \frac{\partial \rho}{\partial t} = 0$$

asks for a charge distribution constant in time. Therefore the only viable possibility is $\rho = 0$.

Obviously, this approximation is too rough and would prevent us from studying in detail the charge distribution in junctions. But its main results must not be forgotten: Current distribution tends to be solenoidal at low frequencies and Kirchoff's law should be approximately satisfied in small junctions.

3.2 Transmission line model

The TL model should provide better results than a quasistatic model but it suffers from its inherent one-dimensional nature. Therefore, it cannot provide a detailed description of the current or charge distributions in the junction because the junction itself is reduced to a connection point in the TL model.

But at least some useful global indications should be obtained about the charge and current behaviour.

The TL model includes displacement current but neglects radiation phenomena. Typically, it should provide reasonable results for problems with overall dimensions below λ/4.

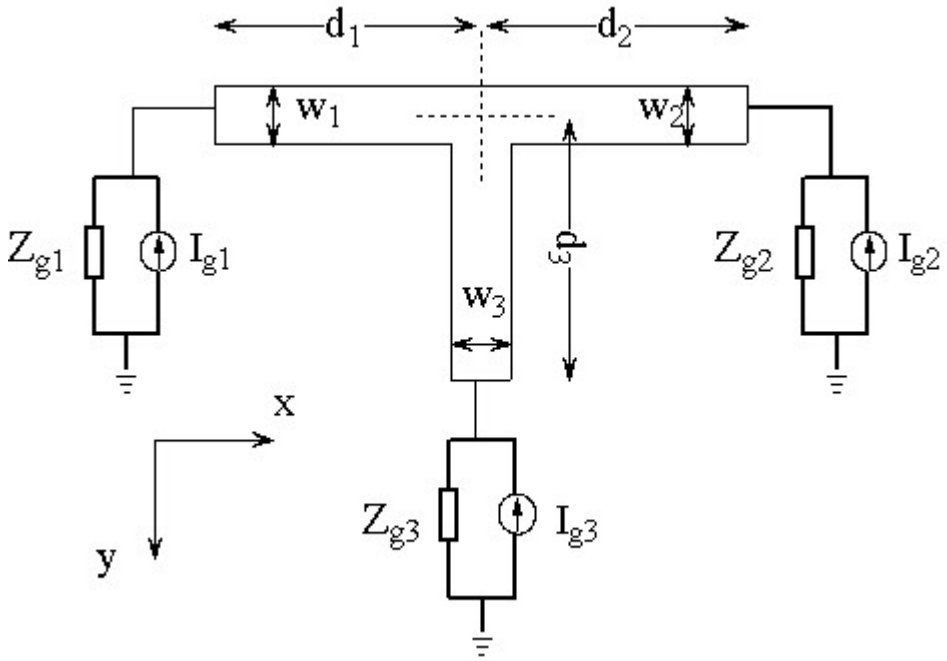

a

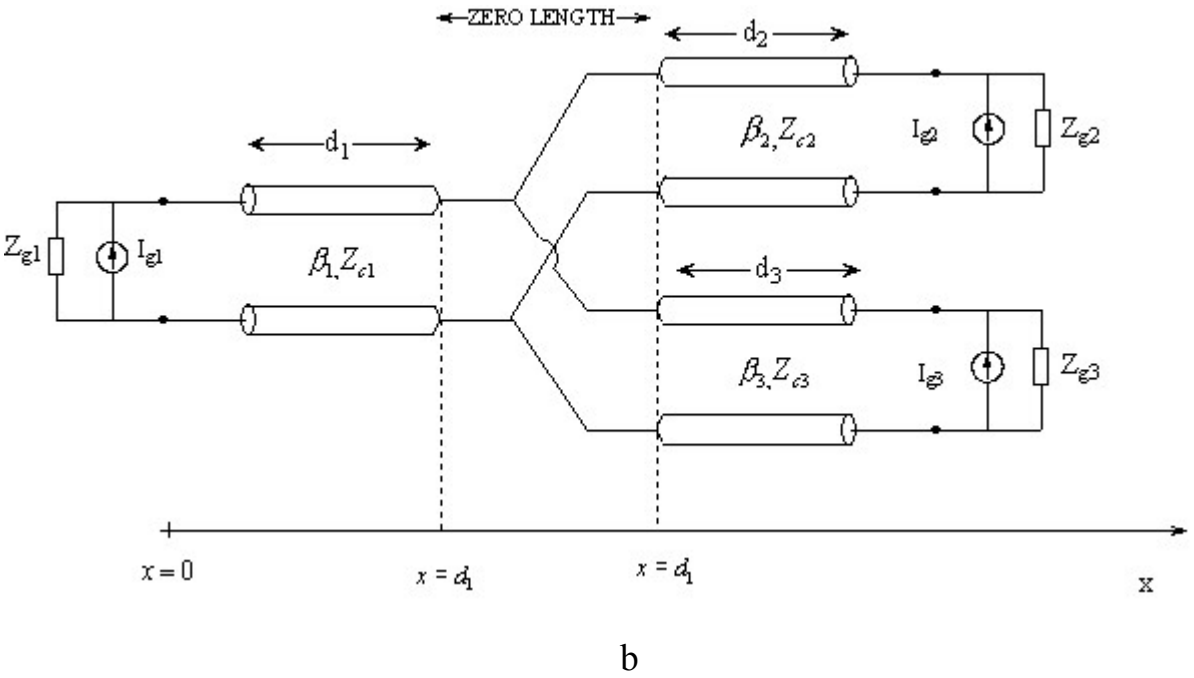

b

Figure 4. Real T-junction (a) and equivalent TL-model (b).

The TL model is depicted in Figure 4. Usually the needed characteristic impedances Z_{ci} are easily obtained as a function of the width w_i and the substrate parameters (ε_r, h). These 3 quantities also allow determination of an effective permittivity ε_{ei} and then $\beta_i = \omega\sqrt{\mu_0 \varepsilon_{ei}}$.

It is important to notice that the TL model cannot account for the orientation of printed strips. Therefore T- and Y-junctions are essentially equivalent in this model.

Also, with reference to Figure 4, if we have a symmetric T with $d_1 = d_2 = d_3$ and $w_1 = w_2 = w_3$, and the load impedances are identical (for instance open circuits $Z_{g1} = Z_{g2} = Z_{g3} = \infty$), the TL model will not predict any difference between a "horizontal" excitation ($I_{g1} = 1; I_{g2} = I_{g3} = 0$) and a "vertical" one ($I_{g1} = I_{g2} = 0,\ I_{g3} = 1$). This prediction seems to go against "physical intuition" and should be verified with a full-wave model.

3.3 Full-wave model

Once seen that the predictions with quasistatic model and transmission line model are incomplete, a study with a full-wave model is done to know in detail which are the current and charge distributions on the junction. The full-wave model used for this purpose is the Mixed Potential Integral Equation (MPIE) [2] solved with the Method of Moments (MoM). A rough mesh is used first to have an idea of the global variation of current and charge along the structure, but of course it does not give a lot of detailed information about their variation on the junction itself. Thus, a complementary study with a finer mesh is done in order to know better the behaviour of this kind of microstrip discontinuities. The investigation has been made for single port and multiport excitation, and for two different frequencies, one for which the longer arm length of the T is equal to λ/6 and so the junction dimensions are much smaller than λ, and for a higher frequency, for which the longer arm of the T is equal to λ/2 but the dimensions of the junction are still small with respect to λ.

4 RESULTS FOR TRANSMISSION LINE MODEL

4.1 Single excitation on generator 1

Currents and charges on branch 1 and branch 2 (see the equivalent model in Figure 4), with a single excitation in branch 1, are depicted in Figure 5 and Figure 6. For comparison it must be taken into account that horizontal coordinates are local ones, and for branch 1 they begin in the generator, whereas for branch 2 and 3 they begin in the junction.

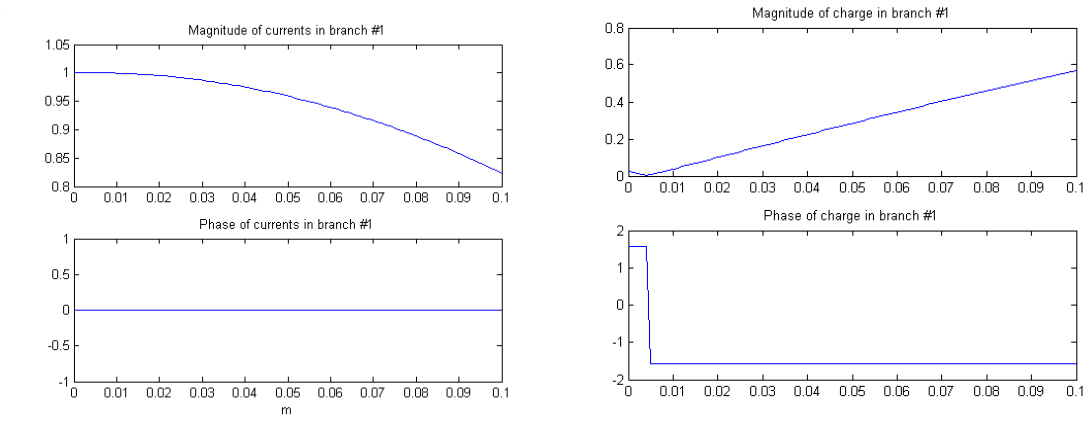

a b

Figure 5. Current magnitude and phase (a) and charge magnitude and phase (b) on branch #1.

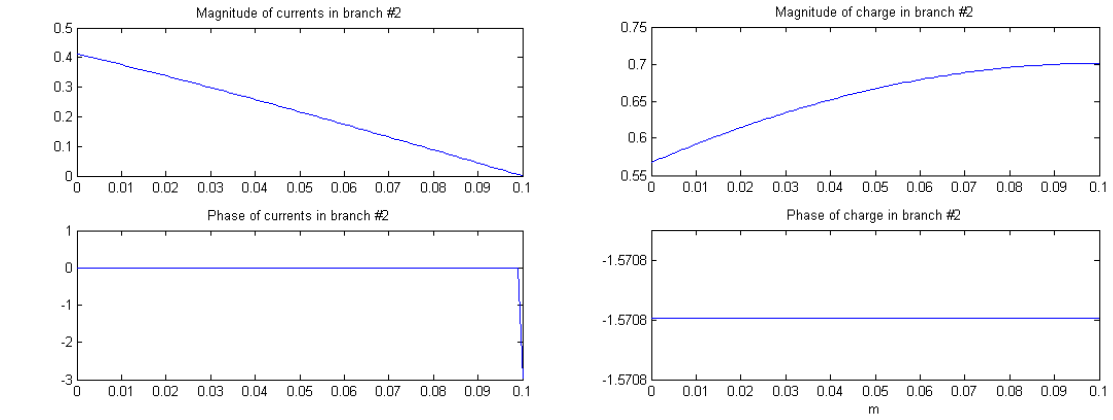

a b

Figure 6. Current magnitude and phase (a) and charge magnitude and phase (b) on branch #2.

The current begins with the value of $I_{g1=1}$ in branch one and it slowly decreases reaching a value *0.82* at the junction. After the junction and in the branch 2, the magnitude has exactly a factor ½ respect branch 1, since it is divided in two branches (the starting current in branches #2 and #3 is ≈ *0.41*), and it follows the same pattern, that is, it becomes smaller and smaller and ends in zero, as it is an open ended line (I_{g2}=0). The same behaviour is expected in branch 3, since a TL model cannot include asymetries due to different relative orientation of branches.

5 RESULTS FOR FULL-WAVE MODEL

5.1 Single excitation on the left horizontal arm

Before "attacking" the problem of a T-junction , a simple line is considered. The charge and current distribution along the line axis is studied having a single excitation in one of the ends. The results are shown in Figure 7 and Figure 8. The charge distribution has a minimum at the beginning of the line, thus, near the excitation, and then increases its value until the end of the line. This increment is more or less linear for low frequencies respect with the size of the line and it becomes more sinusoidal-shaped as the frequency increases, with a minimum in the middle of the line.

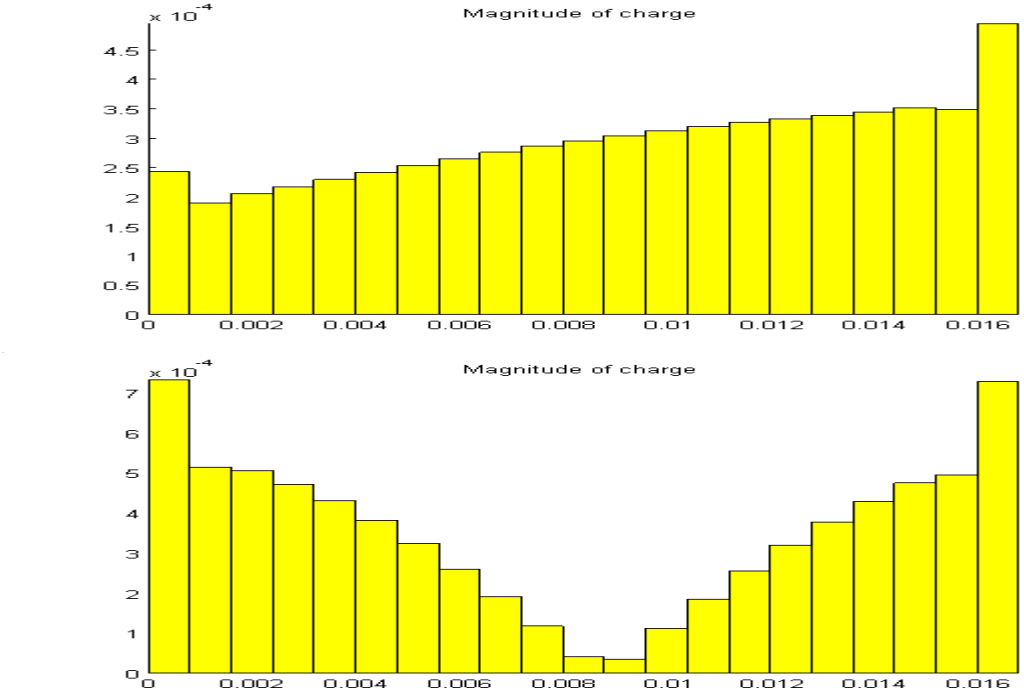

Figure 7. Magnitude of charge distribution on a line with a single excitation on the left for f1=3GHz (up) and f2=9GHz (down).

The magnitude of the current Figure 8 is decreasing until the end of the line, since it is open ended. For low frequency linear behaviour can be observed whereas for high frequencies resonances on the line can be encountered. In our case, we have the first resonance at 9 GHz as can be seen in Figure 8.

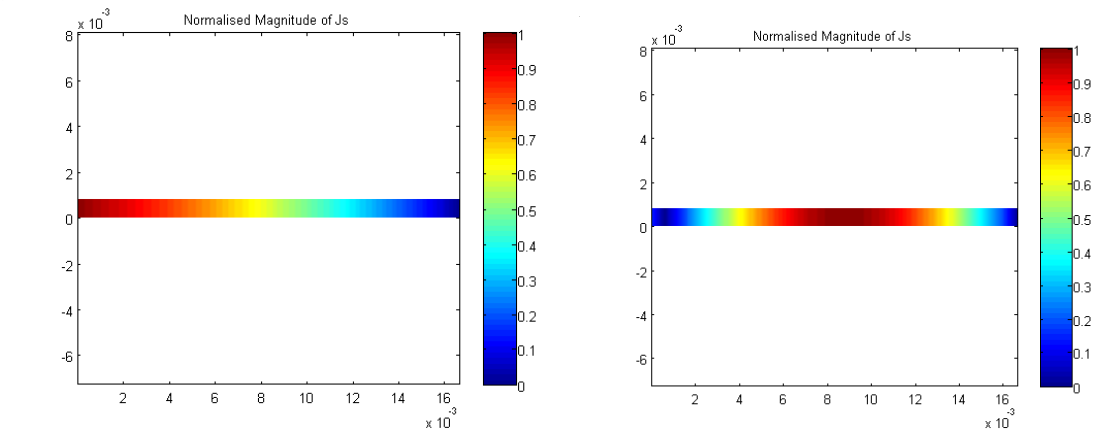

Figure 8. Current distribution on a line with a single excitation on the left for f1=3GHz (left) and f2=9GHz (right).

For the analysis of a T-junction a second line is added perpendicularly to the previous one in the middle. The T consists on 3 arms of the same length.
Adding a discontinuity in the microstrip line to create a T-junction the current flow is disturbed, and so the charge distribution is.

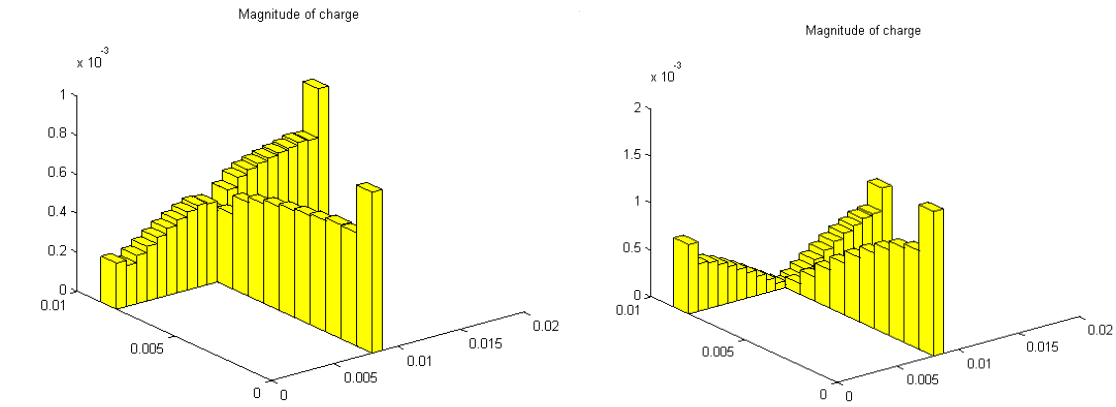

Figure 9. Magnitude of charge distribution for T-junction for f1=3GHz (left) and f2=9GHz (right).

Looking at Figure 9, it can be realized that the charge distribution, for a single excitation on the horizontal arm, grows in a similar way as on the line, but just until the junction. There, for a low frequency what is observed is that the two arms without excitation have, with a scale factor, the same charge and current distribution (seen in Figure 10) as if they were an unbent line. The current flows in the same way in the two secondary arms, as in the transmission line model. The difference is just that as the junction is not reduced to a point, we can see here that the charge has an important decrement in the junction.
In general the imaginary part of the charge is more than 3 orders of magnitude smaller than the real part, thus only magnitude is plotted here, knowing that most of the contribution is due to the real part.

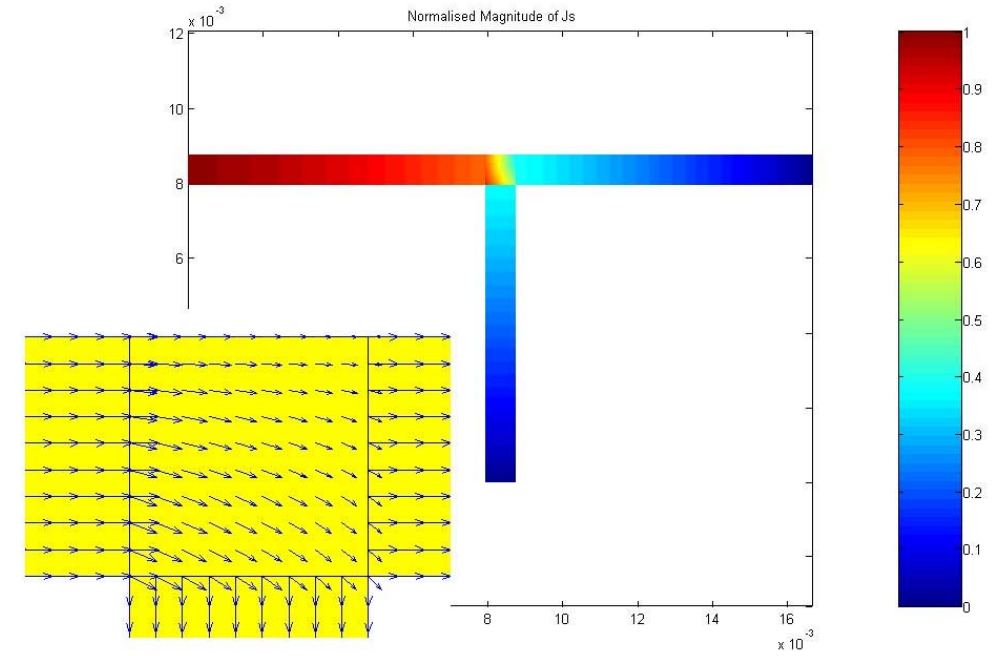

Figure 10. Current distribution for f1=3GHz in the case of single excitation on the horizontal arm.

On the contrary, for f=9GHz there is a different phenomena. Current gives priority to the vertical arm (see Figure 11).

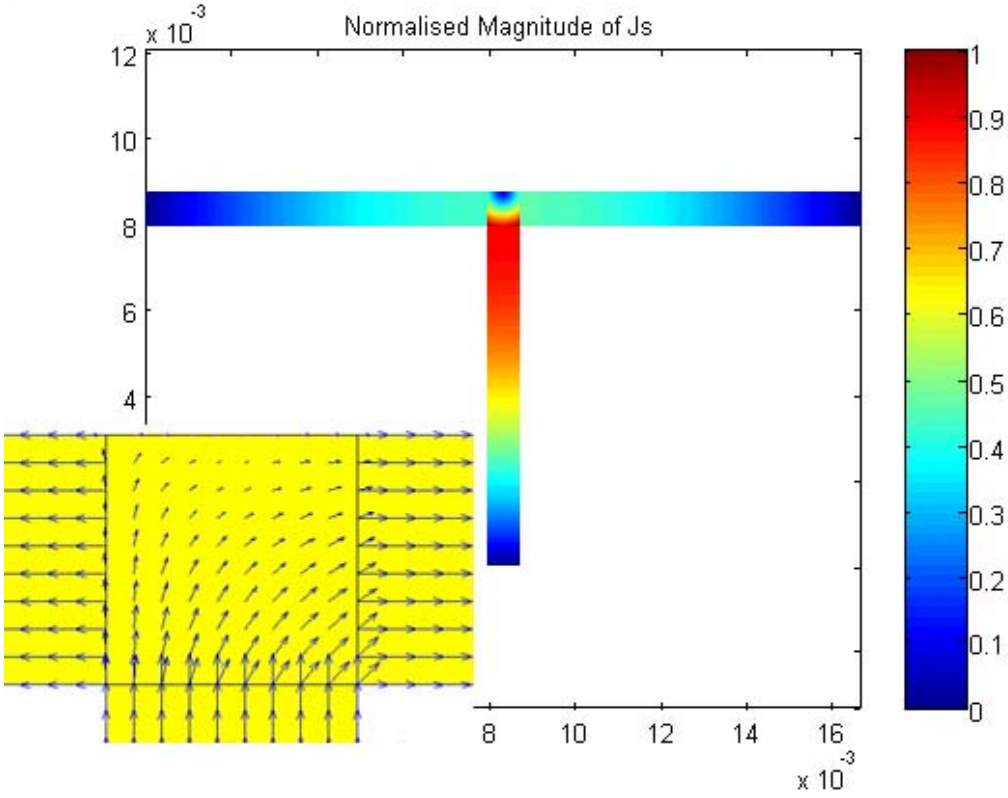

Figure 11. Current distribution for f1=9GHz in the case of single excitation on the horizontal arm.

Current is concentrated in the vertical arm because the fact of putting this third arm in the middle of the structure has killed the first resonance of the former line. For higher order modes with a minimum in the centre this is no longer the case (see Figure 12).

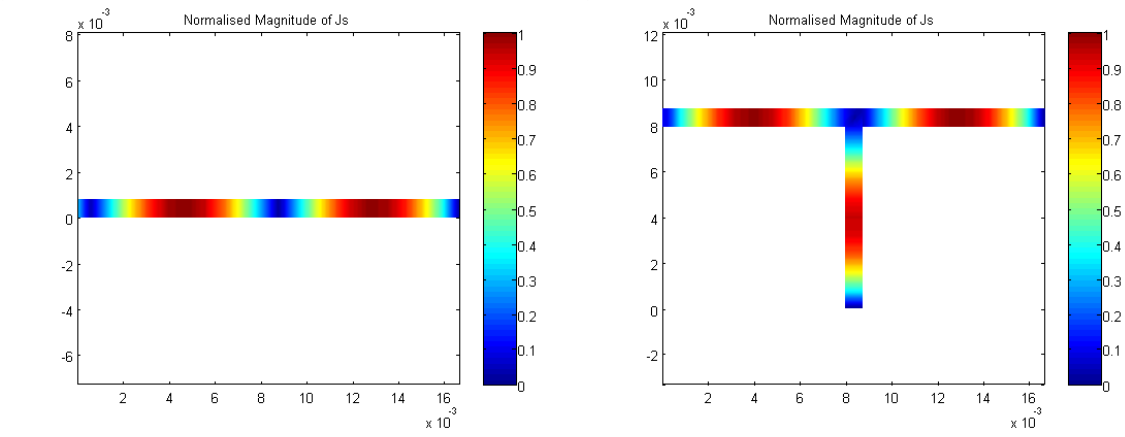

Figure 12. Normalised current distribution of the line and the T-junction for f=6f1, second resonance of the line, in the case of single excitation on the horizontal arm.

5.2 Single excitation on the vertical arm

As expected the excitation in the vertical arm gives a totally symmetric response. Again, for low frequencies it behaves like a line, that is, the charge grows from the arm where the excitation is to the end of the other two arms (Figure 13), and for higher frequencies the shape of the charge distribution is the same as if the excitation was on the horizontal arm.

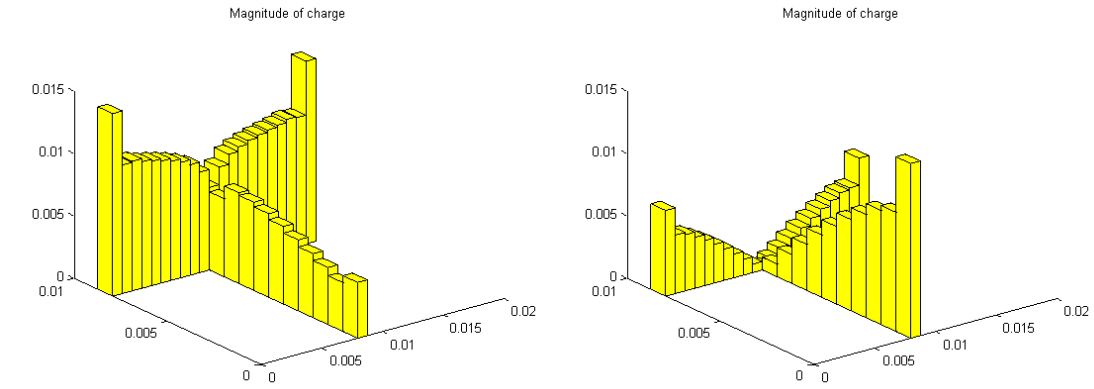

Figure 13. Magnitude of charge distribution for T-junction at f1=3GHz (left) and f2=9GHz (right) with excitation on the vertical arm.

So a first conclusion could be that the global behaviour does not depend on the position of the single-port excitation, because the observed phenomena are globally the same. But this cannot be affirmed for currents and charges in the junction itself in particular, we are only talking of the general shape of the charge and the current.

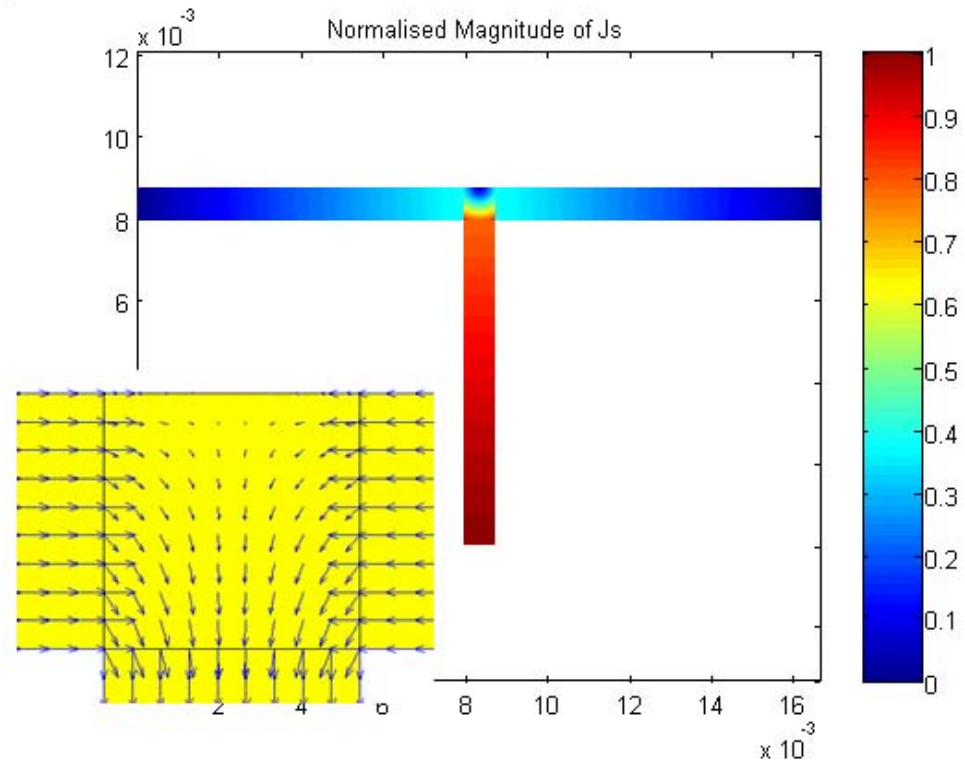

Figure 14.Current distribution for f1=3GHz in the case of single excitation on the horizontal arm.

Looking at the current distributions in Figure 14 and Figure 15, current density at low frequencies is concentrated in the arm with the excitation, as well as at higher frequency.

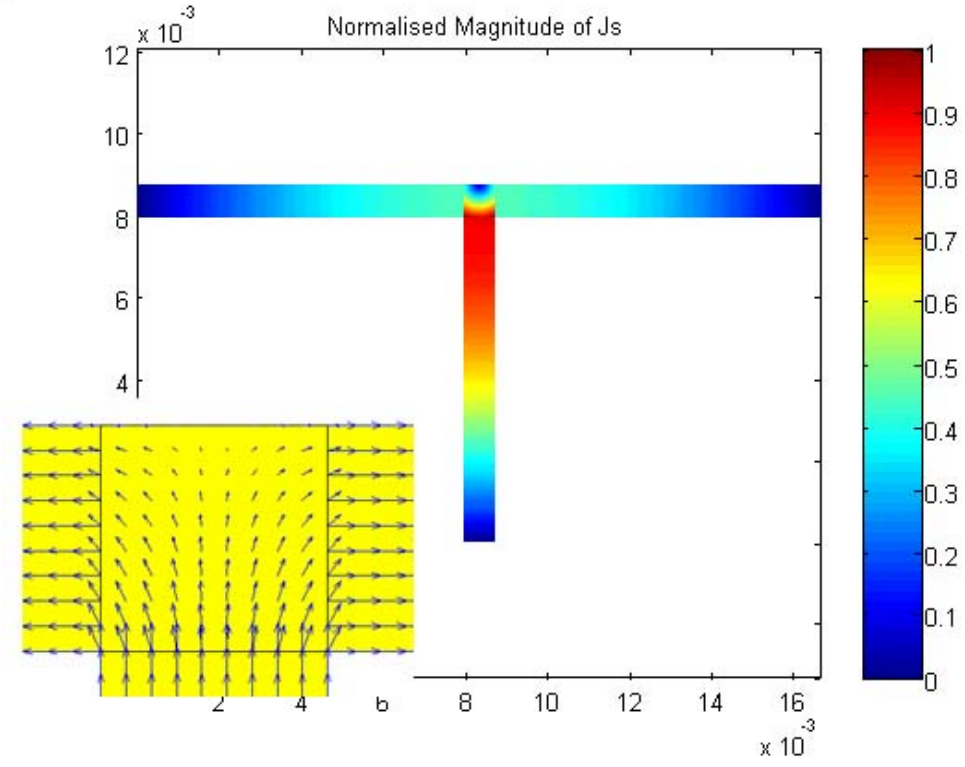

Figure 15. Current distribution for f1=9GHz in the case of single excitation on the horizontal arm.

5.3 Multi-port excitation on the horizontal arm.

If a multi-port excitation of opposite sign is forced on a line the response is expected to be the superposition of two single excitation cases. In the case of the charge, the superposition of two solutions of the kind in Figure 7 is obtained, see Figure 16. Again the variation at low frequencies is a linear one, whereas at higher frequencies it is not.

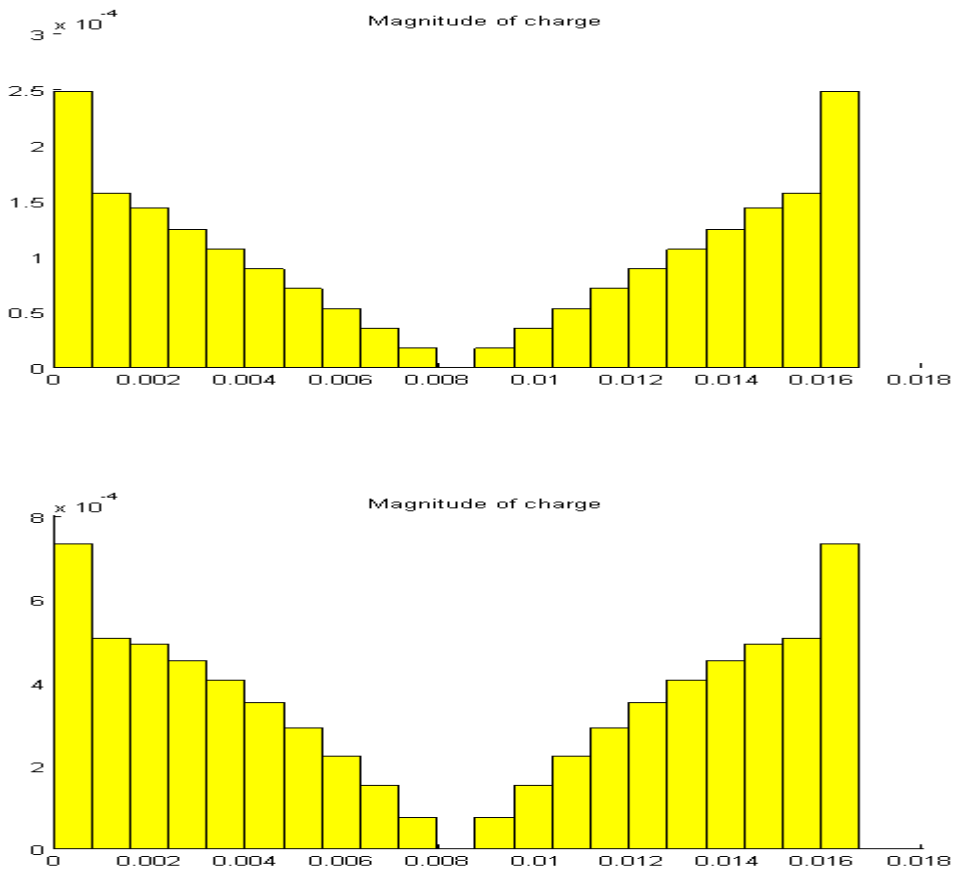

Figure 16. Magnitude of charge distribution on a line with a multiport excitation for f1=3GHz (up) and f2=9GHz (down).

In Figure 17 it is shown that for this kind of excitation in a line there is no significant difference between a low and high frequencies from the point of view of current distributions.

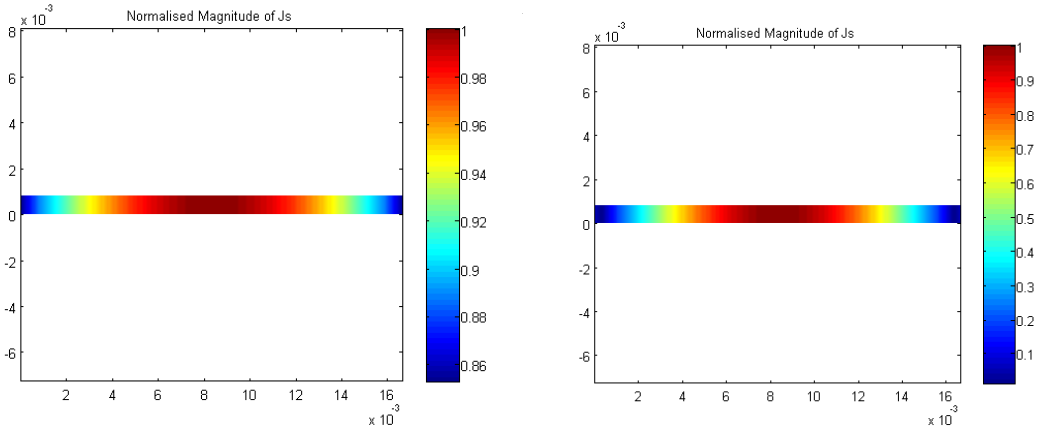

Figure 17. Current distribution on a line with a multiport excitation for f1=3GHz (left) and f2=9GHz (right).

With this kind of excitation the current is enforced to flow on the horizontal arm (Figure 19). So for both low and high frequencies the shape of the charge distribution is the same as if the vertical arm of the T junction was not there as it is corroborated in Figure 18.

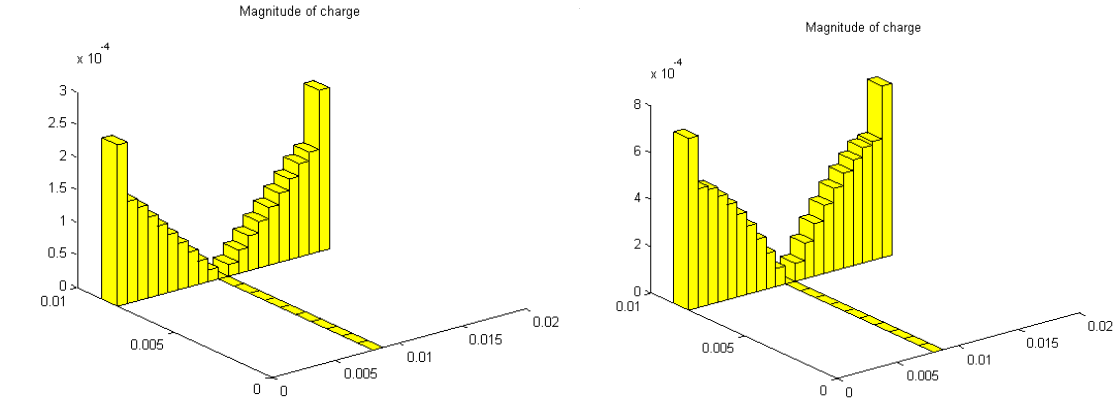

Figure 18.Magnitude of charge distribution on T-junction with a multiport excitation at f1=3GHz (up) and f2=9GHz (down).

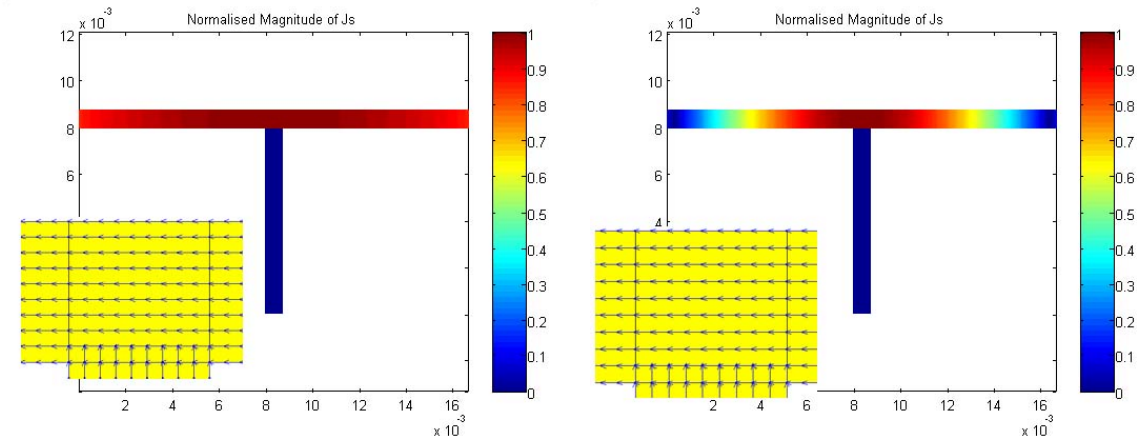

Figure 19. Current distribution on a T-junction with a multiport excitation on the horizontal arm at f1=3GHz (left) and f2=9GHz (right).

5.4 Multi-port excitation on the horizontal and the vertical arm.

Now the multiport excitation with different sign is applied on the left horizontal arm and the vertical one. It is expected a similar effect than in the pure horizontal multiport excitation case, just with the difference that current flow is now enforced in a perpendicular direction.
In Figure 20 it is shown that indeed, charges have the same distribution than in the other multiport case on the left horizontal arm and on the vertical arm. A slight difference, however, is that on the right horizontal arm there is still a residual charge, due to the fact that there is a "leak" of current towards this arm. This effect could not be seen in the plot of current magnitude, but it appears if the logarithm of current magnitude is plotted (Figure 21).

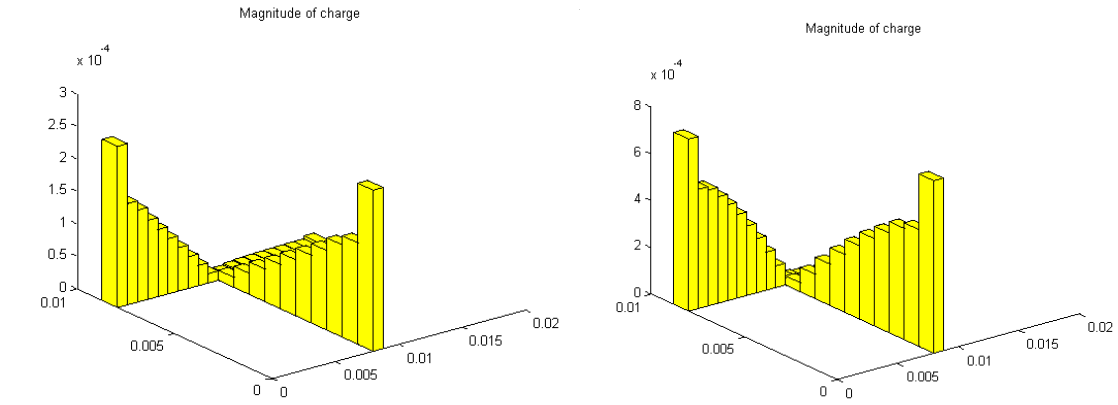

Figure 20. Magnitude of charge distribution on a line with a multiport excitation (horizontal-vertical) at f1=3GHz (up) and f2=9GHz (down).

The enforcement of current flow in the perpendicular arms does not give such a neat result as in the horizontal case, but still, it can be considered that the same effect is happening.

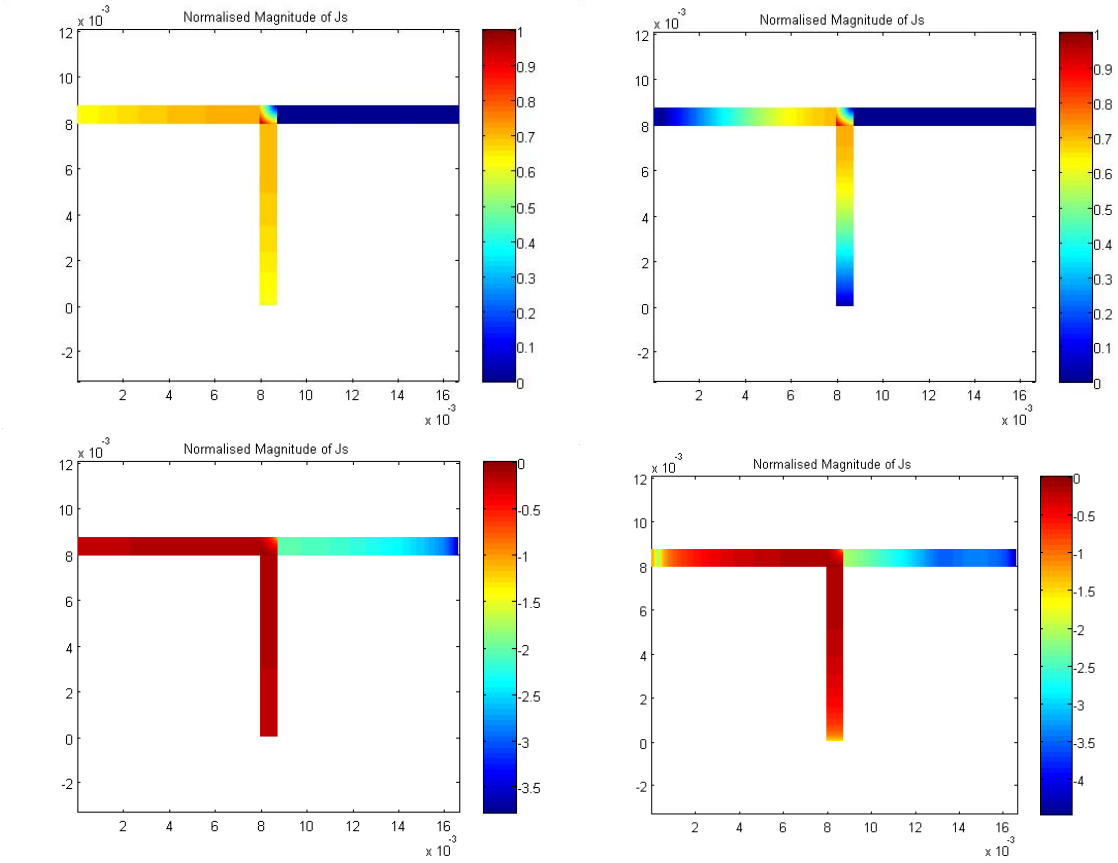

Figure 21. Normalised current distribution on a T-junction with a multiport excitation on the horizontal-vertical arm at f1=3GHz (left) and f2=9GHz (right). The logarithm of magnitude of the current is below.

A rough mesh as it has been used in the precedent analysis is only useful to have a general impression of charge and current behaviour on the T-junction, but it does not give many details on the current and charge distributions on the junction itself. Trying to improve this fact, a finer mesh is used. Concretely, each new cell surface is 1/25 of the cell surface used before. As the results are basically the same than before and in order not to be repetitive, a synthesis is made by means of two tables. Table 1 contains results for f=3GHz and Table 2 for f=9GHz. Results are computed for all the different excitations explained in the precedent pages. The presented results are charge magnitude and current magnitude. As before the

charge magnitude bar plot is given. But in addition to that, a flat colour of the charge magnitude is presented to see its distribution in the junction. But as the magnitude of the charge in a linear scale seems to be constant in the junction, the decimal logarithm of the charge magnitude is presented. As it can be seen in Table 1 and Table 2, when decimal logarithm is taken there is a great enhancement of charge singularities. But ignoring singularities, for low frequencies the charge can be said to be constant in the junction, whereas the same thing cannot be said for high frequencies.

F1=3GHz			
	Magnitude of the charge	**Log10(charge)**	**Normalised Current Density Magnitude.**
Single-port horizontal excitation.	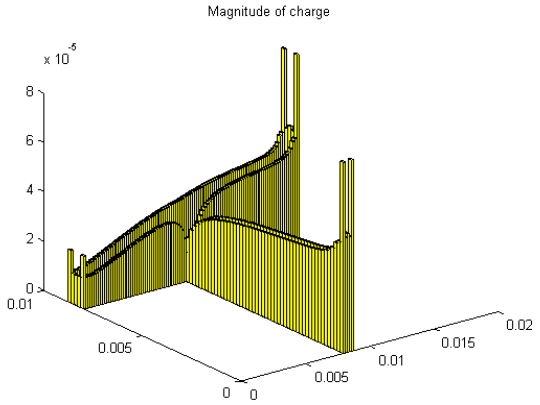	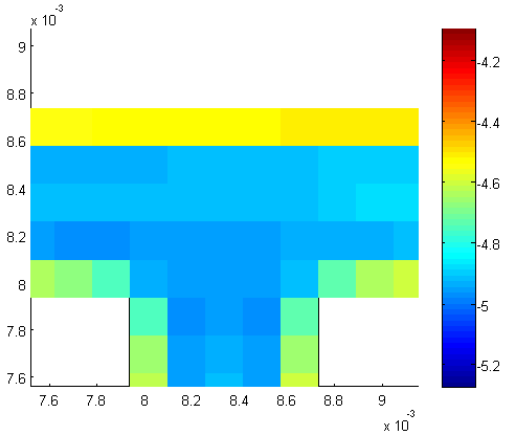	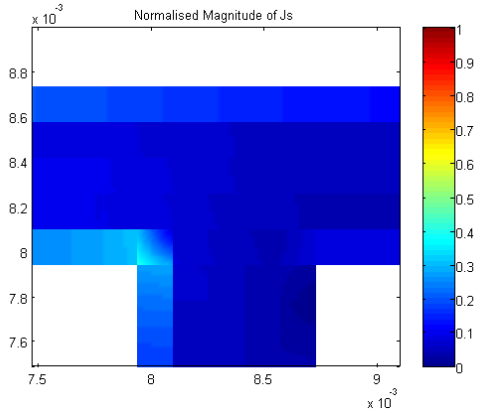
Single-port vertical excitation.	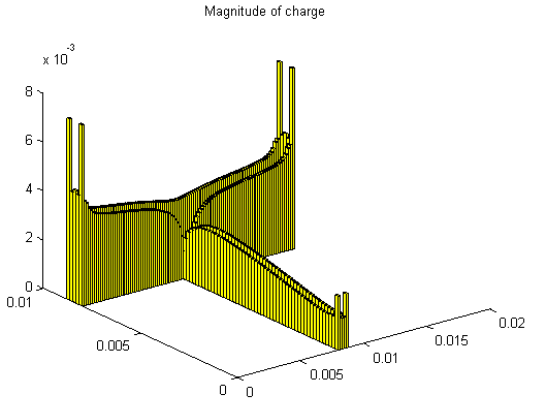	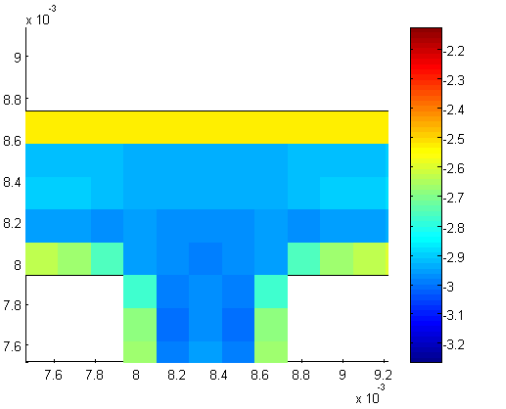	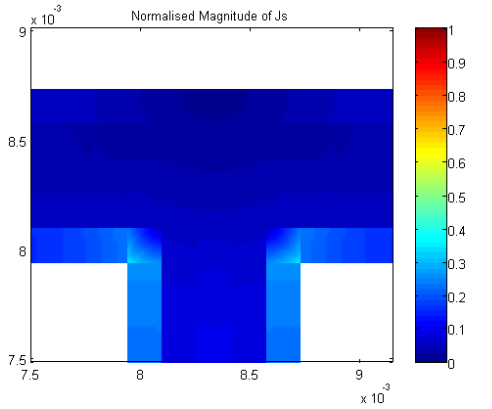

Multi-port horizontal.	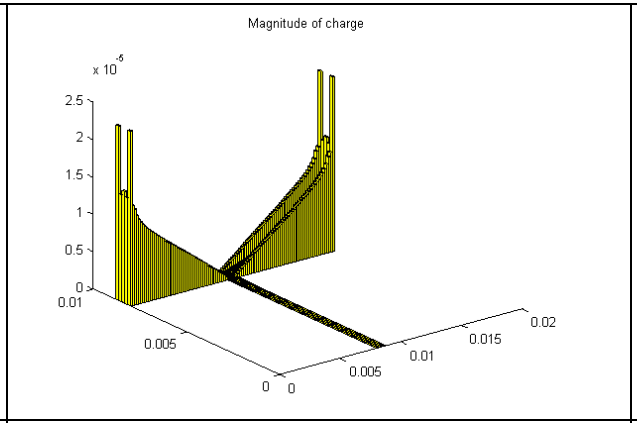	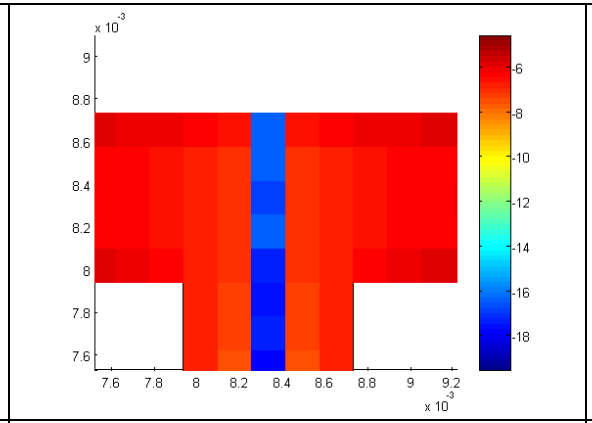	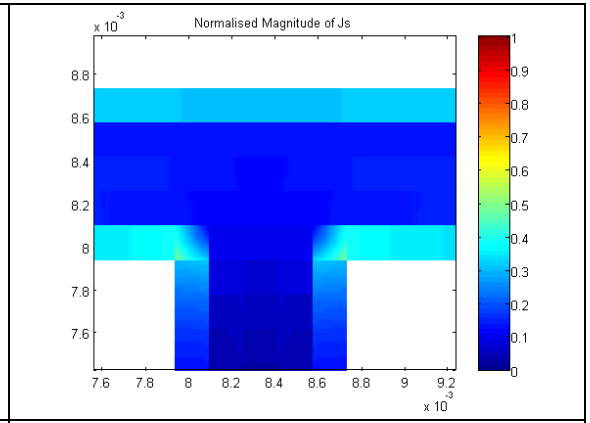
Multi-port mixed.	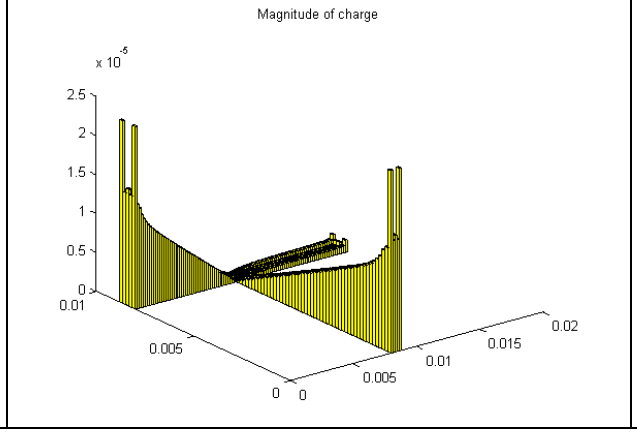	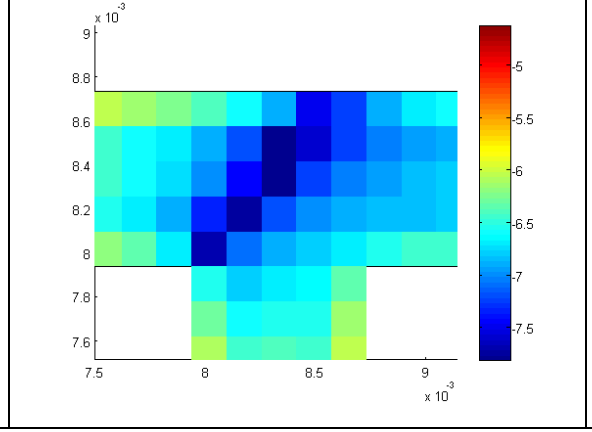	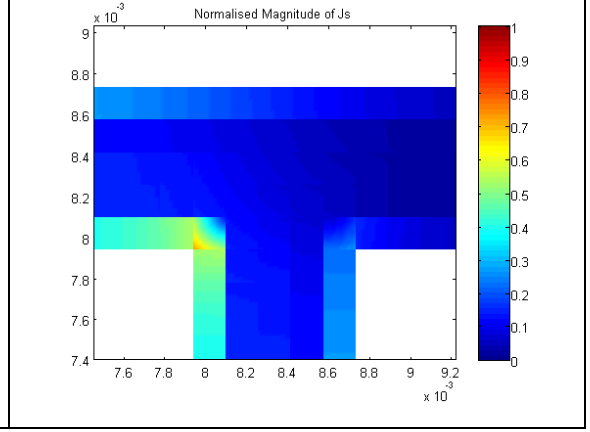

Table 1. Charge magnitude and current magnitude at f=3GHz, for 4 different kinds of excitations.

F1=9GHz			
	magnitude of the charge	**Log10(charge)**	**Normalised Current Density Magnitude**
Single-port horizontal excitation.	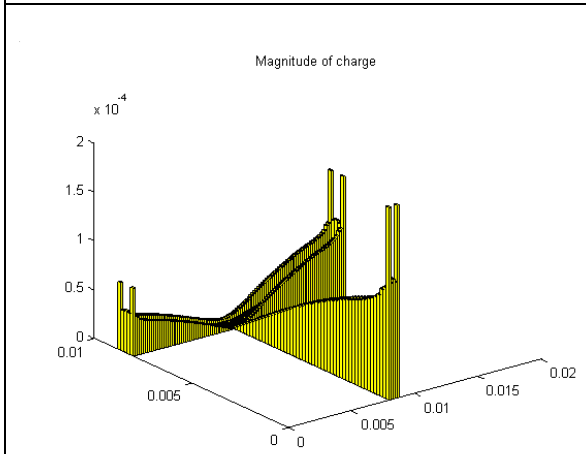	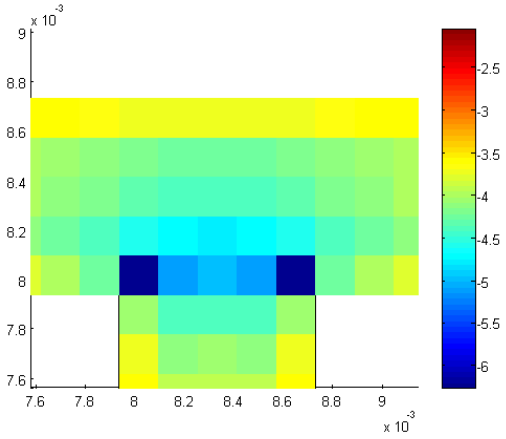	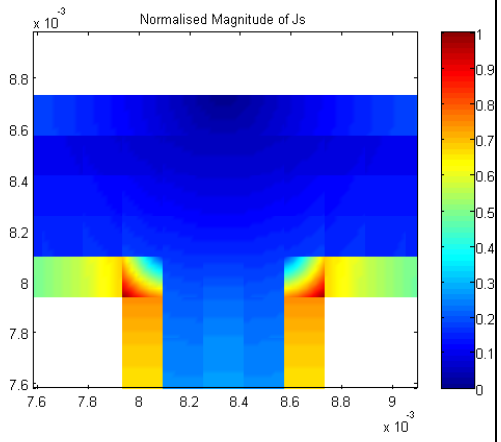
Single-port vertical excitation.	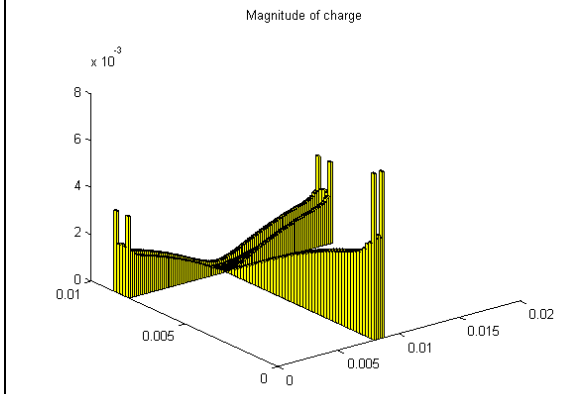	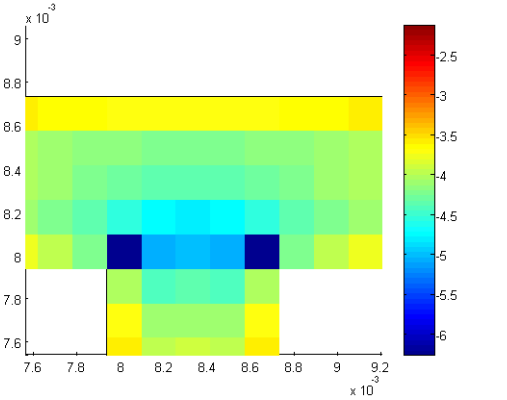	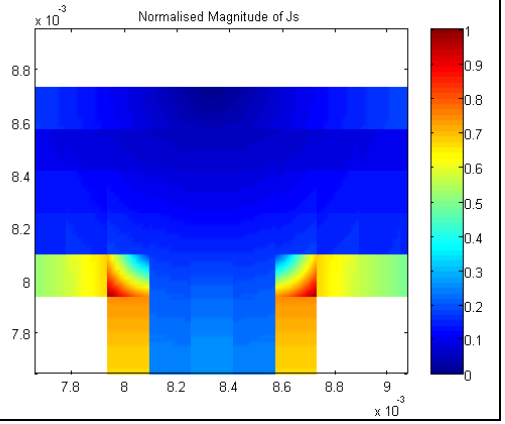

Multi-port horizontal.	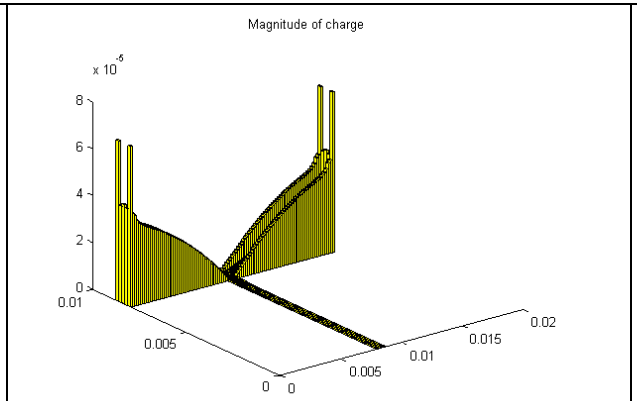	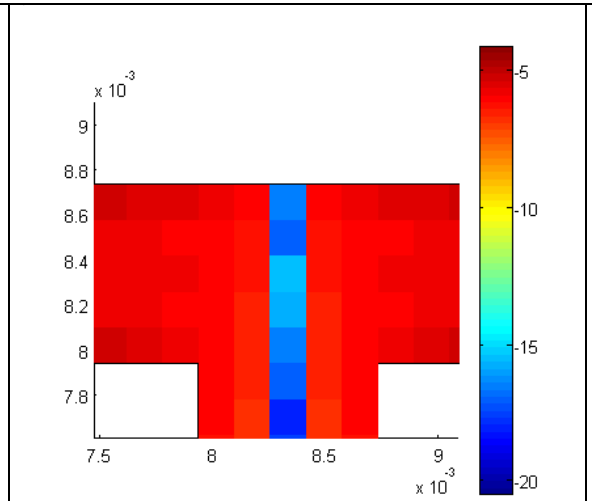	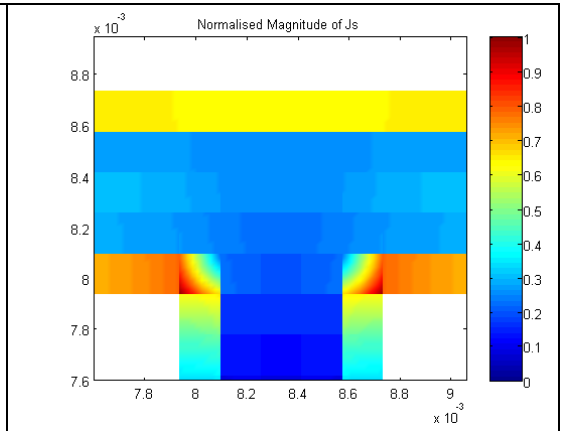
Multi-port mixed.	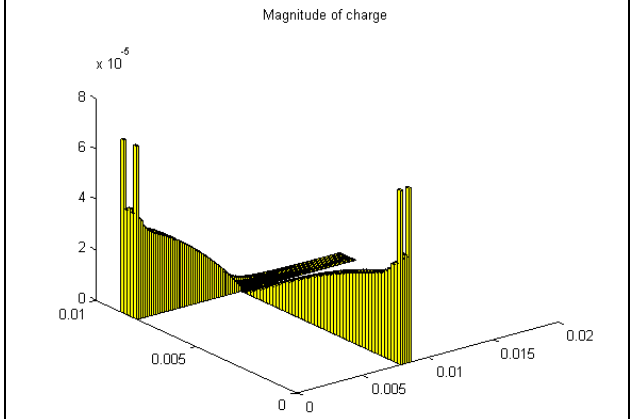	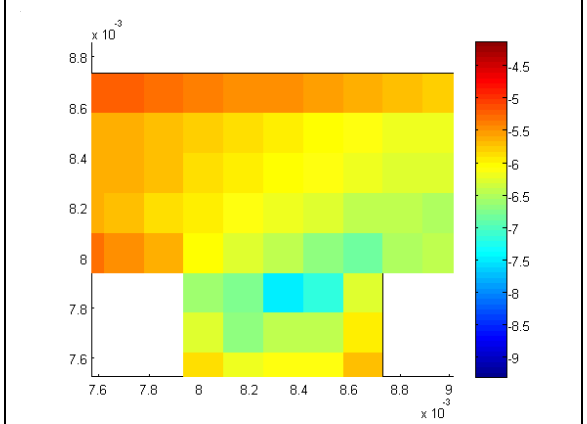	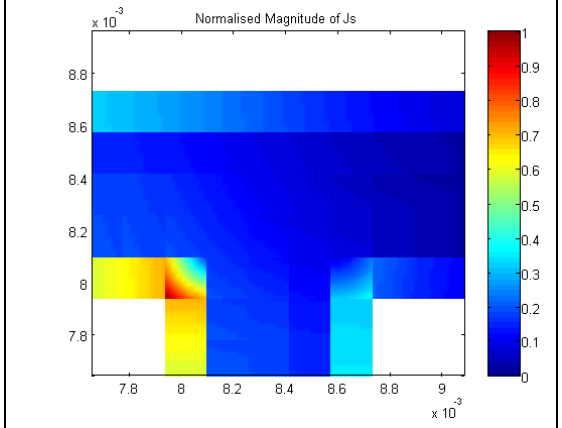

Table 2. Charge magnitude and current magnitude at f=9GHz, for 4 different kinds of excitations.

6 CONCLUSIONS

Different models for analysing printed junctions have been discussed. First, the quasistatic model has led us to two results, namely: The current distribution tends to be solenoidal at low frequencies and Kirchoff's law should be satisfied in small junctions.

Then a transmission line (TL) model has been studied to have some useful global indications about the charge and current behaviour. In this case Kirchoff's law must still be satisfied but opposite to quasistatic approaches, the TL model allows prediction of charge behaviour in the arms connected at the junction. Indeed the TL predictions are frequently a good approximation at the global level.

These global results have been corroborated with a full-wave model. For low frequencies the general behaviour of charge and current along the line for the transmission line model and in the full-wave model is the same, except, of course, in the junction. For high frequencies radiation phenomena take place, and so transmission line model is no longer valid. But even at low frequencies, radiation is generated at the junction. This results in a net decrease of charge level at the junction which has been systematically observed in our numerical experiments. This feature of the charge must be included in the pre-fractal antenna model if accurate predictions are required.

With the full-wave model the structure has been studied once with a rough mesh and once with a very high number of unknows, to know in detail which is the evolution of currents and charges on the T-junction, for different kind of excitation. With a high degree of detail results show with precision the zones where current and charge maxima or minima can be found. For low frequencies, in the junction and without taking into account singularities, the charge can be said to be constant, but it is no longer the case for high frequencies. All this information must be used in order to define a global basis function that reproduces these characteristics, and thus it can be used to substitute the detailed fine mesh in the junction without loss in precision and accuracy of results.

Summarizing, this study has set up the basic strategy for the modelling of connections and junctions in pre-fractal antennas. Some observed effects deserve further study in order to reach a correct interpretation. For instance the electromagnetic behaviour of junctions seems to depend critically on the kind and type of excitation.

At a first glance, this seems to render hopeless a global, unique aproach for junctions in fractals. But save for the case of a junction containing eventually the excitation, most junctions in fractal structures are essentially excited by the fractal itself and hence there is room for a systematic time-saving treatment. This and related questions should be clarified in the next phase of this project.

7 REFERENCES

[1] T.C. Edwards, M.B.Steer, “Foundations of interconnect and microstrip design”, John Wiley and Sons.

[2] J.R. Mosig, “Arbitrarily shaped microstrip structures and their analysis with a Mixed Potential Integral Equation”. IEEE Transactions of Microwave Theory and Techniques. Vol. 36, no. 2, February 1988, pp. 314-213,

DISCLAIMER

The work associated with this report has been carried out in accordance with the highest technical standards and the FRACTALCOMS partners have endeavoured to achieve the degree of accuracy and reliability appropriate to the work in question. However since the partners have no control over the use to which the information contained within the report is to be put by any other party, any other such party shall be deemed to have satisfied itself as to the suitability and reliability of the information in relation to any particular use, purpose or application.

Under no circumstances will any of the partners, their servants, employees or agents accept any liability whatsoever arising out of any error or inaccuracy contained in this report (or any further consolidation, summary, publication or dissemination of the information contained within this report) and/or the connected work and disclaim all liability for any loss, damage, expenses, claims or infringement of third party rights.